SYNAPTIC SCULPTING: TERMINAL SCHWANN CELLS PARTICIPATE IN NEUROMUSCULAR SYNAPSE ELIMINATION

A Dissertation

by

IAN W. SMITH

Submitted to the Office of Graduate and Professional Studies of
Texas A&M University
in partial fulfillment of the requirements for the degree of

DOCTOR OF PHILOSOPHY

Chair of Committee,	Uel J. McMahan
Committee Members,	Mark Zoran
	Steve Lockless
	Mendell Rimer
Intercollegiate Faculty Chair,	Michael Smotherman

December 2019

Major Subject: Neuroscience

ABSTRACT

Impulse transmission from the axons of motor neurons to the myofibers of our muscles is essential for virtually all aspects of our physical behavior. It ultimately drives our ability to move, to breathe and to eat, amongst other essential activities. The sites where the impulse transmission occur are termed neuromuscular junctions (NMJs). They are similar to the synapses that mediate impulse transmission in the brain, which underlies, for example, mental behavior. Due to our dependence on neuromuscular transmission for essential aspects of our vitality and its relatively convenient availability for experimentation, considerable attention has been given to understanding how the NMJ functions, how it forms during ontogenetic development, how it is affected by disease and how it reforms after injury. Most of these studies have been made in non-human vertebrates, where the fundamental mechanisms are highly conserved from lower organisms to humans. My study concerns mechanisms involved in ontogenetic development of NMJs in the mouse, a common model used by neuromuscular experimentalists.

In mouse, each NMJ is formed by the terminal branches of a motor axon. The branches lie in close apposition to a specialized region of the myofiber membrane called the motor endplate. The endplate occupies about 0.1% of the myofiber surface in adult muscles. Synaptic transmission from the axon terminals to the endplate is mediated by molecules of acetylcholine (ACh). As the nerve fires an action potential, when an impulse traveling along a motor axon reaches its terminals at a neuromuscular junction, it evokes the secretion of ACh from the terminals into a narrow crevice between them and the motor endplate. Once secreted, ACh binds to aggregates of acetylcholine receptors (AChR) on the surface of the endplate, triggering an impulse in the myofiber that leads to its contraction. Capping the axon terminals are terminal

Schwann cells (tSCs), the third cellular component of neuromuscular junctions. They play supporting, but essential, roles in the NMJ's activity.

Typically, in mammals there is a single endplate on a muscle fiber. In adults, each endplate is innervated by the terminals of a single axon. On the other hand, at birth, there can be terminal branches of as many as 10 or more separate axons making synaptic contact at a single endplate. Several lines of evidence indicate that the terminals of the different axons compete for sole occupation of the endplate and that the elimination of inputs requires communication between the axon terminals and muscle fiber. Although much has been learned about the nature of the communication driving this transition from poly- to single-innervation our understanding is far from complete. Even less well understood is the behavior of the tSCs during the period of synapse elimination. The aim of my study was to determine in detail the characteristics of tSCs during this period with an eye toward learning whether the tSCs play a direct role in the process.

DEDICATION

I dedicate this dissertation in the loving memory of my mentor, Dr. Wesley J. Thompson. I began my career in science as an undergraduate volunteer in Dr. Thompson's lab. Under his tutelage, I developed a level of respect for science and a love for the process that I had not yet appreciated. Dr. Thompson was the essence of what a mentor should be. He fostered my education in science through rigorous inquisition and training along the way. He provided connections with so many people, especially Dr. Jack McMahan, that are so influential to my progress as a young scientist. More than just science, Wes taught me so much about life. His respect and care he showed for all people and wildlife are something that will never part from me. Not a day passes that I do not reflect on my relationship with Dr. Thompson in some form or another. You will be missed.

ACKNOWLEDGEMENTS

I would like to thank my late advisor and mentor Dr. Wes Thompson for inspiring me and getting me started in science. He has had an incredible impact on my scientific career, thought processes, curiosity, and general outlook on life.

Thanks to Dr. Jack McMahan for his commitment to me personally and my professional development. For most of my graduate studies he served as my co-mentor and had an incredible impact on my understanding of the history of neurobiology, ultrastructure, electron microscopy, and professional development.

Thank you to all of my committee members Dr. Thompson, Dr. McMahan, Dr. Zoran, Dr. Rimer, and Dr. Lockless for their incredible support throughout my time at Texas A&M. They have pushed me to become a better scientist and person through their advice and guidance, pushing me to strive for the very best I can at all times.

Thanks to Michelle Mikesh for all of her support and guidance through my undergraduate and graduate education. She has been integral to developing my skills in the art of electron microscopy and writing in addition to her compassion and guidance through the many trials and tribulations that have accompanied my journey.

Thanks go to all of my fellow students and staff members at Texas A&M and the Institute for Neuroscience. I will always cherish my time here and the progress we all made in improving this program for the betterment of all students here and to come in the future.

A special thanks to my family, especially my mother and grandmother for always inspiring me and expressing unwavering belief and confidence in me for my entire life.

Lastly, I'd like to thank my wife, Jessica, for her support day-in and day-out no matter the circumstances. I know I made it hard to do this throughout the years but I would not have been able to endure without your love and support every day.

CONTRIBUTORS AND FUNDING SOURCES

Contributors

This work was supervised by a dissertation committee consisting of Professor Wesley Thompson (advisor) and Professor Jack McMahan (co-advisor) and Professors Mark Zoran and Steve Lockless of the Department of Biology and Professor Mendell Rimer of the Department of Neuroscience and Experimental Therapeutics.

Most of the electron micrographs used for analysis in Chapter 2 & 3 were taken by Michelle Mikesh of the Department of Molecular and Cellular Biology at The University of Texas at Austin, Dr. Matt Lee in part, performed the confocal microscopy in chapter 3, and all resources were provided by Dr. Wesley Thompson. This work was published in 2013. The tissue for postnatal day 7 and 19 mice analyzed in Chapters 2-3 was dissected and prepared for SEM by Dr. Matt Lee of the Department of Biology and imaged by Renovo Imaging. Dr. Jae Hoon Jung of the Department of Biology in part performed the analyses conducted in Chapter 5.

All other work in the dissertation was conducted by Ian W. Smith.

Funding

Graduate study was supported by a Heep Fellowship from Texas A&M Institute for Neuroscience and Funds from Dr. Wesley J. Thompson.

This work was also made possible in part by the National Institute of Health under Grant Number 2 R01 NS020480-28 and in part by start-up funds of Dr. Wesley J. Thompson from Texas A&M University.

NOMENCLATURE

NMJ	Neuromuscular Junction
EM	Electron microscopy
tSC	terminal Schwann cell
AChR	Acetylcholine receptor
BTX	Bungarotoxin
BDNF	Brain derived neurotrophic factor
LGN	Lateral geniculate nucleus
HRP	Horseradish Peroxidase
DAB	3,3'-diaminobenzidine
P#	Postnatal Day
SC	Schwann cell
ACh	Acetylcholine
SEM	Serial block-face electron microscopy
GFP	Green fluorescent protein
Fig.	Figure
LRP4	Low-density lipoprotein receptor-related protein-4
MuSK	Muscle specific kinase
NRG1-III	Neuregulin-1 type 3
SMA	Spinal muscular atrophy

TABLE OF CONTENTS

Page

Page

LIST OF FIGURES

FIGURE Page

FIGURE Page

LIST OF TABLES

CHAPTER I

INTRODUCTION AND LITERATURE REVIEW OF NEUROMUSCULAR JUNCTION DEVELOPMENT AND SYNAPSE ELIMINATION

1.1 Cellular components of neuromuscular junctions

Impulse transmission between motor neurons and the muscle fibers of skeletal muscles occurs at synapses known as neuromuscular junctions (NMJ). Typically, an NMJ consists of three cellular components: the axon terminals of a motor neuron, the endplate region of a muscle fiber, and the processes of terminal Schwann cells (Figure 1.1) (reviewed in Sanes and Lichtman, 1999). All three components are specialized for unique roles in neuromuscular transmission. What follows is a description of these components and their roles in transmission at adult NMJs.

The axon terminals are specialized for the storage and release of the neurotransmitter, acetylcholine (ACh). Release occurs after an impulse traveling along the axon reaches the axon terminals. ACh molecules are loaded into and stored in membrane-bound synaptic vesicles, which are abundant in the axon terminals (see Figure 1.1). The vesicles congregate at specialized regions along the axon terminal's presynaptic plasma membrane known as active zones. In addition to synaptic vesicles, the active zones include dense protein patches, called active zone material (AZM), and aggregates of voltage-gated potassium and calcium channels. AZM is attached to the presynaptic membrane and the channels are embedded in the membrane adjacent to the AZM. The AZM directs the docking of synaptic vesicles on the presynaptic membrane. The calcium channels open

upon arrival of an impulse and the influx of calcium into the cytosol triggers the fusion of the vesicle membrane with the presynaptic membrane (Harlow et al., 1998). The fusion results in the release of the vesicle's ACh into the synaptic cleft, which separates the presynaptic membrane and postsynaptic plasma membrane of the muscle fiber at the endplate. Axon terminals also contain a second type of vesicle population, dense-core vesicles (DCVs). DCVs are about twice as large as synaptic vesicles (100nm versus 50nm diameter) and are thought to primarily deliver essential proteins, such as agrin, to the synaptic cleft. These proteins aid in the formation and maintenance of synaptic connections at the NMJ, in part, by creating a tight protein matrix linking the pre- and postsynaptic membranes (discussed further below). Mitochondria are also abundant within the axon terminals, where they aid in ionic homeostasis and production of ATP that helps power the fusion of synaptic vesicles, protein interactions and even communication with terminal Schwann cells through binding purinergic receptors on their cell surface (Darabid et al., 2013).

The presynaptic membrane of axon terminals is separated from the postsynaptic membrane of the muscle fiber by ~50nm (roughly the diameter of a single synaptic vesicle). This space, the synaptic cleft, is not an empty-void of extracellular space, but rather, filled with a milieu of proteins arranged in a dense matrix. This matrix, the basal lamina, ensheaths the entire surface of the muscle fiber, passing through the synaptic cleft, and extending into the junctional folds. It also extends to enclose the terminal Schwann cells and axon terminals, similar to a net. Basal lamina is not unique to muscle cells, similar lamina is found around cells throughout the body, consisting of; collagen IV, laminins, and heparin sulfate proteoglycans.

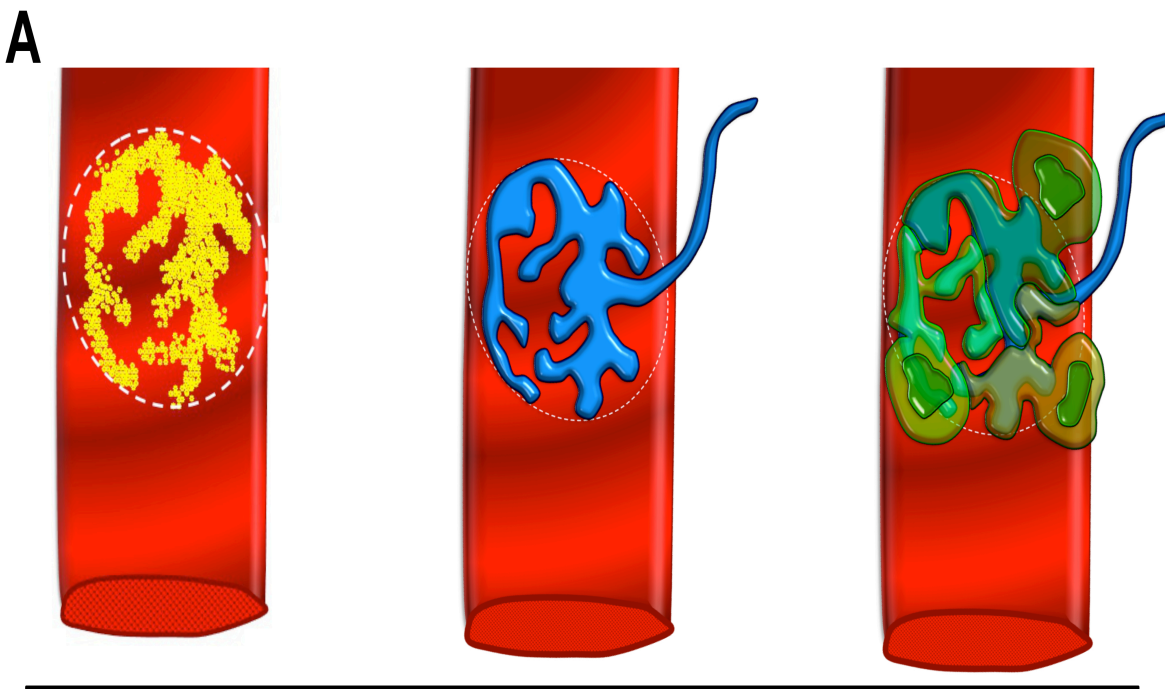

Figure 1.1: Cellular components of the NMJ and synaptic specializations**.** A, The postsynaptic muscle fiber (red) has a centrally located endplate area on its surface, rich with AChR (yellow) that has a branched "pretzel" pattern (top left). A single motor axon and its terminals (blue) contacts the muscle fiber at the endplate, mirroring its contacts to the sites of AChR expression (top middle). Terminal Schwann cells (green) cover the terminal arbors of the axon on the non-synaptic side (top right). B, Cross-section of adult NMJ showing tSC (green) capping the non-synaptic side of the axon terminal (blue) in direct apposition to the muscle fiber membrane (red). Axon terminals are packed with mitochondria (orange), synaptic vesicles (SV) (white), and dense-core vesicles (white w/ black center). Active zone material (black) assembles along the presynaptic surface of the axon terminal and serve to facilitate SV and DCV docking, fusion and release of contents into synaptic cleft. The muscle fiber is undulated at the endplate, with axon terminals residing in gutters lined with junctional folds. The folds are rich with AChR (yellow) and open directly opposite the sites of SV release at AZM. Here acetylcholine released from SVs binds to AChR and initiates muscle contraction. The submembrane space of the muscle is also specialized with organelles such as synaptic myonuclei, ER, Golgi, and mitochondria that contribute to its raised appearance compared to extrasynaptic muscle fiber membrane. Between the axon terminal and the muscle fiber membrane is the basal lamina (BL). The BL at the synapse contains specialized components, detailed in the text, which organize synaptic specializations in all three cell types. Illustration by Ian W. Smith.

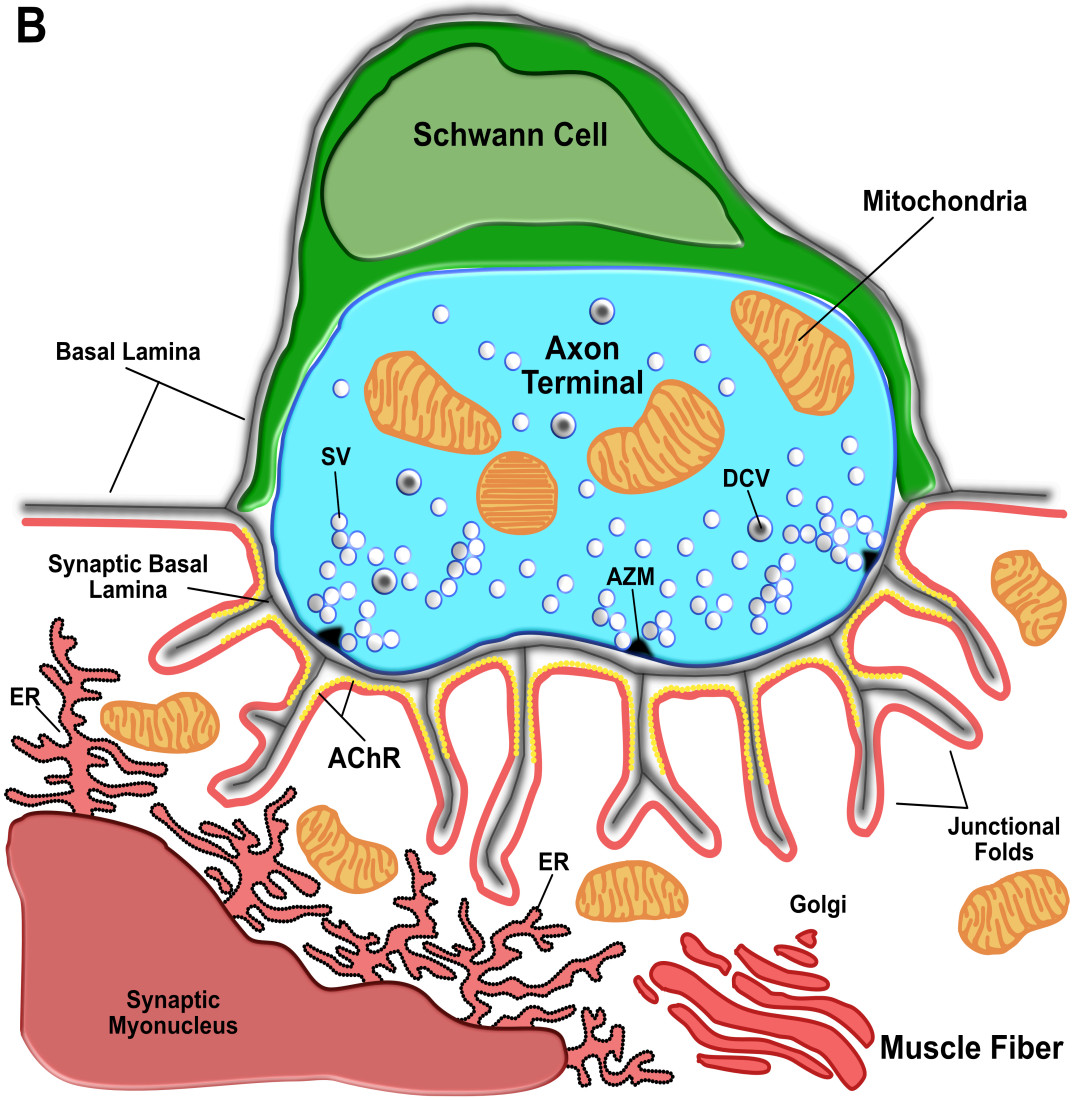

Figure 1.1 Continued

Although these proteins are found throughout the muscle basal lamina, specific isoforms are expressed at the NMJ versus extrasynaptic portions of the muscle fiber. For example, while laminin α2 is found throughout the basal lamina, laminin α4/5 are found exclusively at the adult NMJ in the synaptic cleft portion of the basal lamina. Similarly, laminin β1 is primarily expressed in extrasynaptic regions of the muscle fiber surface while laminin β2 is found predominantly at the NMJ (reviewed in Patton, 2003). Laminins are

crucial to the adhesion of the pre and postsynaptic components. Indeed, in mice lacking laminin β2 there is a lack of synaptic adhesion and stability (Noakes, 1995). The synaptic basal lamina is also enriched with acetylcholinesterase, which serves to sequester and hydrolyze ACh released from axon terminals, helping to modulate the amount of interaction released ACh has with acetylcholine receptors (AChR) in the muscle fiber membrane (Salpeter, 1969; Rosenberry, 1975; Salpeter et al., 1978; McMahan et al., 1978) Additionally, the synaptic basal lamina is rich with agrin, which interacts with transmembrane proteins found in the muscle fiber surface, low-density lipoprotein receptor-related protein 4 (LRP4), and muscle-specific tyrosine kinase (MuSK), which play an important role in establishing and maintaining synaptic connections between the presynaptic membrane of the axon terminals and the postsynaptic membrane of the muscle fiber (Reviewed in Burden et al., 2018). Although these basal lamina proteins are not a major topic of discussion in the studies that follow, it is important to recognize their presence, specific arrangement, and impact on the overall efficacy of neuromuscular synaptic communication. The postsynaptic portion of the NMJ, located on the surface of the muscle fiber, is known as the motor endplate. The majority of the muscle fiber surface is smooth except for the endplate region, which occupies less than 1% of the total muscle fiber surface. The endplate region appears as a hump on the muscle fiber surface and is undulated with synaptic gutters, housing the axon terminals. The elevated surface of the endplate is also due, in part, to the accumulation of mitochondria, myonuclei, associated Golgi apparatus and granular endoplasmic reticulum, all of which is involved in producing proteins specific for the synapse. The proteins are required for mediating the neurotransmitter's effect on the muscle fiber. Thus, the postsynaptic membrane of the

motor endplate is designed for rapid and reliable responses to the ACh released into the synaptic cleft. It is densely packed with AChRs at roughly 1,000-fold higher concentration (~ 10,000/ μm^2) than that of the muscle fiber's plasma membrane found in extra-synaptic membrane, outside of the endplate region (~ 10/ μm^2) (Salpeter, 1985; 1988). In addition to the differences in receptor concentrations, the shape of the muscle fiber membrane at the endplate region is different from that of the extra-synaptic regions. The axon terminals reside in slight depressions of the muscle fiber membrane, gutters, where in-foldings (junctional folds) arise. The majority of AChRs are concentrated along the crests and upper sides of the folds. The mouths of the folds are positioned directly opposite the active zones in the presynaptic membrane, where vesicles fuse and release their ACh (Bartol et al., 1991). Processes of Schwann cells cover the portion of the axon terminals facing away from the muscle fiber membrane. Terminal Schwann cells differ from Schwann cells along the parent axons. For example, Schwann cells along the axons form myelin that sheaths the axons and have different protein expression patterns from those of terminal Schwann cells (reviewed in Woodhoo and Sommer, 2008). Myelin aids in the rapid transmission of nerve impulses along the axons. Terminal Schwann cells are typically considered to provide axon terminals with trophic support for maintenance of synaptic transmission. Despite their roles at neuromuscular junctions being much less understood than those of the axon terminals or motor endplate, the importance of Schwann cells to the vitality of neuromuscular junctions is evident from what happens in their absence. Genetic ablation of terminal Schwann cells at adult NMJs results in complete dismantling of both the presynaptic and postsynaptic apparatus while their deletion in embryonic development

results in the inability to form NMJs, leading to death of the animal at birth (Wolpowitz et al., 2000; Reddy et al., 2003; Barik et al., 2016).

1.2 Prenatal formation of NMJs

While the previous section described the composition of adult NMJs, it is important to understand how these synapses are formed. This process begins in early embryonic development. Motor axons are derived from somata in the neural tube (Leber et al., 1990). Myoblasts arise from the dermatomyotomal portion of the somite (reviewed in Brand-Saberi et al., 1996), and terminal Schwann cells from the neural crest (reviewed in Kastriti and Adameyko, 2017). Following their differentiation, all three cells travel long distances to their peripheral muscle sites to form NMJs. Upon arrival at their peripheral destinations, myoblasts fuse, end-to-end, forming multinucleated myotubes that develop into muscle fibers. Soon after the formation of myotubes motor axons, accompanied by Schwann cells enter the peripheral muscle site and begin branching, extending processes toward multiple muscle fibers (See Figure 1.2) (Reviewed in Le Li et al., 2017). Although there is some discrepancy as to whether the Schwann cells lead or follow the axons to their muscle targets, most of the evidence suggests that axons lead Schwann cells during embryonic development (Riethmacher et al., 1997). However, Schwann cells do lead axons back to the NMJ during reinnervation after peripheral nerve injury (Son and Thompson, 1995; Son et al., 1996; Trachtenberg and Thompson, 1996; Trachtenberg and Thompson, 1997). At this time, the muscle fibers express AChR diffusely along their surface with small, pre-patterned clusters of AChR that form in the absence of the nerve, “aneural plaques” (Bevan and Steinbach, 1977; Kummer et al., 2006). As the motor axons make contact with the

muscle fiber surface, they contact aneural plaques as well as non- Although several molecules have been proposed to cause this postsynaptic differentiation, McMahan and colleagues showed that agrin, synthesized by motor neurons, and released from their terminals is a primary driver for this postsynaptic differentiation (McMahan, 1990; Rimer et al., 1997). Indeed, in the absence of neural agrin, postsynaptic differentiation is severely impaired (Gautam et al., 1996; reviewed in Sanes et al. 1998). Once released from the axon terminals, neural agrin forms a large portion of the synaptic basal lamina at the NMJ where it interacts with its co-receptors, postsynaptic transmembrane proteins Lrp4 and MuSK (reviewed in Burden et al., 2018).

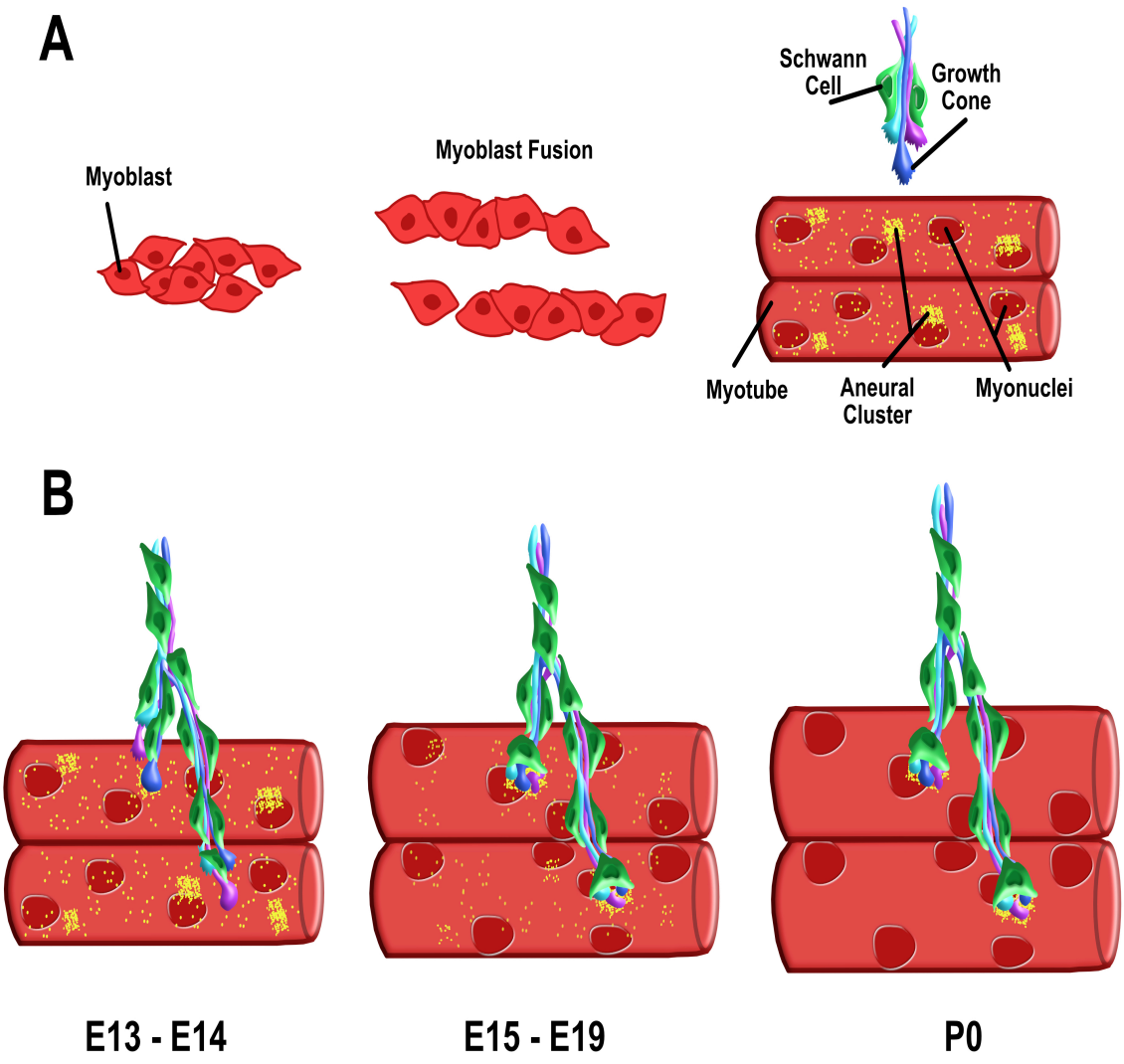

Figure 1.2: NMJ formation. A, Prior to the arrival of motor axons and tSCs, myoblasts aggregate and fuse into myotubes. Upon fusion, myotubes begin to express AChRs and small, primitive AChR clusters (aneural clusters, yellow) that are distributed in a broad middle region of the myofibers.. B, ~ E13-14 motor axons begin to make contact with the muscle fibers at sites of pre-clustered AChRs and at sites that are unclustered. Over the course of late embryonic development (E15-19), axons continue to make contact with the muscle fibers and AChRs continue to aggregate at these sites, reducing their expression at non-synaptic regions of the muscle fiber surface. By birth (P0), muscle fibers are contacted by rudimentary terminals of multiple motor axons and AChR expression is almost undetectable beyond the endplate regions where axons contact the muscle fiber and are capped by a single tSC. Illustration by Ian W. Smith.

The activation of the Lrp4-MuSK complex leads to downstream activation of the AChR-aggregating protein, rapsyn. As more axons come to poly-innervate these existing NMJs over the remaining days of gestation (E14-E20 in mice), this complex signaling network is activated and strengthened, leading to more dense aggregation of receptors

beneath the axon terminals and reduced expression elsewhere on the muscle fiber surface (Lin et al., 2008).

Thus, after meeting at their peripheral destinations (the site of the muscle), axons, accompanied by Schwann cells, establish their contacts with individual muscle fibers and initiate the formation of the NMJ in late embryonic development. Although the synapses have been formed, there are many morphological changes that will occur over the first few weeks of postnatal development that lead to the NMJ structure observed in the adult.

1.3 Postnatal maturation of neuromuscular junctions

Once NMJs have formed during embryonic development they undergo many morphological changes during postnatal maturation. At birth, multiple motor axons are observed converging at a single muscle fiber endplate (Tapia et al., 2012), where the acetylcholine receptor patterning resembles a small ovoid-plaque, measuring ~60 μm^2, with a uniform concentration of acetylcholine receptors throughout (Marques et al., 2000). At this time, the terminal branches of each axon converging on an endplate occupy a roughly equal amount of the plaque (Balice-Gordon and Lichtman, 1993). The processes of a single terminal Schwann cell cover all of the axon terminals from the different axons at this point (Love and Thompson, 1988; Brill et al., 2011). Over the first few weeks of postnatal life, all three of these components undergo considerable remodeling and growth.

Presynaptic remodeling occurs, primarily, through the elimination of redundant motor axons at the endplate. Over the first two weeks of postnatal life, the axon terminals of individual axons will be removed, sequentially, from the endplate. Only one of these axons will remain to occupy the endplate in the adult, which eventually will be roughly

ten-fold larger than observed at birth. (Redfern, 1970; Brown et al., 1976; Bixby and Van Essen, 1979; Balice-Gordon & Thompson, 1988; Balice-Gordon and Lichtman, 1993; Tapia et al., 2012). Similarly, the endplate is remodeled during this period. While the endplate is initially an evenly distributed plaque of AChR, contacted by the multiple motor axons, it is transformed to a pretzel-like pattern, mirroring the terminal arborization of the remaining axon. (Steinbach, 1981; Marques et al., 2000).

The terminal Schwann cells undergo considerable changes as well during this period of postnatal life. First, they proliferate at the NMJ. There is single terminal Schwann cell present at birth, while just days, later 3-4 will occupy that same space. While their numbers stay relatively stable after this initial proliferation, terminal Schwann cells organize their coverage of the endplate during the same period where axons are eliminated and the endplate is transformed from plaque to pretzel. After initial proliferation, terminal Schwann cells have intercalated coverage of the endplate, that is, they show no clearly defined territories. However, they show well-segregated coverage of the adult endplate (Brill et al., 2011). Thus, all three cellular components undergo a considerable period of remodeling during the first few weeks of postnatal life.

1.4 Synaptic competition and elimination

The stark morphological difference between newborn and adult NMJs is largely a result of synapse elimination (summarized in Figure 1.3). This process unfolds as the multiple motor axons initially converging on an endplate are gradually eliminated, until only one remains. (Redfern, 1970; Brown et al., 1976; Bixby and Van Essen, 1979; Balice-Gordon and Thompson, 1988; Balice-Gordon and Lichtman, 1993; Tapia et al., 2012).

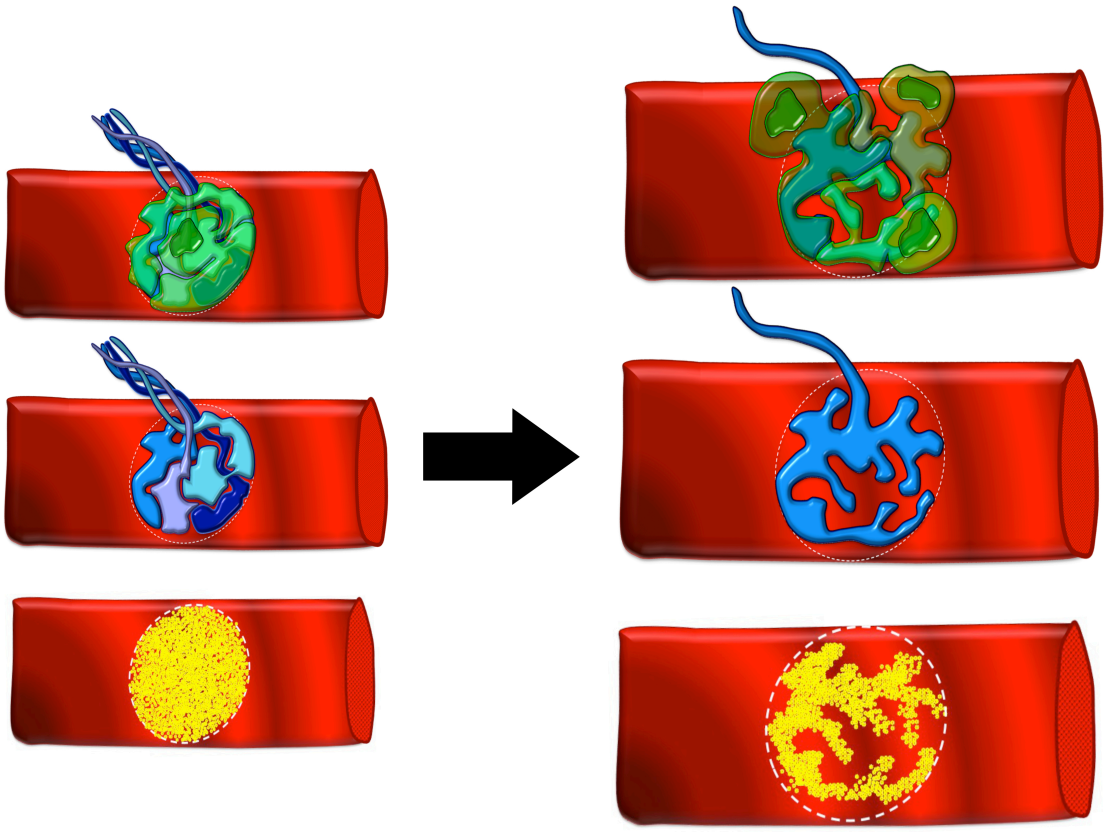

Figure 1.3: Morphological changes to NMJ structure during the course of postnatal development and synapse elimination**.** (Left) At birth each NMJ is covered by a single terminal Schwann cell (green), with the terminals of multiple motor axons (shades of blue, middle left) making contact with a uniform plaque of AChR (yellow) at the endplate zone of a single muscle fiber (red). Following synapse elimination the NMJ has grown considerably (right). Adult NMJs have multiple terminal Schwann cells that occupy distinct coverage areas of the endplate (top-right), where the terminals of a single motor axon remain (blue, right middle) where the branching pattern of the axon terminals is precisely matched by the expression of AChR (yellow, bottom right) in the postsynaptic muscle fiber membrane (red). Illustration by Ian W. Smith.

The numerous studies aimed at identifying mechanisms involved in synapse elimination agree that primary factors driving elimination of axons relate to synaptic activity and the spatial constraints of the endplate (Rosenthal and Teraskevich, 1976; Colman et al., 1997; Personius and Balice-Gordon, 2001; Walsh and Lichtman, 2003; Turney and Lichtman,

2012). Thus, synapse elimination is generally thought to be the result of an activity-dependent competition amongst the separate axons for sole occupation of the endplate.

Importantly, the reduction in axons at the endplate and the remodeling of the AChR pattern from plaque to pretzel occur during the same period of postnatal development (summarized in Figure 1.4). Many lines of evidence suggest that there is a high mutual affinity for axon terminal contact and regions of AChR expression in the muscle fiber membrane at the endplate (Rich and Lichtman, 1989; Hesselmans et al., 1993, Balice-Gordon and Lichtman, 1993; Balice-Gordon and Lichtman, 1994; Walsh and Lichtman, 2003). As motor neurons navigate into the muscle during gestation, their motor axons branch and project toward individual muscle fibers. Prior to axon contact, acetylcholine receptors are diffusely distributed along the length of the entire muscle fiber surface (Lin et al., 2008). After the axons touch-down, receptors aggregate at the site of contact and become markedly reduced elsewhere on the surface of the muscle fiber. This aggregation of receptors established the endplate region (Hesselmans et al., 1993). The high affinity between the pre and postsynaptic components is appreciable at adult NMJs as well, where the intricate branching pattern of the motor axon terminals at the muscle fiber surface is precisely mirrored by the expression of AChR at the endplate (Desaki and Uehara, 1981). Additionally, affinity is observed after peripheral nerve injuries. Following injury, the axon terminals contacting the endplate are degenerated and retract away from the endplate while the receptor patterning remains for an extended period (Kang et al., 2007). During the repair and regeneration process, as the motor axon returns to the endplate, it will tend to re-occupy those regions of the postsynaptic receptor patterning in the same fashion that it had

prior to the injury, rather than establishing new endplate regions (Rich and Lichtman, 1989; Kang et al., 2007).

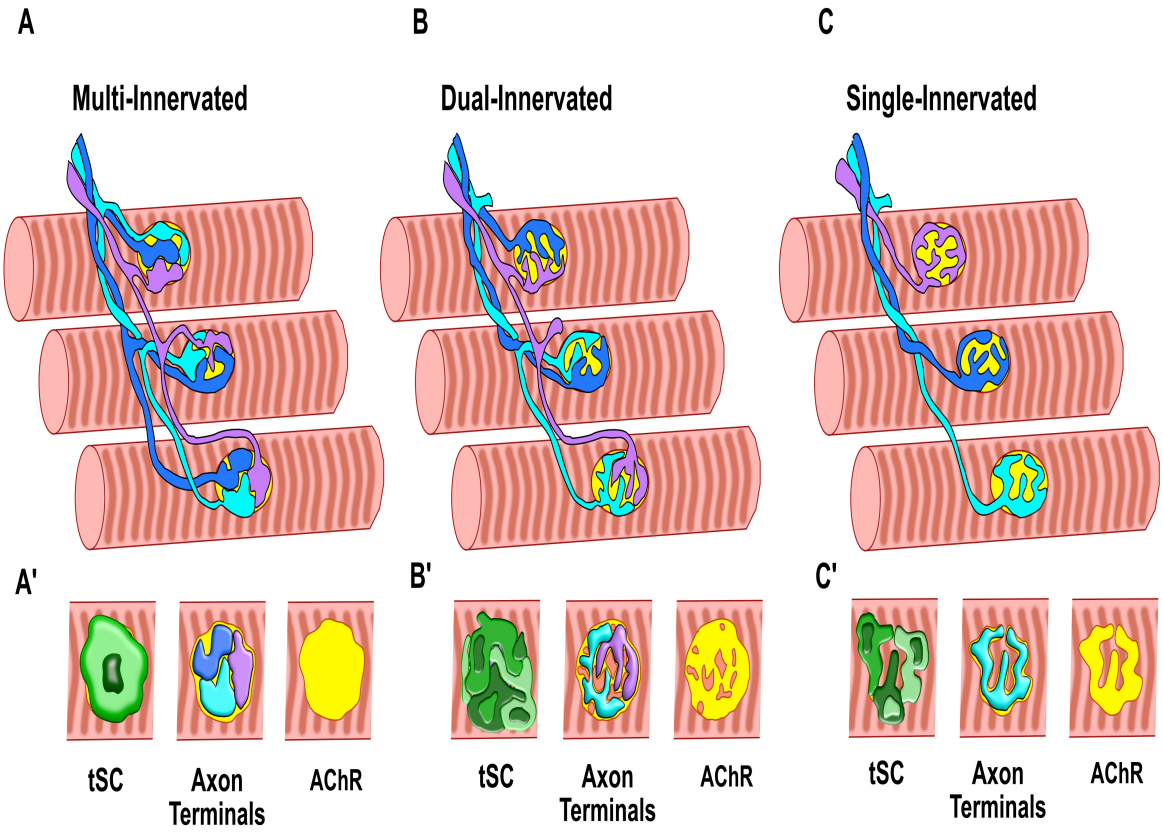

Figure 1.4: Schematic of neuromuscular synapse elimination and morphology maturation. (A) Each motor neuron (shades of blue) extends terminal arbors to multiple muscle fibers (red) where multiple motor axon terminals occupy a single endplate rich with AChR (yellow). (A') Each NMJ initially has a single terminal Schwann cell (green), multiple motor axons making synaptic contact (dark blue, light blue, purple) atop a uniform plaque of AChR (yellow). (B) Axons compete for occupation of the endplate, with losing axons being eliminated from the endplate (notice each endplate has less axons than it began with). (B') Each NMJ experiences a proliferation of terminal Schwann cells that are highly intermingled in their coverage (3 Schwann cells different shades of green), elimination of axons (dark blue axon has been lost), perforation of original AChR plaque (yellow-remaining AChR). (C) Adult NMJs have a single axon innervating each muscle fiber. (C') Terminal Schwann cells segregate their coverage of the adult endplate, single axon (light blue) remains occupying territory previously occupied by competing axons, AChR (yellow) becomes tightly restricted to regions contacted by the axon terminals. Illustration by Ian W. Smith.

Collectively, these observations suggest that the substrate for competition between the separate axons at poly-innervated NMJs in neonates is indeed the AChR-rich membrane of the endplate region on the muscle fiber.

Increased activity by axon terminals is understood to induce aggregation of AChR beneath them (Balice-Gordon and Lichtman, 1994). In fact, receptor density is shown to vary from one region of the endplate to another, based on the differing activity level of the terminals occupying those sites. For example Balice-Gordon and colleagues have shown that blocking transmission from one axon terminal at the endplate results in the loss of receptors at that site, while regions that maintain activity show increased receptor density (Balice-Gordon and Lichtman, 1994). Although those experiments were performed at adult NMJs, the same principles are suggested to apply to synaptic competition, during the period of synapse elimination (Balice-Gordon and Lichtman, 1993). At birth, the terminal arbors of each axon converging at an endplate, occupy fairly equal portions of the receptor plaque (Personius and Balice-Gordon, 2001). Assuming consistent frequency of active-zones, with equal postsynaptic contact, each axon terminal should have similar release of acetylcholine when they fire an action potential. Differential-firing rates between the different axons could affect competitive balance. However, at birth, firing rates of the separate axons are reported to be highly synchronous, negating any effect on competitive balance. The synchronicity is proposed to be the result of gap junction connections between the cell bodies of the separate motor neurons in the spinal cord (Personius and Balice-Gordon, 2001). Thus, at birth, there is competitive balance between all of the different axons occupying a single endplate.

As postnatal development ensues, gap junction connections diminish between axons, and, in turn, the relative patterns of their activity and strength begin to diverge (Personius and Balice-Gordon, 2001). As a result, the balance of power begins to shift, with some axons becoming stronger, while others weaken, with regard to activity

(Rosenthal and Terskevich, 1976; Balice-Gordon and Thompson, 1988; Colman et al., 1997). The diverging activity pattern of the different inputs, in turn, translates to unequal activation of the AChR beneath them, respectively. The concept that local differences in receptor activation are capable of causing remodeling of AChR accumulation in the adult NMJ suggests that more active axon terminals will retain and/or add receptor density beneath them while the less active axon terminals will tend to have reduced expression of AChR (Balice-Gordon and Lichtman, 1993; 1994). Thus, as activity and strength profiles of the separate axons begin to diverge during synaptic elimination, it may contribute to the remodeling of the postsynaptic receptor patterning. Indeed, reduced receptor expression has been observed at sites of eliminated axon terminals during synapse elimination (Riley, 1977; Balice-Gordon and Lichtman, 1993). Through the course of synapse elimination, the loss of terminal arbors from less active axons continues along with a progressive perforation of the initial acetylcholine receptor plaque at the endplate. These focal reductions in synaptic activity may account for the progressive transformation of the initial receptor plaque, known to occur via acute perforations in AChR labeling. Thus, as perforations continue and receptor expression becomes confined to sites of winning axon terminals the plaque is gradually sculpted into the intricately branched pretzel-like morphologies observed at mature endplates (Marques et al., 2000).

1.5 Schwann cells during synapse elimination

The behavior of terminal Schwann cells during the period of synapse elimination has been less examined than that of the motor axon terminals and the muscle fiber. Schwann cells are thought to play an important role in the guidance of axons to their peripheral muscle fiber targets during embryonic development and during re-innervation after peripheral nerve injury (Nguyen et al., 2002; Barik et al., 2016; Son and Thompson, 1995; Son et al., 1996; Trachtenburg and Thompson 1996; Trachtenburg and Thompson, 1997). In fact, they may be important for the preservation of the NMJ following peripheral nerve injury, as they remain at the NMJ, in tight association with the endplate, in the absence of the nerve (Culican, 1998; Hesselmans et al., 1993). It has even been suggested that they are capable of quantal release of ACh after nerve injury during denervation at the NMJ (Birks et al., 1960). Although interesting, there is not a consensus on this behavior, as others have concluded that terminal Schwann cells do not release ACh (Miledi and Slater, 1968).

Importantly, terminal Schwann cells have been reported to engage in phagocytic activity against motor axons as they retract during synapse elimination and after peripheral nerve injury (Love and Thompson, 1988; Kang et al., 2007; Song et al., 2008). Specifically, Schwann cells become much more dynamic in extension of processes and respond to axon terminal withdrawl through phagocytic engulfment of shed axonal debris, “axosomes”, during the retraction of axons once they have been eliminated during postnatal development (Awasaki and Ito, 2004; Song et al., 2008; Fuentes-Medel et al., 2009). This is a critical behavior for ensuring clearance of cellular debris and clearing the extracellular environment for the return of axons during reinnervation after injury.

However, according to my studies, and in agreement with studies from the central nervous system, this behavior does not appear to be limited to passive clearance of debris after axons have been eliminated from their postsynaptic targets. Studies examining the role of microglia in central nervous system development have shown that microglia are especially active in pruning and eliminating entire portions of synapses in the binocular zone of the lateral geniculate nucleus (LGN) during developmental synapse elimination (Paolicelli et al., 2011). Moreover, this phagocytic activity appears to play an important role in the correct progression of synapse elimination and synaptic specificity refinement as mouse models with mutations to complement receptors on microglia show significant deficits in their ability to correctly segregate the binocular organization from the left and right eye in these animals (Schafer et al., 2012). Similarly, in a mouse model of lysosomal storage disease, the timing to complete synapse elimination was severely delayed at NMJs compared to wildtype counterparts (Song et al., 2008). This delay indicates that the phagocytic role of terminal Schwann cells during the period of synapse elimination plays an important role in the maturation of these synapses.

Thus, the focus of my work is aimed at gaining an in-depth characterization of terminal Schwann cell behavior during the early postnatal period of synapse elimination. In the following chapters I will show evidence for and argue that (1) terminal Schwann cells prune axon terminals during the period of synapse elimination, (2) they make extensive contact with the postsynaptic membrane during this period, competing with axon terminals for the AChR rich postsynaptic landscape, (3) they remodel their contacts to be restricted to the edges of axon terminals in the adult, and (4) that this postsynaptic occupation,

transient to the period of synapse elimination, can be modeled as a driving force for synaptic competition and elimination.

CHAPTER II

TERMINAL SCHWANN CELLS PRUNE PRESYNAPTIC AXON TERMINALS DURING NEUROMUSCULAR SYNAPSE ELIMINATION*

2.1 Introduction

The formation of circuits in the nervous system relies not only on synapse formation but also on turnover, a process termed "synapse elimination." Such elimination has been most extensively studied in the case of the rodent neuromuscular junction (NMJ). Each motor neuron initially over-connects with the fibers in the muscle to which it projects (Brown et al., 1976). Each muscle fiber is innervated by multiple motor neurons within the single acetylcholine receptor (AChR) plaque near the center of each fiber. Then, during the first 2 postnatal weeks, all but one of these inputs is lost from each fiber. Compelling evidence that the motor neurons compete with each other for occupancy of each plaque has come from vital imaging (Walsh and Lichtman, 2003): as each axon withdraws from contact with the synapse, another expands to fill the vacated space. Laser ablation of one of two remaining axons results in the rapid expansion of the unablated axon into the territory of the ablated axon (Turney and Lichtman, 2012). Thus, synapse elimination has largely been explained in terms of interaxonal competition at the NMJ.

---

*Portions of this chapter reprinted from Journal of Neuroscience, 33(45), Ian W. Smith, Michelle Mikesh, Young Il Lee, & Wesley J. Thompson, Terminal Schwann cells participate in the competition underlying neuromuscular synapse elimination, 17724-36, Copyright (2013), with permission from Journal of Neuroscience.

Glia, called terminal Schwann cells (tSCs), are present at the neonatal junction (Brill et al., 2011) but have not been considered to play a direct role in the competition. However, SCs do play a major role in the destruction of the losing axons once they are eliminated from the muscle surface (Bishop et al., 2004). As losing axons withdraw from the synapse, forming so-called retraction bulbs (Riley, 1977), tSCs phagocytose pieces of them (i.e., "axosomes") (Bishop et al., 2004). tSCs also are important for the maintenance of axon terminals as their ablation in frog tadpoles reduces the growth of NMJs (Reddy et al., 2003). SC deletion in mice (Wolpowitz et al., 2000) results in loss of muscle innervation and motor neuron death. Interestingly, microglia in the CNS have been recently proposed to play a role in the postnatal elimination of retinal ganglion cell inputs to the lateral geniculate nucleus (Schafer et al., 2012), as well as synapse elimination in the hippocampus (Paolicelli et al., 2011).

In this study I show that tSCs participate in the process of neuromuscular synapse elimination through phagocytic degradation of motor axons and their terminals during early postnatal development. Using fluorescence microscopy and serial transmission electron microscopy, I show this behavior is observed as early as the day of birth (P0) and peaks during the early postnatal period of synapse elimination.

2.2 Terminal Schwann cells show elevated levels of phagocytic activity during the period of synapse elimination

In order to determine phagocytic activity by tSCs at NMJs during the period of synapse elimination, we used a marker for lysosomal organelles, Lysotracker-Red, incubating nerve-muscle preparations in the dye. We found abundant staining, in the form of small puncta, at these NMJs. The puncta were co-localized with both labeling of axons and their terminals (anti-neurofilament: 2H3, and vesicular proteins: SV2) as well as tSCs (transgenic for S100-eGFP). Moreover, we found considerable amounts of Lysotracker puncta within the region of the NMJ in the plane of AChRs and within tSCs (Figure 2.1 A). This suggests that the phagocytic activity of the terminal Schwann cells is occurring very near the synaptic surface, rather than in axons retracting well away from the synapse as shown previously by Song et al. (2008). Puncta were highly present during the first postnatal week (P0, P3, P5/6) and continued to decline into the second postnatal week at P10 and P21, towards the end of synapse elimination (5.5 +/- 0.7 at P0, n=20; 3.4 +/- 0.4 at P3, n=27; 3.3 +/- 0.5 at P5/6, n=31; 2.9 +/- 1.0 at P10, n=9; 0.4 +/- 0.1 at P21, n=20; and 0.3 +/- 0.2 at P120, n=19) (Figure 2.1 B). Thus, it appears tSCs are engaging in a developmentally regulated phagocytic activity at developing NMJs during the period of synapse elimination.

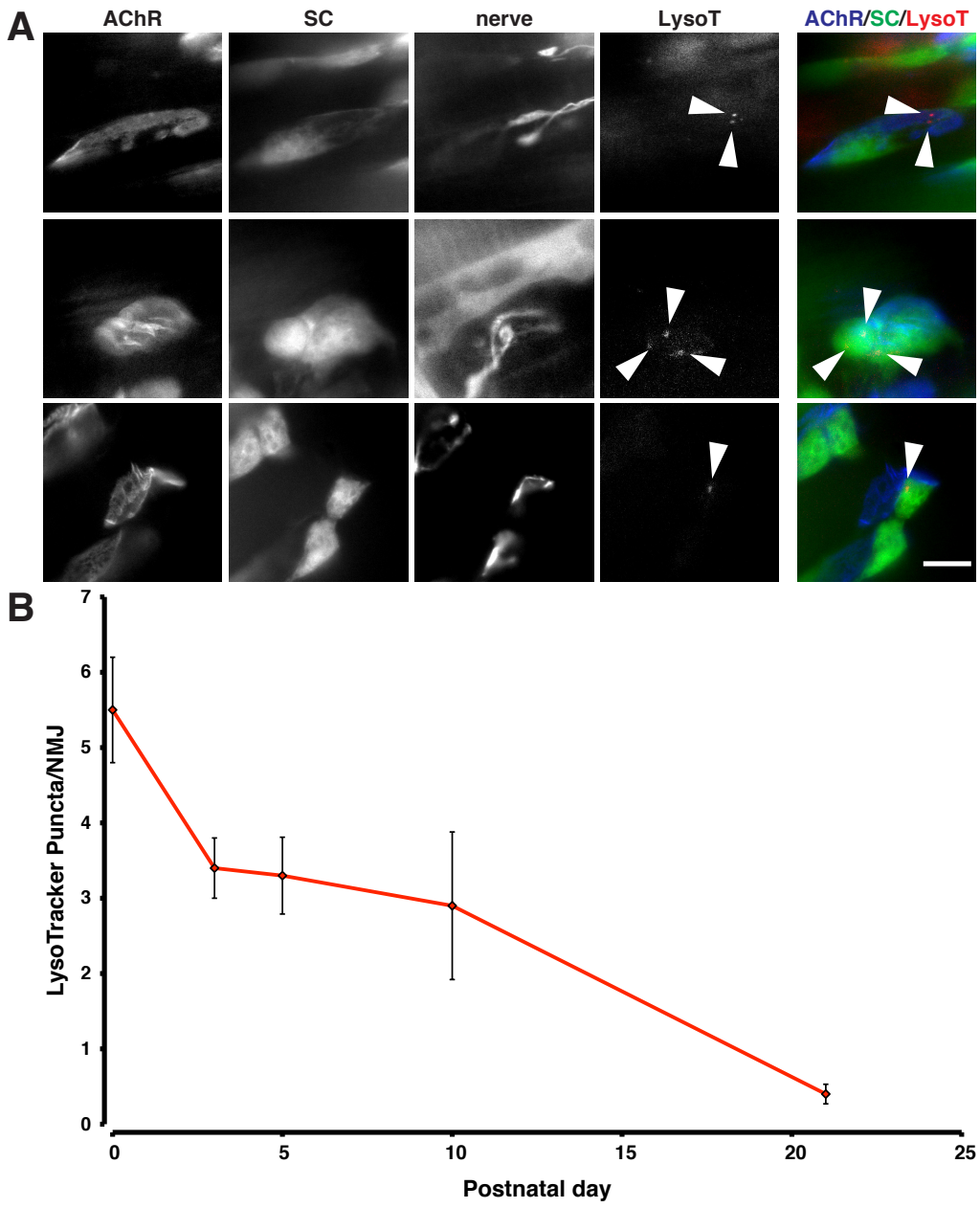

Figure 2.1: A marker for acidic organelles (Lysotracker-Red) shows developmentally regulated activity in tSCs. (A) Transgenic mice expressing GFP in SCs were labeled for postsynaptic AChR, presynaptic nerve terminals (neurofilament and SV2) amd acidic organelles (Lysotracker-Red) in P3 sternomastoid muscles. Lysotracker-positive puncta were found in the plane of the AChR, apparently contained within SCs; arrowheads show corresponding points in the panels. (B) The number of puncta per NMJ decrease with postnatal development. Scale bar: 10 μm.

2.3 Terminal Schwann cells phagocytose nerve terminals in synaptic contact with muscle fiber during synapse elimination

Light microscopy examination of phagocytic activity by tSCs at developing NMJs suggested that this activity was not restricted to retracting axons above NMJ, as suggested in previous reports (Bishop et al., 2004, Song et al., 2008). This would suggest that tSCs are actively participating in the process of synapse elimination rather than passively cleaning up shed axonal debris as they retract from the synapse. In order to determine if tSCs were in fact degrading intact axon terminals at the synaptic surface of the NMJ we performed serial electron microscopy through 24 NMJs in sternomastoid muscles at P0, P3, and P7. Examination of serial sections of neonatal NMJs, throughout the period of synapse elimination, shows that tSCs prune and degrade axon terminals at the synaptic surface. tSCs are observed degrading intact axon terminals as early as the day of birth (P0) (Figure 2.2). This activity continues throughout the period of synapse elimination, as this behavior is observed in EM data sets at P3 and P7 NMJs as well (Figures 2.3 and 2.4). This behavior is most pronounced at P3, where approximately one-fourth of all degradation in axons was found within 350nm of the postsynaptic membrane. This indicates that this activity is not isolated to retracting axons but rather is directly involved in the elimination of axon terminals. A series of sections that illustrates several features observed is shown in Figure 2.5. Here, a tSC (Figure 2.5 A, asterisk) extends a ~300nm diameter cytoplasmic finger (Figure 2.5 A, black arrow) that penetrates the axon terminal, reaches 1800nm into the interior, but does not emerge on the opposite side of the terminal.This finger even bifurcates part-way into the terminal (Figure 2.5 G). Similar to the P0 and P7 terminals shown in Figures 2.2 and 2.4, this P3 terminal is in synaptic contact with the muscle fiber,

as it has synaptic vesicles, some of which are gathered into clusters near the presynaptic membrane.

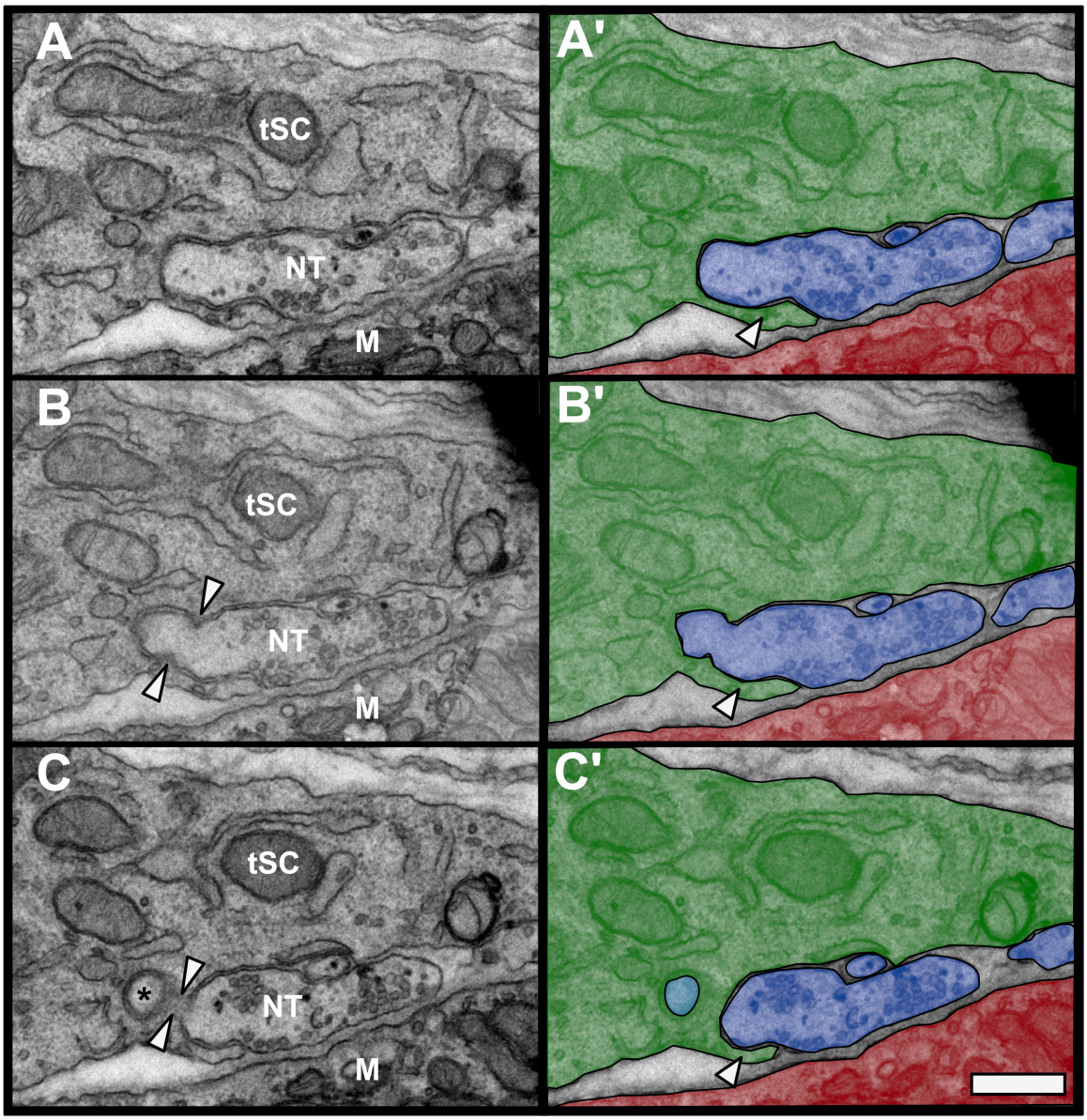

Figure 2.2: Terminal Schwann cell pruning of intact axon terminal at P0 NMJ. (A-C) 3 consecutive sections (~65nm each) showing tSC pruning (arrows B, C) of axonal material from an intact axon terminal (NT) at the synaptic surface of the muscle fiber (M). tSC pruning results in axosome (asterisk, C) to be degraded, fully enclosed by tSC. (A'-C') the same set of images shown in (A-C) segmented by color (tSC-green, NT-Blue, muscle fiber – red). Notice tSC process also intruding between the axon terminal and postsynaptic membrane of the muscle fiber (arrow, A'-C'). Images taken with TEM at 16.5 kX, scale bar 500nm.

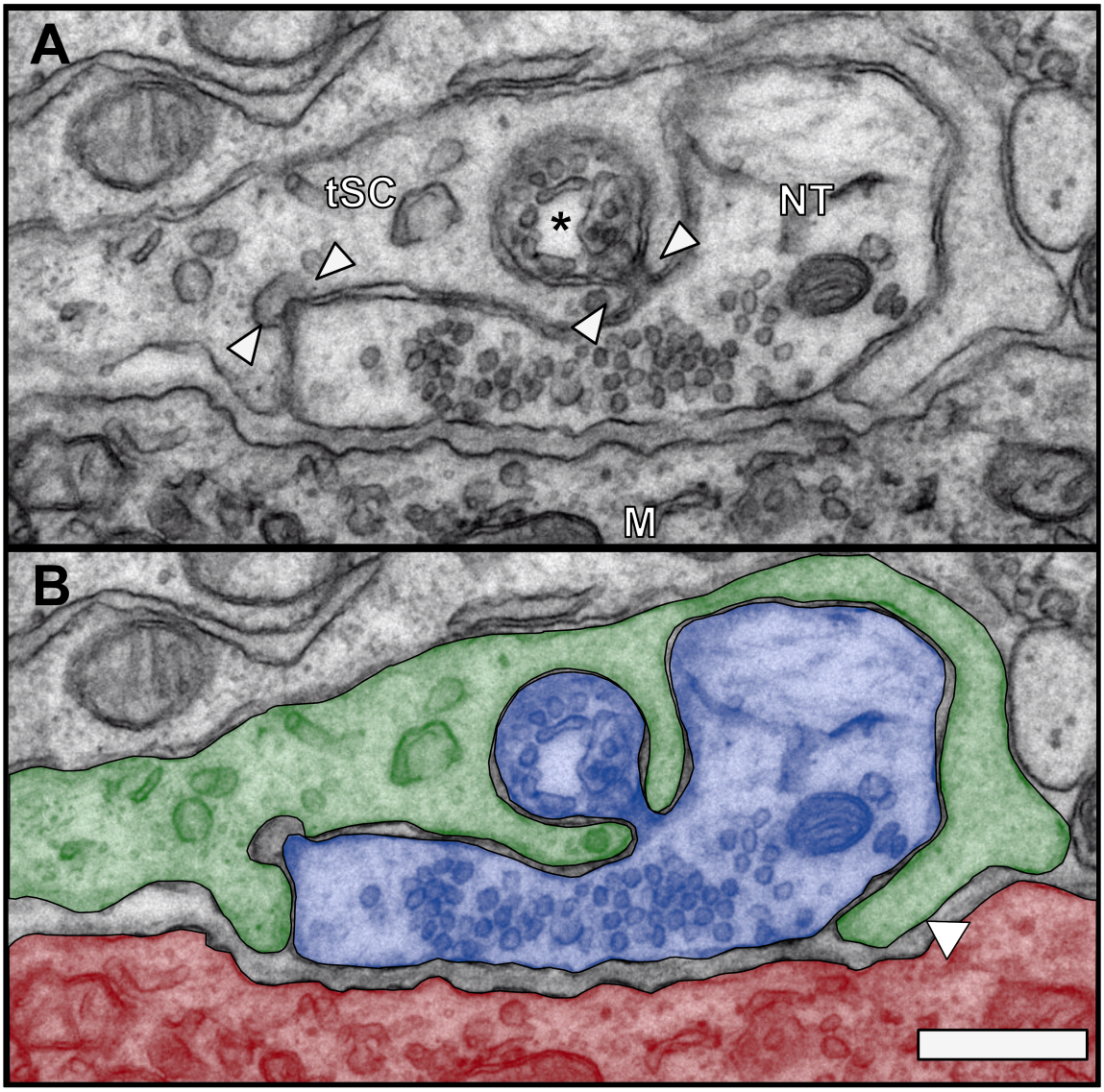

Figure 2.3: Terminal Schwann cell pruning intact axon terminal at P3 NMJ. (A) Single EM from the series shown in Fig. 2.5. Terminal Schwann cell (tSC) shown pinching off portions of axon terminal (NT) in direct contact with muscle fiber (M), forming axosome (asterisk). (B) Same image as above, segmented for ease of identifying cell types and boundaries. Notice tSC again separating axon terminal from the postsynaptic membrane via extension of processes into the synaptic cleft (arrow, B). Scale bar, 500nm.

This bouton joins, through small tSC-wrapped neuritis, one of the major axons entering the NMJ (see Figure 2.9A, axon 2). Thus, this tSC finger appears to penetrate an intact axon terminal. In seven NMJs reconstructed at P3, we observed 14 clear incidences of such tSC

fingers inside the axon terminals (Figure 2.6). Similar Schwann cell fingers were observed in the case of retraction bulbs by Bishop et al. (2004) and were shown to be very dynamic in vital imaging. However, these observations were of the destruction of recently eliminated axons and their retraction bulbs at the NMJ. Here we show that immature axon terminals in synaptic contact with the muscle fiber are also subject to tSC-mediated phagocytosis. Near the base of the tSC finger in Figure 2.5, a double membrane, "phagocytic vesicle, ~ 400nm in diameter at its maximum, appears in the tSC cytoplasm. This vesicle is still partly joined to the cytoplasm of the axon terminal (diameters 42.2 +/- 0.6 nm, n=24 in the terminal; 41.6 +/- 0.9 nm, n=22 in the vesicle). Adjacent is a second, 400nm vesicle is located entirely within the tSC cytoplasm (Figure 2.5 F, G). This vesicle also has two membranes, but its contents are much more electron lucent, the membranes, particularly the inner one, are more complicated and the few darkly staining structures within the inner membrane are less distinct and identifiable. This second vesicle appears to be in the process of degradation and likely represents a later stage in the processing of the phagocytic vesicle forming to its right. Similar instances of phagocytic vesicles were observed at P0 and P7 NMJs and can be observed in Figures 2.2 and 2.4. Such phagocytic vesicles were also reported by Bishop et al. (2004) during the destruction of retraction bulbs.

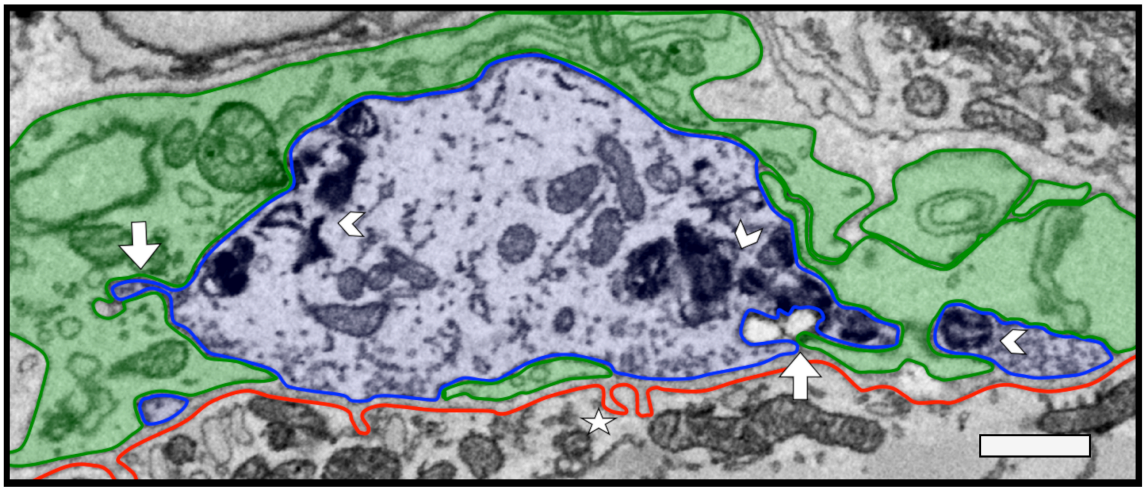

Figure 2.4: Terminal Schwann cells continue to phagocytose intact nerve terminals during later stages of synapse elimination. EM cross-section of NMJ in sternomastoid at postnatal day 7 (P7) showing Schwann cell (green) and nerve terminal (blue) in contact with postsynaptic membrane of muscle fiber (red). Schwann cells compete for postsynaptic contact, intercalating processes between the nerve terminal and muscle fiber, physically blocking sites of AChR on secondary folds from nerve terminal contact (stars). Additionally, Schwann cells continue to penetrate and phagocytose intact nerve terminals (arrows) similar to observations made at P3. Sites of Schwann cell attack are always observed with characteristic indicators of axon degeneration and damage (arrow heads). These observations indicate Schwann cells remain in an activated state into the second week of postnatal maturation. Micrograph imaged with block-face scanning electron microscopy, scale bar = 0.5 µm.

Throughout the sections of NMJs at P0, P3, and P7, we encountered material contained within tSCs at the NMJ that had the appearance of the second type of phagocytic vesicle described above. This material, described variously in previous reports as membrane whorls, honeycombs, lysosomal bodies, and multivesicular bodies, was found in tSCs in close association with axon terminals. These were far more numerous than the instances of tSC-enclosed material that contained synaptic vesicles. A likely explanation is that the synaptic vesicles rapidly disintegrate after phagocytosis. These observations also make it likely that most of the debris found in the synaptic area is that of axons and not that of tSCS. There is no evidence in our micrographs of loss of tSCs or their processes during the early stages of synapse elimination, even though Brill et al. (2011) report that the processes of neonatal tSCs are quite dynamic, in contrast to those in the adult. In fact, our

results indicate the number of tSCs increases at the NMJ from P0 to P3. This is consistent with a previous report, showing that tSCs are being added to NMJs during this period rather than lost (Love and Thompson, 1998).

2.4 Schwann cells attack and consume portions of axon terminals from all axons at multi-innervated NMJs during synapse elimination

We mapped the specific location of degradation events at NMJs from P0 (n=3), P3 (n=3), and P7 (n=2) using serial electron microscopy data sets. We found they were distributed apparently randomly to portions of all the axons at the junctions. This degradation was investigated more in-depth via the individual segmentation of the debris found at these sites for all three time-points. Thus, we generated volumetric information about the debris associated with each axon (examples of this degradation are shown at a P3 in Figure 2.6). The tSCs appear to be randomly removing parts of each axon terminal on the muscle fiber surface. Although some axons appear to be experiencing more degradation than others it is not clear that any individual axon is being selectively eliminated from the NMJ. This was true for P0 NMJs that were multiinnervated as well (see Figure 2.8A). Therefore, it is clear that, although this type of consumption by tSCs may play a role in driving synapse elimination, it does not appear to be selecting a winner. Moreover, it is clear from examination of NMJs in which the individual tSCs were segmented, that consumption of axon terminals occurs in all the tSCs present, rather than a select subset of them. This observation is compatable with the lack of apparent segregation of tSCs contacts according to axon of origin at this stage in development.

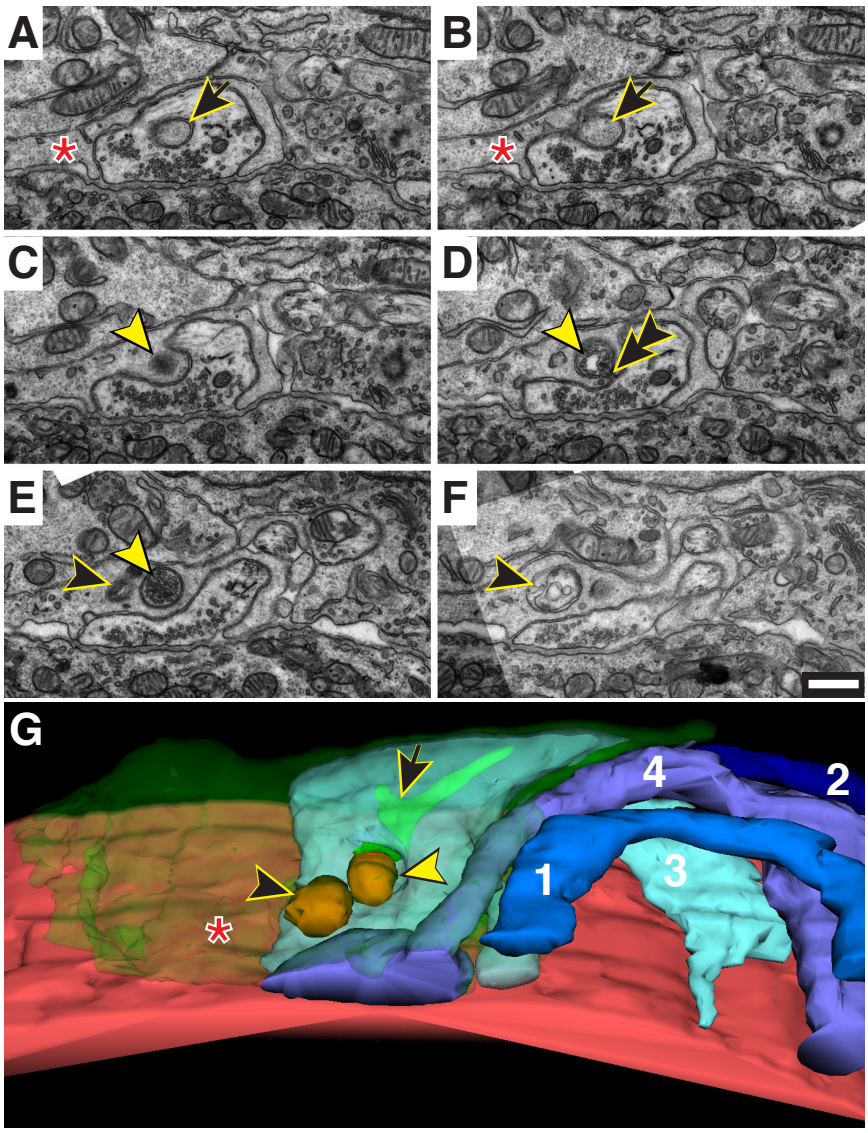

Figure 2.5: EMs of tSC phagocytosing a P3 nerve terminal. Select images from a serial set of EMs showing process of a single tSC (indicated by asterisk) and its relationship with a synaptic bouton in a P3 NMJ (NMJ-4). A, A finger of SC cytoplasm located inside the nerve terminal (black arrow). Note the two membranes. The finger extends 1800 nm into the terminal and bifurcates into two branches (shown in G below) but never emerges on the other side of the terminal. B, The site where the finger enters the nerve terminal. C, Near the base of the SC finger, a darker mass (yellow arrowhead) indicates the edge of a "phagocytic" vesicle that becomes visible inD.D, A phagocytic vesicle-containing cytoplasm of nerve terminal that is almost pinched off from the SC (double black arrowhead). E, The phagocytic vesicle in D is now completely surrounded by SC cytoplasm and appears to contain synaptic vesicles. The beginnings of a purported second phagocytic vesicle are located just to the left of this one (black arrowhead). F, The second vesicle first seen in E. This vesicle appears to contain mostly clear contents suggesting a further step in degradation. A–C, Adjacent 65 nm sections. C, D, Two sections apart. D, E, Three sections apart. E, F, Four sections apart. The serial sections for this portion of this junction are shown in Movie 2. G, Surface rendering of a small portion of this NMJ, showing one of the SCs (translucent green fill and marked with asterisk as in A), the muscle surface (red), the phagocytic vesicles (orange, marked with arrowheads as in panels above), and four axons present (1, 2, 3, 4, filled with color). The orange phagocytic vesicles derived from axon 3 are located next to the penetrating SC finger (black arrow). Scale bar: F, 500 nm.

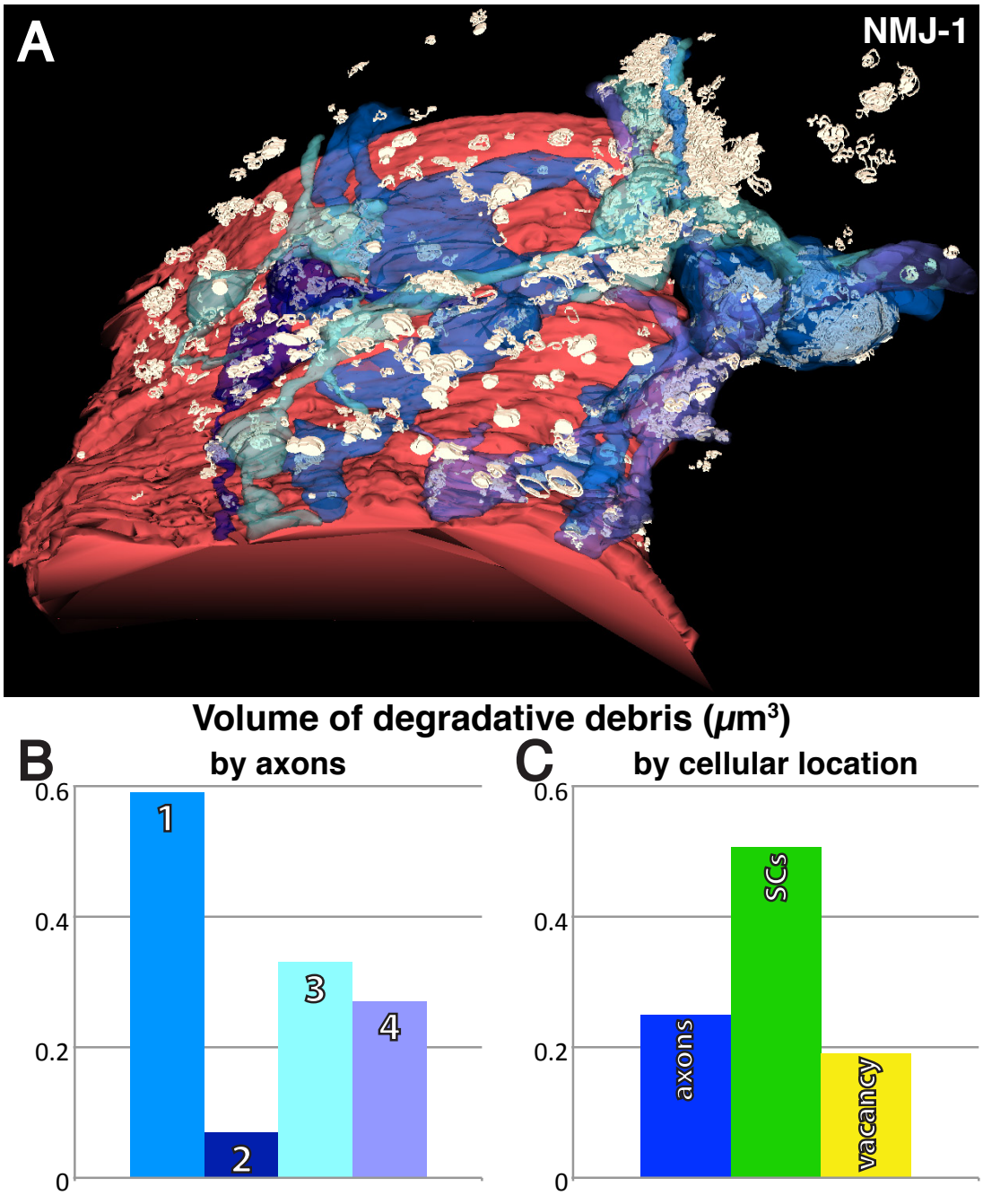

Figure 2.6 Location of degradation in P3 NMJ. A, White structures represent an outline of the degraded material in NMJ-1.Much of the debris here appears above the junction but is actually located in SCs that are not shown here. B, Volume of degraded debris in each of the axons illustrated in A. C, Volume of degraded debris found in axons, SCs, and vacancies for the NMJ in A.

2.5 Vacant areas along the synaptic surface of the muscle appear to be sites previously occupied by eliminated axons

Within the serial sections, most of the space where axons enter the NMJ as well as within the NMJ itself (but not other spaces between the muscle fibers) was filled with cells and cellular processes. However, there were some distinct vacancies where no cell or processes were present (Figure 2.7 A-C). Most of these sites were contiguous between sections. When we reconstructed these vacant spaces through the sections, their contiguity became more obvious (Figure 2.7A). These contiguous spaces resembled, in their size and shape, in their orgin near the entry of the nerve, and their proximity to and course along the muscle fiber surface, the axons still in synaptic contact. Moreover, these vacancies contain free-floating cellular debris that appears to be axonal in orgin (i.e., they contain synaptic vesicles and membrane whorls), as well as having, in some instances, direct connections to axons undergoing degradation (Figure 2.7 C). Examples of these vacancies were observed at all P0, P3 and P7 NMJs imaged with electron microscopy. Together these findings suggest that the vacant spaces were recently occupied by axon terminals. Thus, although it is impossible to be certain that these vacant spaces are not a consequence of tissue processing, the overall quality of fixation and organelles within the micrographs, the ordered arrangement of the spaces within the endplate region, the absence of such spaces in older material (P16 and P40 adult sternomastoid), and the presence within some of the spaces of intact and well-fixed SC processes indicate that the spaces are not artifact. Interestingly, such vacancies have been reported in the fruit fly CNS during the pruning of axon terminals during metamorphosis (Awasaki and Ito, 2004).

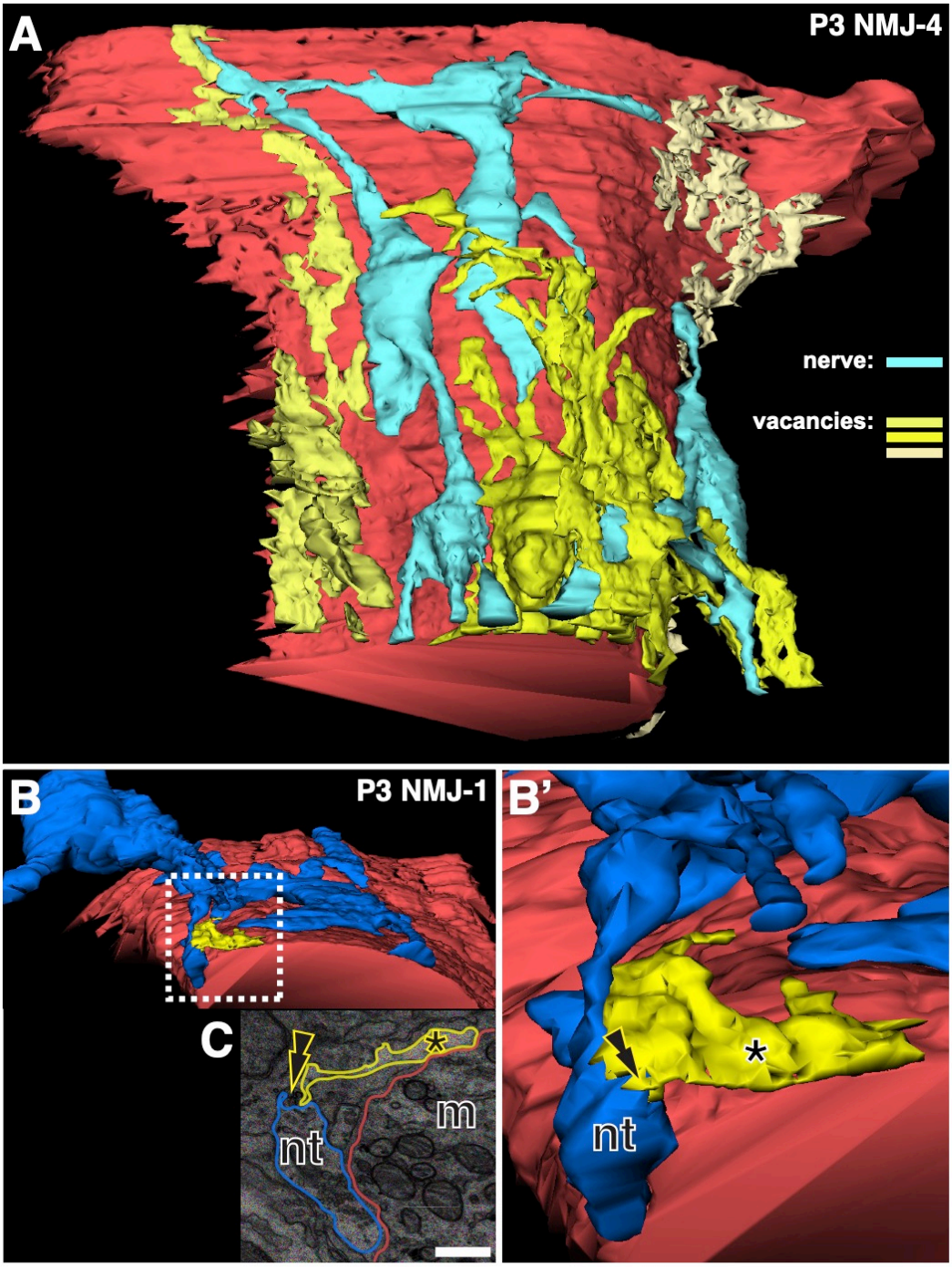

Figure 2.7: Unoccupied sites (vacancies) in P3 NMJ. A, Surface rendering of the three largest contiguous vacancies (shades of yellow) present in presynaptic area of NMJ-4. One of the four axons still innervating this NMJ is shown in blue for comparison. B, One of the axons innervating another P3 NMJ (NMJ-1) (Fig. 2.1C royal blue), and a vacancy (yellow). This vacancy appears to originate off a branch of the blue axon. This axon and vacancy are shown at higher magnification in B'. C, EM section through the blue nerve terminal (nt), muscle (m), SC, and the vacancy (asterisk). Scale bar: C, 1μm.

These vacancies are also present in figures of previous studies of the ultrastructure of neonatal NMJs, although not commented on (Bixby, 1981; Korneliussen and Jansen, 1976; Riley, 1981; Tapia et al., 2012).

We know from our reconstructions of P0 NMJs that the number of axons present at P3 NMJs is reduced from that of birth. This is also in agreement with the studies of Tapia et al. (2012) indicating that there is a reduction of inputs during this time period. Therefore, these spaces could represent the sites occupied by recently eliminated axon(s). Moreover, 58 of the 88 vacant sites observed on the surface of the muscle at P3 had, located next to them, an intact axon terminal. This supports the suggestion of Turney and Lichtman (2012) and the fluorescence imaging of synapse elimination by Walsh and Lichtman (2003) that individual axon terminals contacts lost during elimination are re-occupied by neighboring axons. However, it also seems likely, given the adjacency of axon terminals of many of the axon terminals on the muscle fiber surface at earlier developmental timepoints (Bixby, 1981; Kelly and Zacks, 1969; Korneliussen and Jansen, 1976) the tSC filled spaces at P3 that some of these vacant sites never become reoccupied or become occupied by tSCs alone. Even in the experiments in which axons have been ablated (Turney and Lichtman, 2012), the re-occupancy of the territory of the ablated axon is not immediate and appears inexact, even when visualized with light microscopy.

Scrutiny of these vacancies suggested that some of them did not result from the loss of an entire competing axon from the synapse but rather are eliminated branchlets of axons still present at the synapse (Figure 2.7 B, B', C). Indeed, in 12 cases for one of the P3 NMJs, we could follow vacancies present at the muscle fiber surface through an obvious, vacant pathway to an axon branch that led to other, intact axon terminals. Eleven of these

12 branchlets contained degraded material, most of which was within 350nm of the fiber surface. Moreover, all of the axons present at the synapse had such eliminated branchlets, consistent with the observation that all of them are undergoing some turnover. Although they were examined in more detail at P3 NMJs, instances of branchlet pruning sites were also observed at all P0 and P7 NMJs using serial electron microscopy. These observations are consistent with previous studies (Keller-Peck et al., 2001; Tapia et al., 2012) showing that, not only are individual axon terminals removed, but the branch giving rise to them as well.

2.6 Degradation events within tSCs fall dramatically by the end of synapse elimination

We compared the incidence of terminal Schwann cell phagocytosis of axon material during the course of synapse elimination by examining NMJS at P0, P3, and P7 timepoints as shown above as well as during two later stages in the sternomastoid muscle by light and electron microscopy.

At P16, the fibers in the sternomastoid are almost all singly-innervated, and by P40 the NMJs should have achieved approximately their adult configuration in terms of the pretzel present on the muscle fiber surface (Balice-Gordon and Lichtman, 1993). Although at P16 some tSC processes penetrating the axon terminals remained and degraded axonal material was still apparent in the tSCs, the incidence was approximately half that present at P3 and the total volume of debris decreased by ~ 80% (Figure 2.9 A,C). This finding suggests that remodeling of the synaptic connection is less extensive, but is not yet complete by P16, even after single innervation is achieved. This is consistent with previous

reports (Walsh and Lichtman, 2003) that NMJs continue to undergo minor changes after synapse elimination until ~ P21 and also serves as yet another indication that tSCs do not select the winner by their activity as this selection has been completed by P16. The phagocytic activity of the SCs and degradation of axonal material was even less frequent at P40 (Figure 2.9 B, C). Thus, there is a developmentally regulated phagocytic activity of SCs. A developmentally regulated phagocytosis by tSCs is also suggested by observing the number of lysotracker puncta per NMJ.

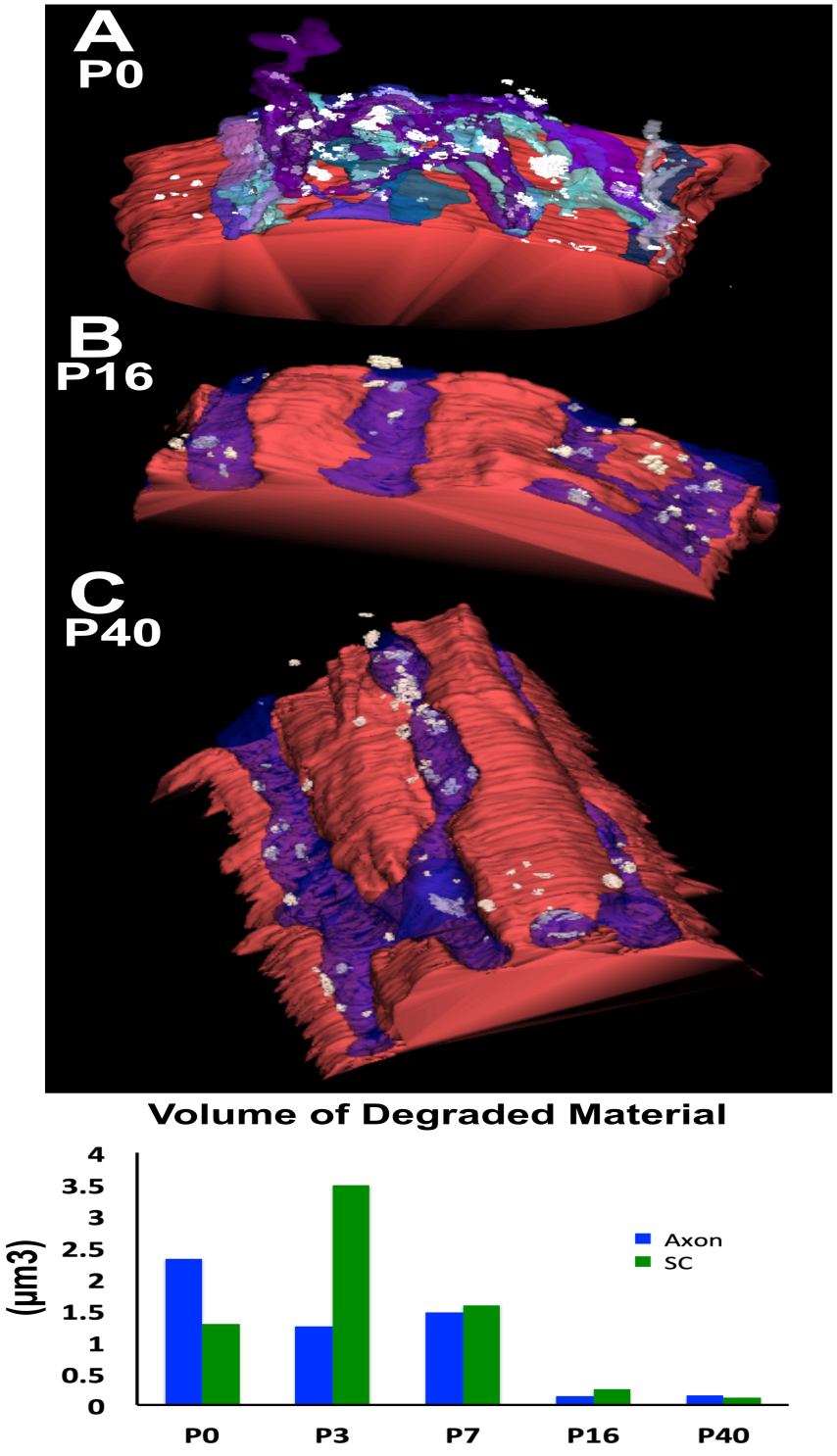

Figure 2.8: Phagocytic activity of tSCs diminishes toward the end of synapse elimination and into maturity. (A), Surface rendering of a P0 NMJ, (B) P16 NMJ, and (C) a P40 NMJ showing the muscle surface (red) and the innervating axon (blue). A, B, C, White structures mark the outlines of phagocytic activity and axonal debris located in tSCs (cells not shown) and within axons for each. D, As the junction matures to single innervations, the phagocytic activity declines as shown by the volume of degraded material found at each P0, P3, P7, P16, and P40.

2.7 Discussion

Our experiments document novel behaviors of tSCs at NMJs that have major implications for the roles these cells play in sculpting synapses during development.

First we show that tSCs engage in phagocytosis of nerve terminals. Glial phagocytosis is not novel. Bishop et al (2004) reported phagocytosis by tSCs during synapse elimination in the mouse, but axons undergoing phagocytosis had been eliminated from the surface of the muscle and were withdrawing (as "axosomes" shed from "retraction bulbs"). So in this case, the glia were involved in consuming the losing axon(s) once disconnected from the muscle. No role in the elimination events at the synapses was identified or proposed. Similarly, phagocytosis of the degenerating nerve terminals is seen after peripheral nerve injury in adult rodent muscle (Miledi and Slater, 1970). Glial activity in the remodeling of the fly nervous system at metamorphosis (Awasaki and Ito, 2004; Watts et al., 2004) and the fly larval neuromuscular junction (Fuentes-Medel et al., 2009) has been documented, but this activity seems important for removal of debris rather than the remodeling itself. More recently, Paolicelli et al. (2011) have documented microglial activity in the removal of whole synaptic structures from the dendrites of developing hippocampal dendrites. Schafer et al (2012) have documented microglial activity in the developmental pruning of synapses in the lateral geniculate nucleus. In both cases, this microglial phagocytosis is activity driven; moreover, some molecules involved in this phagocytosis have been identified and shown to delay this process if genetically ablated. However, the process determining which inputs are lost remains less clear. The neuromuscular junction offers distinct advantages for these types of issues. It is possible to study the process longitudinally in time at individual synapses (Walsh and Lichtman,

2003), to manipulate the activity of individual inputs (Buffelli et al., 2003), to surgically and optically eliminate individual inputs or even parts of inputs (Turney and Lichtman, 2012), and to even examine the relative competitiveness of individual presynaptic inputs at various postsynaptic targets (Kasthuri and Lichtman, 2003). Moreover, with serial electron microscopy, it is possible to examine every input to a single postsynaptic cell as these inputs are confined within a small, circumscribed area on the muscle fiber surface (i.e., the endplate) (Tapia et al, 2012). In this way, it has been possible in the present study to show that all synapses onto the postsynaptic cell undergo attack by the tSCs. Thus, this activity cannot be stated to select the winner definitively. There are several glia at the synapse; and although they ultimately partition the synapse amongst themselves (Brill et al., 2011), all of them at each NMJ participate in this activity. The role for glia at the NMJ (and perhaps in the CNS as well) appears to be driving synapse turnover, and this turnover plays a role in the interneuronal competition (see discussion below).

If SCs phagocytose all of the terminals present at polyneuronally innervated junctions, how do they manage to effect elimination of all but one axon? A possibility was recently suggested by Turney and Lichtman (2012). These investigators report a number of observations following up on vital imaging (Walsh and Lichtman, 2003), showing that the various inputs at each NMJ compete with each other for occupation of the the synaptic space on the surface of the fiber, with the victor ultimately expanding its territory at the expense of the losers(s). They show that laser ablation of one of the axonal inputs to a dually-innervated junction results in the rapid reoccupation of the territory of the ablated axon by the unabalted axon. They even show, in a singly innervated, adult junction, that laser ablation of a portion of the terminal arbor results in new growth of the same terminal

to reoccupy the vacated space. From this they conclude that a mechanism that removes portions of any input results in compensatory growth by the other input(s). They model a process of random elimination of portions of the terminal arbor of each axon at polyneuronally innervated junctions combined with a random reoccupation of the vacated space by any of the adjacent terminals at the endplate. This model can account for the segregation of inputs into adjoining domains within the endplate (a behavior observed from vital imaging), followed by eventual loss of inputs, resulting ultimately in single innervation. Our observations assign the role of random removal of axon terminals from the surface and creating vacancies within the endplate to SCs. Thus, SCs would drive synapse elimination without selecting the winner. Presumably, some of the sites that become occupied by SCs are not reoccupied by nerve terminals; such represents only a slight modification of the Turney and Lichtman (2012) model and could presumably help convert a uniform plaque of receptors into one that has discontinuities in the distribution of receptors (i.e., a pretzel of receptors) (however, see Kummer et al. 2004).

Such a model of SC consumption of nerve terminals in synaptic contact with the muscle fiber is not inconsistent with any previous studies of manipulations that change the rate or outcome of synapse elimination. All one would have to assume, for example, is that the manipulation favored the growth of one axon over the other axons at the NMJ. For example, as in the visual system, the more active axon at a polyinnervated junction is favored in the competition and ultimately displaces the less active axon(s); such could be explained by the more active axon(s) having a greater tendency to grow within the endplate experiencing turnover. Similarly, motor neurons that innervate larger territories might be proposed to be better (or worse) at reoccupation of vacated spaces.

The SC destruction of inputs reported here is seldom dramatic enough to produce obvious features of Wallerian degeneration, as previously reported (Rosenthal and Teraskevich, 1977). However, ther are subtle but clear anatomical signs when one examines junctions in serial sections. Hence, some of the controversy over the anatomical signs of synapse elimination can be explained.

These experiments suggest obvious next steps to show whether SCs are necessary for synapse elimination. One possible caveat to such experiments is that SCs might be essential in other ways for the synaptic development and their removal causes failure of innervation (Wolpowitz et al., 2000). It also seems quite likely that, as in the case of the hippocampus and lateral geniculate nucleus where elimination is slowed but not prevented upon genetic alterations in phagocytic activity, elimination is so crucial to neural development that no single mechanism will completely explain it.

2.8 Methods

Animals. Wild-type C57B/6 mice of either sex, obtained from The Jackson Laboratory and bred in a colony at the University of Texas and Texas A&M University, were killed on postnatal day 0 (P0), P3, P5, P6, P7, P10, P16, P19, P21, or P38-P40 by intraperitoneal injection of Euthasol (Virbac Animal Health). Experimental procedures were approved by the University of Texas and Texas A&M University Institutional Animal Care and Use Committee.

Electron microscopy and reconstruction. Animals were perfused transcardially with 0.1 M sodium cacodylate buffer, pH 7.4, followed by the same buffer containing 2% PFA and 3% glutaraldehyde. Sternomastoid muscles were removed and fixed overnight at room temperature in the same fixative. Muscles were washed with cacodylate buffer and stained en bloc in 1% osmium tetroxide, 1% ferrocyanide in cacodylate buffer for 5 h, washed with water, and then stained in 1% aqueous uranyl acetate for 2 h. Muscles were dehydrated in graded alcohols and acetone, then embedded in Epon 812. Regions containing neuromuscular junctions were located by thick (0.5–1 μm) sections made on a Leica Ultracut UTC Ultramicrotome with glass knives, stained with 1% toluidine blue, and examined under a light microscope. Blocks were further trimmed using a 45 degree cryotrim tool (Diatome) and serial 65 nm (silver) sections cut with a 35 degree diamond knife (Diatome). Sections were mounted on formvarcoated Synaptek slot grids (Electron Microscopy Sciences) and observed under a FEI Technai Spirit electron microscope with an AMT Advantage HR digital camera. NMJs were identified by the apposition of nerve terminals to within ~50 nm of the muscle fiber surface in the presence of SCs. Digital images of individual NMJs and the immediately surrounding area were captured from each

section at a magnification of 16,500. At this magnification, ~6–12 overlapping images were acquired to include the entire extent of the NMJ. These individual images were then montaged by manual manipulation in Adobe Photoshop to create a single image. Such montaged images over 70–150 serial sections were then imported into the software program Reconstruct (Fiala, 2005), calibrating the pixel dimensions in the images to known distances in the specimen. In software, the montage in each section was aligned linearly to each adjacent montage using 6–8 objects common in both and starting with the central montage in the stack and working toward each the first and last montage. Once aligned, structures of interest in each section were segmented (traced) using the tools provided in the software. Measurements and 3D renderings of these structures were then generated in software.

In total, we made extensive serial sections from a total of 10 NMJs at P0, 8 at P3, 6 at P7, 2 at P16, and 4 at P40. One P3 muscle provided all 8 NMJs, although two other animals were used to provide 40 semiserial or nonserial sections to confirm the observations made in the serial sections. Of the 8 serially sectioned P3 junctions, 1 (NMJ1) has been completely reconstructed for all parameters reported here, 5 (NMJs 2, 3, 4, 7, and 8) have been completely reconstructed, except that their SCs were not individually identified, and 2 have been partially reconstructed (NMJs 5 and 6). Two animals were used for the serially sectioned P16 muscles; an additional 2 short serials and 10 nonserial sections were made. At P40, 3 animals were used and the four NMJs had between 54 and 231 sections, and approximately a dozen individual sections were made.

Fluorescence microscopy. Fluorescent labeling of NMJs was performed as described previously (Hayworth et al., 2006, Kang et al., 2007, Lee et al., 2011). Briefly,

C57B/6 mice carrying an S100-GFP transgene (to fluorescently label SCs) were anesthetized as described above and transcardially perfused with PBS, pH 7.4. Sternomastoid muscles were dissected and fixed with 4% PFA, pH 7.4, then blocked and permeabilized with a blocking solution (0.2% BSA-fraction 5, 0.3% Triton X-100, 0.1% NaN3). Presynaptic nerve terminals were labeled with a mouse antineurofilament antibody (2H3; Developmental Studies Hybridoma Bank) and an antibody against a vesicular protein: SV2 (Developmental Studies Hybridoma Bank) or synaptophysin (Invitrogen). AChR-rich plaques were identified using a fluorochrome-conjugated alpha-BTX (Invitrogen). The acquisition of confocal fluorescence images of neuromuscular junctions was performed on a Leica TCS SP5 upright microscope using Leica LAS AF image acquisition software with a 63x oil-immersion objective with a NA of 1.4. Maximum intensity projections and orthogonal slices of image stacks were generated using ImageJ. The presence of tSC somata not in contact with the postsynaptic surface and the curvature of the postsynaptic muscle fiber prevented an accurate measurement of tSC apposition to the AChR-rich portion of muscle membrane through en face views. In attempt to improve our ability to resolve this apposition, we made orthogonal, virtual sections in both the XZ and YZ planes through confocal z stacks near the center of the synapse. Portions of AChR-rich membrane apposed by tSCs and their processes and the lengths of tSC process that overshoot the postsynaptic surface were measured using iVision software (BioVision Technologies) and computed as a percentage of length of the AChR-positive membrane and found to be 98.1 +/- 0.4% and 4.5 +/- 0.5%, respectively. A total of 46 NMJs from 5 pups were examined in this fashion.

A fluorescent label for acidic organelles (LysoTraker Red DND-99; L-7528, Invitrogen) was used to confirm the presence of and quantify degradative bodies/organelles at developing and mature NMJs, a method described previously (Song et al., 2008). Briefly, S100-GFP transgenic mice were killed as described above and perfused transcardially with oxygenated-Ringer's solution (Oxy-Ringer's). Sternomastoid muscles were dissected and pinned in a Sylgard dish in Oxy-Ringer's. Muscles were then bathed, in the dark, in Oxy-Ringer's solution with LysoTracker- Red (1 μM) for a total of 30 min, replacing the solution every 4 min to maintain oxygenation. After LysoTracker-Red staining, muscles were washed in Oxy-Ringer's 3 times for a total of 15 min. The muscles were fixed in 4% PFA, pH 7.4, and prepared for immunofluorescence as described above.

Numerical data are reported as mean +/- standard error.

CHAPTER III

TERMINAL SCHWANN CELLS COMPETE WITH AXON TERMINALS FOR POSTSYNAPTIC CONTACT DURING SYNAPSE ELIMINATION*

3.1 Introduction

During the process of synapse elimination at developing NMJs, it is presumed that the different axons converging at a single endplate compete for sole occupation of the NMJ. The substrate for the competition is most commonly proposed as the plaque of AChRs on each muscle fiber. Each plaque, oval in shape, becomes remodeled into a "pretzel" during elimination (Marques et al., 2000; Slater, 1982). If a toxin (alpha-bungarotoxin [α-BTX]) that blocks AChRs is puffed onto discrete portions of the receptor site, effectively silencing these portions of the synapse (Balice-Gordon and Lichtman, 1994), the blocked receptors and the overlying nerve terminal are lost, provided neuromuscular transmission continues through the remainder of the synapse. Thus, differential synaptic efficacy could drive input elimination and postsynaptic remodeling.

The serial electron microscopy study described in chapter 2 revealed that terminal Schwann cells (tSCs) affect this competition through phagocytic pruning of the axon terminals. However, during this investigation we recognized a second behavior of the tSCs that may influence this competition.

---

*Portions of this chapter reprinted from Journal of Neuroscience, 33(45), Ian W. Smith, Michelle Mikesh, Young Il Lee, & Wesley J. Thompson, Terminal Schwann cells participate in the competition underlying neuromuscular synapse elimination, 17724-36, Copyright (2013), with permission from Journal of Neuroscience.

tSCs at neonatal NMJs occupy a surprisingly high amount of the muscle fiber surface during the period of synapse elimination. This is in stark contrast to what is observed in the adult, where tSCs just cap the mature axon terminals and only make contact with the postsynaptic surface in thin strips on either side of the axon terminals.

In this chapter I show that axon terminals contact only a fraction of the presumed endplate during the early stages of synapse elimination and that during this period tSCs proliferate and make extensive contact with the postsynaptic surface. Moreover, during this period, tSCs expand their coverage of the postsynaptic surface, coming to occupy more of the muscle fiber surface than axon terminals, in part, by intruding between axon terminals and the muscle fiber surface. Lastly, the extensive postsynaptic coverage observed by tSCs appears to be transient to the period of synapse elimination as their processes are restricted to just capping the axon terminals in the adult. These observations suggest that tSCs may aid in promoting synapse elimination through competition for the postsynaptic membrane.

3.2 Motor neurons make bouton-like contacts within the receptor plaque at neonatal NMJs

Serial, ultrathin cross-sections were made through ten NMJs at postnatal day 0 (P0) and eight NMJs at postnatal day 3 (P3) in sternomastoid muscles of neonatal mice. The electron micrographs (EMs) of these serial sections were aligned using computer software. Structures of interest were outlined or "segemented" in each section (Figure 3.1 B, 3.2 B), and 3D surface renderings of these segmented structures were constructed in software (Figure 3.1 C, 3.2 C,D). Thirteen of these NMJs (6 of the P0 and 7 of the P3) were completely reconstructed for these segmented structures. The first structures segmented

were axons that touched the muscle surface (compare colored fills of axons in Figures 3.1 B, 3.2 B). Axons were identified by the presence of synaptic vesicles, neurofilaments, and the lighter color of the axoplasm compared with surrounding cells (particularly Schwann cells (SCs)), and their processes. Each terminal bouton could be followed through the sections to its axon of origin. On the basis of multiple processes entering them, all 13 of the extensively segmented junctions were polyneuronally innervated (Figures 3.1 C, 3.2 C) by 3-9 axons. Axons were more simple in structure at P0, with an average of 2.2 +/- 1.4 branchpoints per axon (7 junctions, 33 axons). By P3 the axons were much more woven around one another, having 8.4 +/- 1.5 branch-points per axon (3 junctions, 12 axons). At both time points, the axons touched the muscle fiber with bouton-like structures, coming within 50 nm of the muscle fiber surface (43.5 +/- 1.3 nm at P0, 48 +/- 0.7 at P3). Most of these axon terminals showed an accumulation of synaptic vesicles facing the muscle fiber, but there were not many obvious cases of active zone material (as described in Chapter 1). These observations are in agreement with prior results of Tapia et al. (2012), who used similar reconstructions to show that muscle fibers in the mouse are polyinnervated at this early stage of postnatal life. P0 NMJs had on average 5.4 axons per NMJ while only 4.3 axons were present at P3 NMJs. Indeed this is also consistent with previous reports by Tapia and colleagues, suggesting that synapse elimination is well underway just days after birth. The observations of poorly differentiated presynaptic structures and an absence of postsynaptic differentiation agree with previous descriptions of early rodent and rabbit NMJs (Kelly and Zacks, 1969; Korneliussen and Jansen, 1976; Riley, 1977; Teravainen, 1968). P0 and P3 NMJs were also examined by fluorescence microscopy to obtain information for comparison with the EMs.

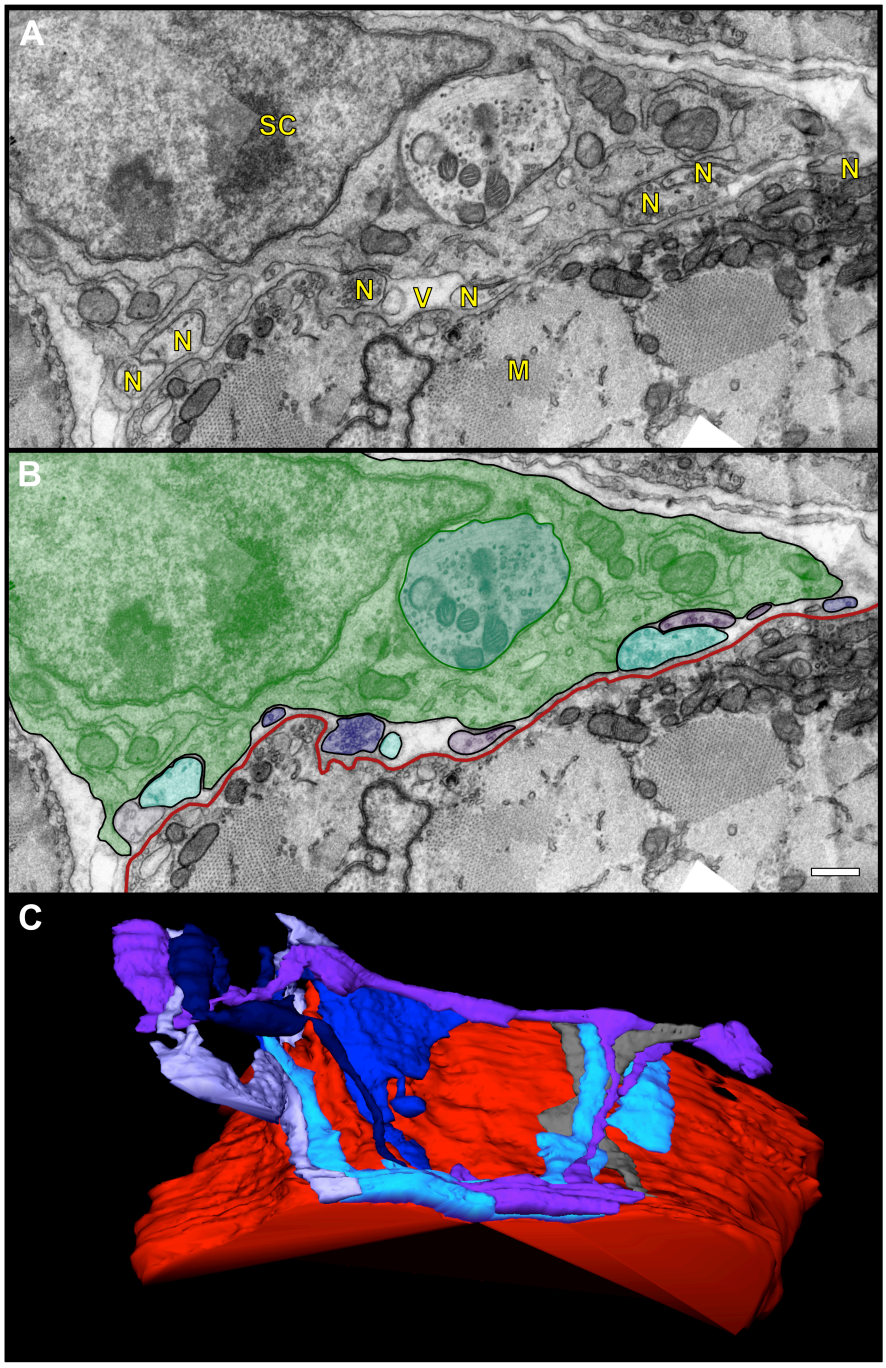

Figure 3.1: Several motor axons innervate sternomastoid NMJs at P0. (A), Montage of individual micrographs spanning the entirety of the NMJ in a single thin section of a P0 mouse sternomastoid muscle fiber (NMJ-7). Nerve terminals (N) with synaptic vesicles come within ~50 nm of the surface of the muscle fiber (M); there are no junctional folds at this stage of development. The nerves and terminals are associated with SCs, one of which have nuclei at edges of this montage. Vacancies (V) are present, some of which extend to the surface of the muscle. (B), Segmentation of the muscle fiber surface, the terminals and axons, and SCs at this same NMJ. Red line represents the muscle fiber surface. Each of six separate axons, determined by their cytoplasmic continuity from section to section, was segmented and is filled with a different shade of blue. The places where the nerves come within 50 nm of the muscle surface interrupt the red line with a line the same color as the nerve terminal. The single SC contacting these terminals was segmented and filled green. (C), Surface rendering of a series of 76 sections of this same NMJ. The axons retain the colors in B. Scale bar: 500nm.

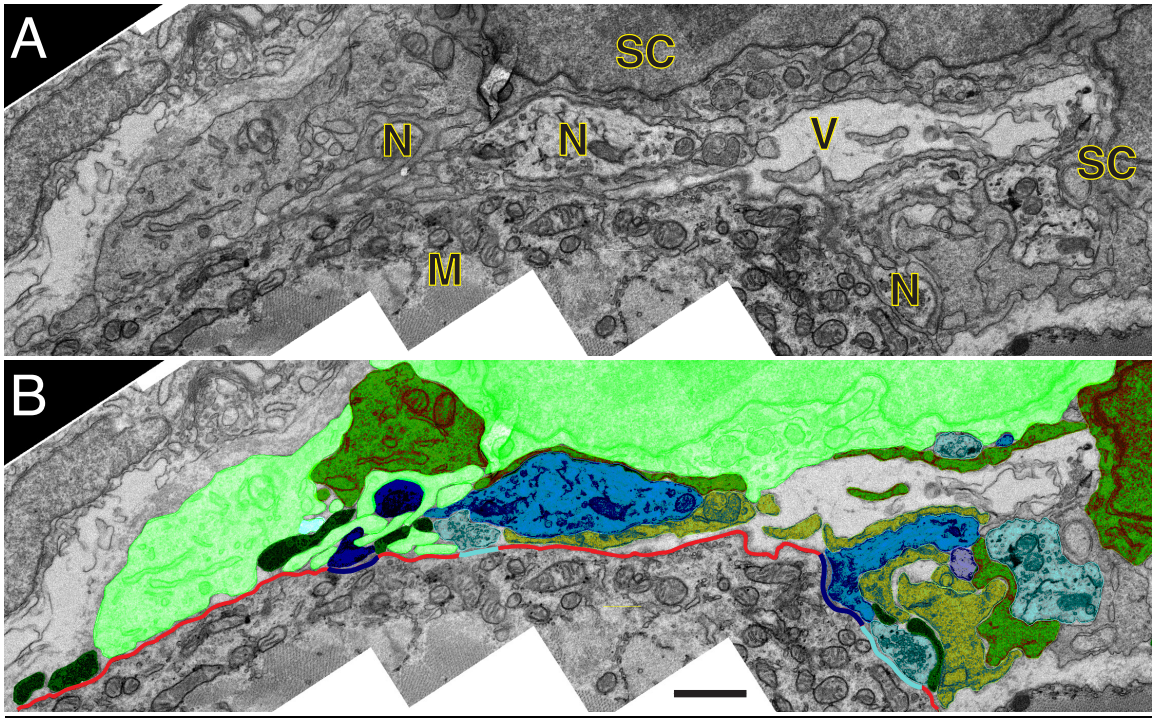

Figure 3.2: Several motor axons innervate sternomastoid NMJs at P3 and make bouton-like synaptic contacts over the surface of an oval AChR-rich plaque. A, Montage of individual micrographs spanning the entirety of the NMJ in a single thin section of a P3 mouse sternomastoid muscle fiber (NMJ-1). Nerve terminals (N) with synaptic vesicles come within_50 nm of the surface of the muscle fiber (M); there are no junctional folds at this stage of development. The nerves and terminals are associated with SCs, two of which have nuclei at edges of this montage. Vacancies (V) are present, some of which extend to the surface of the muscle. B, Segmentation of the muscle fiber surface, the terminals and axons, and SCs at this same NMJ. Red line represents the muscle fiber surface. Each of four separate axons, determined by their cytoplasmic continuity from section to section, was segmented and is filled with a different shade of blue. The places where the nerves come within 50 nm of the muscle surface interrupt the red line with a line the same color as the nerve terminal. Each of four SCs contacting these terminals was segmented and filled with a different shade of green. C, Surface rendering of a series of 139 sections of this same NMJ (location of above montages is indicated with an arrowhead). The axons retain the colors inB.D, Surface rendering as in C, but with the SCs added. Examined en face, the SCs appear to be a sheet over the junction. E, Confocal images in gray of each the AChR (with BTX), nerve (with antibodies against neurofilament and SV2, followed by a second antibody), and SCs (GFP expressed under the S100 promoter) in a P3 NMJ. Top,Maximum projections of each label. Bottom, XZ slice through the confocal stack at the position indicated by the white lines in the top in E. Arrowheads and the asterisks indicate points in the slice and the maximal projection. We conclude from this type of observation that, in the EMs, we can delineate the AChR plaque by the lateral extent of the SCs. Scale bars: B, 1µm; E, 5µm.

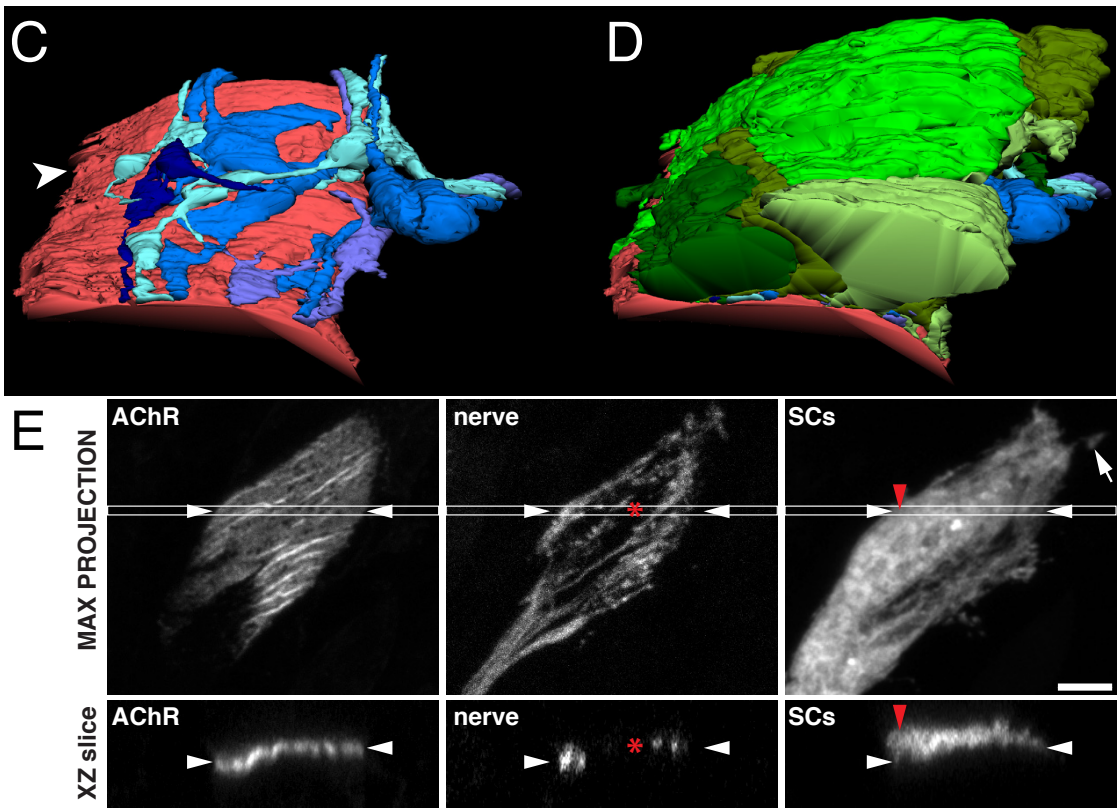

Figure 3.2 Continued

Presynaptic and postsynaptic structures were identified by a variety of fluorescent labels: alpha-BTX for AChRs, antibodies to neurofilaments, and synaptic vesicle protein SV2 for axons and axon terminals, and transgenic expression of GFP in tSCs.

These images show that the synapses and axonal branches leading to them at P0 and P3 occur within an oval plaque of receptors on each muscle fiber (see also Marques et al., 2000; Slater, 1982) (Figure 3.2 E). Confocal analysis shows at P0 these receptor plaques occupied an average surface area of 156 μm^2 and extended, on average, ~ 19 µm along the length of the fiber and ~7 µm across. Similarly, P3 NMJs had an average receptor plaque of 179 μm^2 and extended, on average, ~20µm in length, and ~12µm across the fiber. The BTX staining was mostly contiguous and uniform at both P0 and P3 NMJs.

At P3 there were occasional small holes in most plaques (each < 0.4μm^2 and in sum occupying <4% of the total area). Some receptor plaques had significantly larger "perforations", such as described in later stages of development (Marques et al., 2000). The SCs, examined in confocal stacks to exclude cell bodies located a short distance above the muscle fiber surface, showed remarkable co-localization with the AChRs (Figure 3.2 E, quantification in materials and methods). SC processes appeared to cover almost the entire plaque. The tSC processes at P3 commonly extended to the edges of the AChR plaque; with occasional processes extending beyond it (Figure 3.2 E). The axons appeared to contact much of the AChR-rich plaque, although, given the resolution of the light microscope, it is not possible to distinguish between the actual terminals and the axons leading to them. It is possible that this may over-estimate the degree of contact axons terminals actually make with the postsynaptic surface.

Thus, NMJs are still polyneuronally innervated by postnatal day 3, and this polyneruonal innervation is established within the receptor plaque whose outlines can be delineated by the lateral extent of SC processes. Although these observations are not particularly novel, they point out particular features that serve as a crucial foundation for the results that follow.

3.3 Nerve terminals at P0 and P3 contact only a fraction of the AChR plaque

Within software, we reconstructed the extent of each axon's close apposition (~43nm) at P0 (Figure 3.3) and (~49 nm) at P3 to the muscle fiber surface (Figure 3.4). We arbitrarily call this area the nerve "footprint" on the surface of the muscle fiber. We wanted to relate this footprint to the AChR-rich plaque. This was not possible to do directly at the time because our EMs had no label for AChRs. However, the fluorescence micrographs clearly show that the axons contact the muscle within this plaque. Moreover, the lateral edges of the SCs are co-extensive with the edges of the plaque (Fig 3.2 E). Therefore, we are confident that the plaque of AChRs can be estimated in the EMs by the lateral extent of the SCs and their processes. We also know that from the fluorescence micrographs at P3, that all but ~ 4% of this area of the muscle membrane should contain a high density of AChRs. To assure we were assessing comparable areas both in fluorescence and electron microscopy, we measured the extent of this EM-delineated plaque in ten reconstructed NMJs at P0 and seven NMJs at P3, averaging 39 μm^2 and 123 μm^2 respectively, certainly within the range of the plaques observed from fluorescence microscopy. Thus, despite the manner in which we began serial thin sectioning (within a few sections of first sign of axon contact with the muscle surface) we reconstructed most of the NMJ contact in each of these P0 and P3 junctions.

For the P0 and P3 NMJs that were reconstructed, the footprint of each axon, as well as the total footprint of all axons per NMJ was determined (Figure 3.3 B, 3.4 B). At P0 individual axons occupied from 0.2 to 9.4 μm^2 on the surface of the muscle with an average total axon footprint of 20.6 +/- 3.6 μm^2 (n=10). P3 NMJs had individual axons occupy 0.5 to 20.4 μm^2 on the muscle fiber surface with an average of 24.0 +/- 4.4 μm^2

(n=7). This shows, comparing the total plaque area estimated above, that, surprisingly, axon terminals contact roughly 50% of the total area at the day of birth (Figure 3.3 B) and less than 25% at P3 (Figure 3.4 B). The footprint reconstructions also reflect that the contacts made by the axons are mostly small discontinuous areas on the muscle fiber surface (Figures 3.3 C, 3.4 C). The axons leading to these terminals, if they had been viewed from above by fluorescence, would show much more extensive terminal contact than actually occurs (compare the positions of the terminal branches in Figures 3.1 C and 3.2 C with the actual footprints in Figures 3.3 C, 3.4 C). This indicates that the fluorescence images of axons would overestimate their actual synaptic contact area.

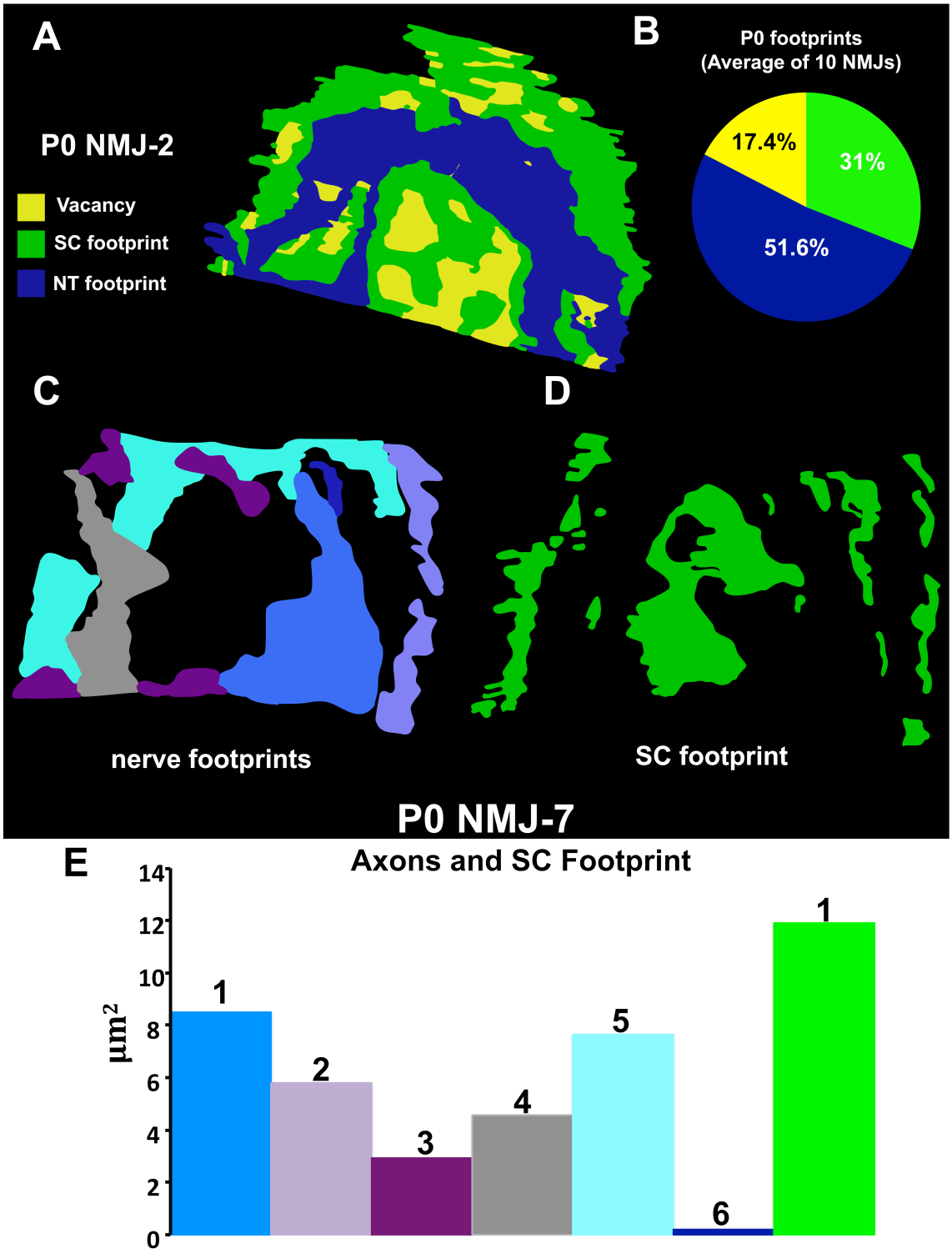

Figure 3.3: Axon terminals occupy the majority of synaptic footprint at P0. (A), The "footprint" (i.e., surface rendering of the sites on the muscle where any nerve (blue, nerve footprint) or SC (green, SC footprint) approaches within 50nm of the muscle surface at one NMJ (NMJ-2) at P0. Yellow areas represent vacancies. (B), The average fraction of the AChR plaque (i.e., the total area of the muscle covered by SC, nerve, and vacancies) contacted by each nerve (blue), the SCs (green), or a vacancy (yellow) at 10 P0 NMJs. (C), The footprints of individual axons at NMJ-7 and, below, the area of the footprint of each axon, retaining the blue shading in Figure 3.1. D, The footprints of the single SC at NMJ-7 and, below the area of the footprint of the individual SCs, retaining the green shading in Figure 3.1.

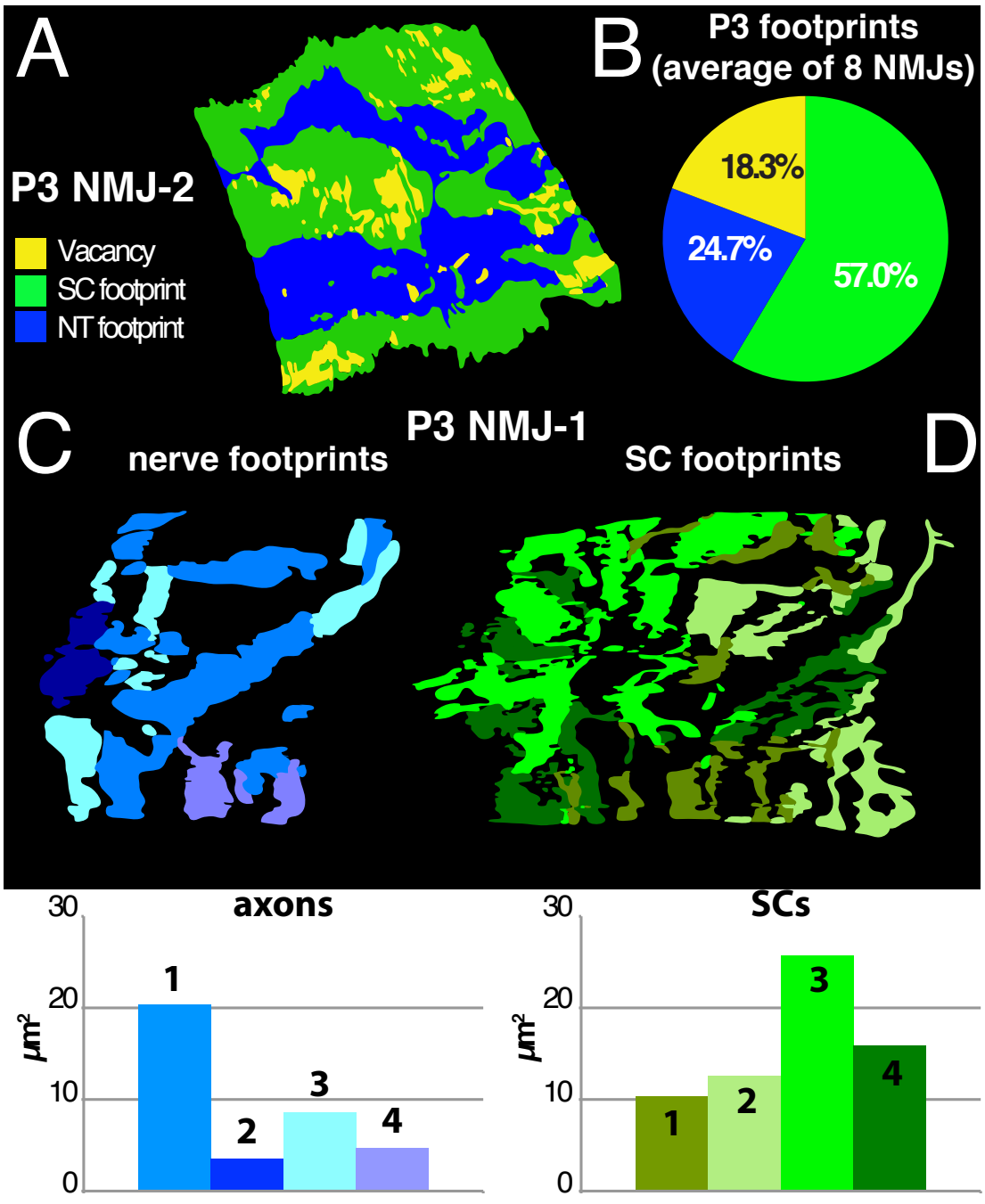

Figure 3.4: The nerve contact area within the AChR plaque is half that of the tSCs at P3. (A), The "footprint" (i.e., surface rendering of the sites on the muscle where any nerve (blue, nerve footprint) or SC (green, SC footprint) approaches within 50nmof the muscle surface at one NMJ (NMJ-2) at P3. Yellow areas represent vacancies. (B), The average fraction of the AChR plaque (i.e., the total area of the muscle covered by SC, nerve, and vacancies) contacted by each nerve (blue), the SCs (green), or a vacancy (yellow) at 8 P3 NMJs. (C), The footprints of individual axons at NMJ-1 and, below, the area of the footprint of each axon, retaining the blue shading in Figure 3.2. (D), The footprints of the 4 SCs at NMJ-1 and, below the area of the footprint of the individual SCs, retaining the green shading in Figure 3.2.

Collectively, these observations indicate that the effective synaptic area at neonatal NMJs is only a fraction of the overall receptor plaque on each multiply-innervated fiber. Even if as is presently thought, the competition during synapse elimination is for synaptic territory and the winning input comes to occupy all the territory of its competitors, much remains unexplained. Considering the P3 NMJs, if all the contacts present at this time become occupied by a single axon at the end of synapse elimination, the expected receptor pretzel with its contiguous gutters of receptors would not be the result (see, e.g., Figure 3.4 C). Comparing the axon footprints from P0 to P3 also suggests that, even as competition for territory occurs, there is growth in the synaptic contact area. However, even with increasing synaptic contact area of the axons, they still occupy an even smaller portion of the receptor plaque by P3. The more interesting result here may be that a considerable portion of what would be presumed to be the synapse from the fluorescent receptor labeling is unoccupied by the nerve during these early stages of development.

3.4 Terminal Schwann cells proliferate after birth and individual Schwann cells contact several terminal boutons

Light microscopic examination of NMJs using the transgenic labeling of SCs with GFP and AChRs with fluorescent α-BTX shows that tSCs proliferate at NMJs after birth (Figure 3.5). While P0 NMJs often have a single tSC (average 2, n= 20 NMJs), by P3 there are an average of 3 tSCs per NMJ (n=27 NMJs). This proliferation was confirmed by EM examination. As described above, these SCs extend to cover almost the entirety of the AChR plaque but very little beyond it. These observations are consistent with previous

reports (Brill et al., 2011) but provide very little information on the exact cellular relationships of the cellular elements here.

EM examination revealed an average of 1.3 tSC bodies (based on number of separate nuclei) at 10 P0 NMJs (range, 1-2), and an average of 3.4 cell bodies at 8 P3 NMJs (range, 2-5). On the basis of their location, above the synaptic site, and their close contact with the nerve, we are confident in identifying these cells as tSCs. In contrast to the cytoplasm of the axons and their terminals, these cells are more darkly stained and contain prominent Golgi apparatus and endoplasmic reticulum, features not present in the axons or their terminals (Figures 3.1 A, 3.2 A). Thus, as early as the day of birth, the innervation of the muscle is intimately associated with tSCs and their processes; it was rare to find any portions of the nerve uncovered.

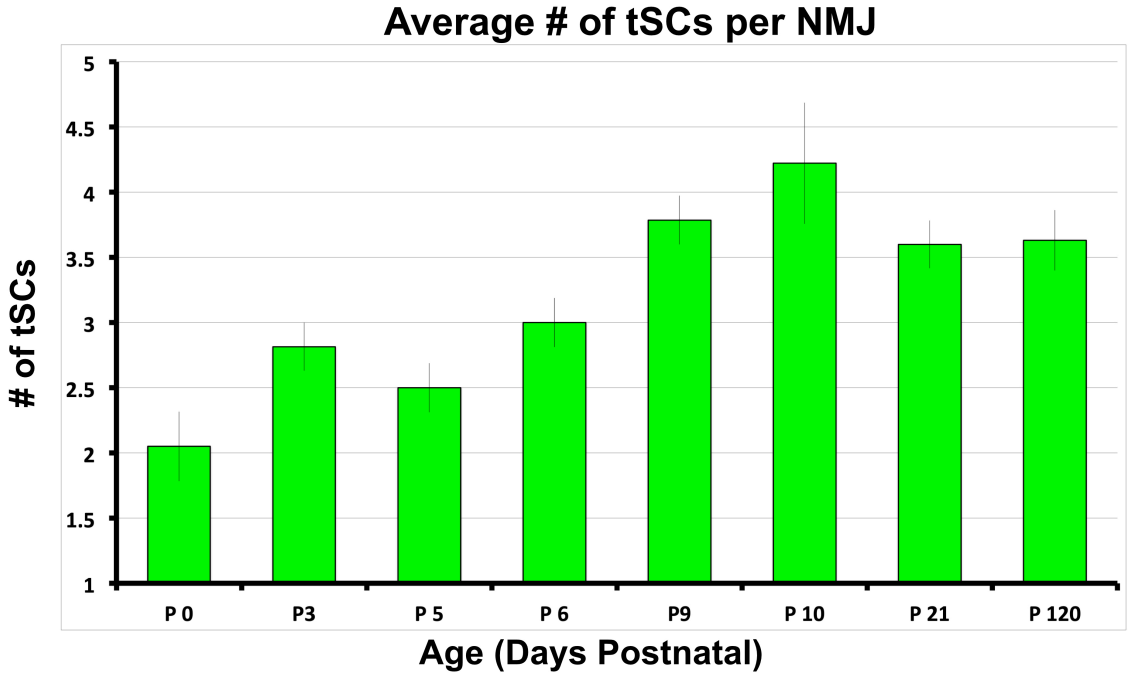

Figure 3.5: Light microscopy observations of terminal Schwann cells during synapse elimination. NMJs were labeled with fluorescently-conjugated btx in mice transgenic for GFP in tSCs and imaged at P0, P3, P5, P6, P9, P10, P21, and P120. Each NMJ was scored for number of terminal Schwann cells per NMJ at each time-point. Results were plotted to compare average tSCs per NMJ during postnatal development, showing that tSCs proliferate shortly after birth and maintain 3-4 tSCs per NMJ into adulthood. Variance shown as SEM.

Processes emerge from the somata of these cells and surround the individual axons as they enter the synaptic site and the small branches that lead to and between each axon terminal on the muscle surface. Each terminal is covered on its non-synaptic surface (Figures 3.1 A,B and 3.2 A,B). The contacts between the nerves and the Schwann cells and between Schwann cells themselves are very close. At P3, this was commonly on the order of 10-15 nm. This contrasts with the contacts between the nerve and the muscle, described above, and the SCs and muscle, described below that are 3-4 times as wide. The branching of processes from the tSCs are very complex. The close apposition of these processes, the fact that they fold back on themselves, and their sheer number make identifying the processes of individual cells difficult at P3 NMJs when multiple cells are present. As an illustration, we followed each of four contacts of a single SC onto the surface of the muscle back to the soma and found an average of 8.2 +/- 1.3 branch points along the way. At both P0 and P3 NMJs, each tSC abutted the terminal boutons and axons of more than one motor neuron (Figure 3.3, 3.4), as has been reported previously (Brill et al., 2011; Tapia et al., 2012). Indeed, at NMJs with multiple SCs at these early timepoints, there is little evidence of segregation ("tiling") of the processes of the individual SCs present at more mature junctions (Brill et al, 2011).

3.5 Terminal Schwann cells make extensive contact with the postsynaptic membrane at P0 and outstrip the contacts of axon terminals by P3

In every EM section of the NMJs at P0 and P3, we observed intimate contacts between the tSCs and the muscle fiber surface (Figures 3.1 A,B and 3.2 A,B). These SCs approached to within 50 nm of the muscle fiber surface, similar to the distance separating

the early nerve terminal contacts from the muscle surface. Often this close contact was maintained for a considerable distance, extending in some cases longer than 3.4 μm along the muscle fiber surface. The extent of this contact differs dramatically from the EMs of adult NMJs where the SCs are seen to cap the nerve terminals and primarily contact the muscle fiber only near the edges of the nerve terminals (Matthews-Bellinger and Salpeter, 1983; and see below). Others have previously commented on these Schwann cell contacts with the muscle surface in neonates (Korneliussen and Jansen, 1976; Rosenthal and Taraskevich, 1977; Tapia et al., 2012) and even shown by autoradiography using radiolabeled BTX that they occur at sites containing AChRs (Matthews-Bellinger and Salpeter 1983; Hesselmans, 1993). However, no quantitative assessment of these contacts has yet been made. In order to evaluate the extent of these tSCs contacts, we examined sets of aligned, serial electron micrographs at multiple postnatal time points.

The area of the muscle fiber surface contacted by tSCs (i.e., the "SC footprint") were reconstructed in software (Figure 3.3, 3.4). Surprisingly, we found that the tSCs contacted substantial portions of the postsynaptic membrane at P0, and made greater postsynaptic contact than the axon terminals by P3 (compare Figures 3.3 B, 3.4 B). Indeed, almost all the space in the plaque not occupied by the nerve was occupied by tSC contacts. Thus, the tSC footprint accounted for, on average, 31% of the plaque area at P0 and 57% at P3 (n=10 at P0 and n=8 at P3). In contrast, the axon footprint, accounted for 51.6% at P0 and 24.7% at P3 (Figure 3.3 B, 3.4 B). There were some places where the tSCs were located larger distances from the muscle fiber surface, and this surface was unoccupied by axon terminals; these sites we termed "vacancies" (first described in Chapter 2); accounting for 17.4% at P0 and 18.3% at P3, of the plaque area (Figure 3.3 B, 3.4 B). Each

of the tSCs present at each NMJ made these intimate contacts with the muscle fiber surface (Figure 3.4 D), and there was no obvious pattern in the way the terminal Schwann cells partitioned their contact of the plaque, when multiple cells were present.

That terminal Schwann cells are in such intimate contact with the areas on the muscle fiber surface, presumed to contain dense AChRs and, as inferred by other studies (Culican et al., 1998), with other synaptically enriched molecules associated with this plaque, suggests that axons, to expand their contacts, must displace tSCs from their contacts or only occupy territory abandoned by other axons. Considering this, it may be suggested that there is a form of competition between axons and tSCs for physical contact with the muscle fiber membrane within the developing AChR plaque during synapse elimination.

3.6 Terminal Schwann cells expand their postsynaptic contact after birth and extend fingers to intrude between axon terminals and the muscle fiber surface

As mentioned above, terminal Schwann cells increase their contact with the postsynaptic membrane, as they proliferate after birth. Given the evidence suggesting a competition between terminal Schwann cells and axon terminals for contact with the postsynaptic membrane, we examined the interfaces between axon terminals and Schwann cells. At ~ 60% of the axon terminal boutons of P3 NMJs, terminal Schwann cell processes were located between the axon terminal and the muscle fiber surface (Figure 3.6). These processes were in close proximity to the muscle fiber surface (52 +/- 1.2 nm) and closely associated with the axon terminal (17 +/- 0.5 nm). Because the basal lamina remains between these intruding processes and the muscle fiber surface, it appears that the tSCs

enter the synapse between the linkages of the nerve terminal membrane to the basal lamina. The average length of intruding processes was 730 nm, but these lengths were highly variable, with some being much shorter and some much longer.

Such glial processes have been proposed as a means of "synaptic stripping" at various sites within the nervous system. They do not represent extraordinary behavior of such cells: they are, for example, apparent during the early stages of degeneration of motor axon terminals after nerve section (Jirmanova' and Thesleff, 1972; Miledi and Slater, 1970). This glial behavior is also observed in central neurons whose peripherally projecting axons are severed (Ronnevi, 1978), and in autonomic ganglia in cases where the supply of trophic materials from the target is interrupted (Nja and Purves, 1978). Here we propose that these terminal Schwann cell processes are a sign of the early competition between motor axon terminals and the glial cells for contact with the muscle fiber surface. There appears to be something especially attractive about the surface of the neonatal endplate, as opposed to the rest of the muscle fiber surface. It may be the presence of AChR, because the light microscopic observations show that Schwann cells are coextensive in their coverage with the edge of the AChR plaque at these neonatal NMJs (Figure 3.2 E).

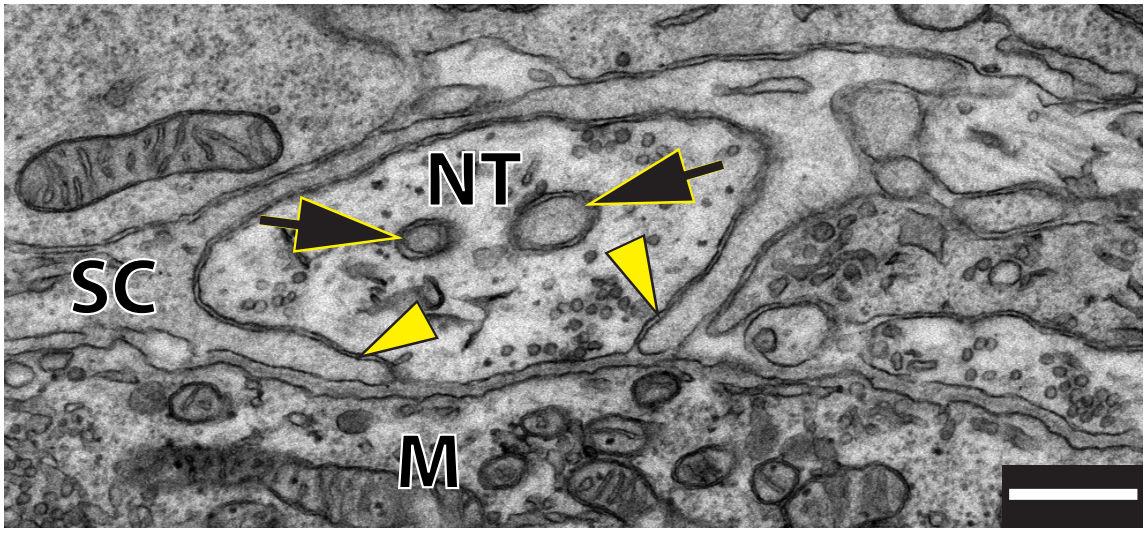

Figure 3.6. Example of Schwann cell fingers separating nerve terminal from muscle fibers. A single image from the same series as in Fig. 3 and in Movie S2. Black arrowheads mark fingers that intrude between the nerve terminal (NT) and the muscle (M). Basal lamina is still present between the Schwann cell (SC) and muscle.Black arrows mark the birfurcated Schwann cell finger within the nerve terminal. Scale bar, 500 nm.

3.7 Schwann cell occupancy of the synaptic site doubles between P0 and P3 while nerve occupancy is halved

Electron microscopy of random samples of NMJs early after birth has shown that nerve terminals abut each other on the muscle surface and has suggested that the arrival of SCs separates these nerve terminals from each other (Korneliussen and Jansen, 1976). If true, then one would predict dramatic changes in the occupancy of the synaptic site by axons and SCs during this period. We performed serial electron microscopy of 10 junctions at P0, reconstructed the axon terminals and SCs, and identified those portions that came within 50 nm of muscle surface in surface renderings, creating “footprints” of each (measured, as described above, as a percentage of the total area).We also measured the vacancies present. The number of axons present at each site fell slightly from P0 to P3: from an average of 5.4 at P0 (range, 3–9) to an average of 4.3 at P3 (range, 3–7). This is

fewer inputs than reported by Tapia et al. (2012) at P0, and the difference maybe explained by sampling. For example, our sample may have been biased toward smaller, secondary myotubes, whose fibers are generated and innervated later (Kelly and Zacks, 1969; Ontell et al., 1988). The critical observation is that the nerve terminal footprints at P0 were twice the size as those at P3 (51.6 +/- 4.7% at P0 vs 24.7 +/- 3.5% at P3). In contrast, the SC footprints at P3 were twice those at P0 (31.0 +/- 2.9% at P0 to 57.0 +/- 2.5% at P3). This shows that the relative nerve contact with the receptor plaque is halved during this period, whereas the SC footprint is doubled. The footprint of the vacancies did not change appreciably from P0 to P3 (P0 = 17.4 +/- 3.4%; P3=18.3 +/- 1.4%). This suggests that the SCs are increasing their contact with the synaptic site at the expense of the axons. Such a conclusion is true even if the total area of each type of contact is compared. Although there is a small increase in the area of the receptor plaque between P0 and P3 (~15%), this increase cannot by itself explain the shift in relative SC and nerve footprints. Computed as an actual area, the total nerve footprint declined (81.1 μm^2 to 44.2 μm^2), whereas the SC footprint increased (47.8 to102.0 μm^2) from P0 to P3. In the absence of time-lapse electron microscopy, this argues strongly for competition between the SCs and the nerve. The possibility that SCs merely occupy synaptic territories abandoned by the nerve seems unlikely, given the intrusive and phagocytic activities of these cells reported here and Chapter 2.

3.8 Schwann cells restrict their contacts with the muscle fiber as synapse elimination proceeds

Further evidence of continued remodeling comes from the examination of the disposition of tSCs at synapses at P7, P16, P19, and P40. The ratio of the axon footprint to the tSC footprint (i.e., the ratio of the muscle fiber surface contacted by the axon terminals to that contacted by the tSCs) changes from 3:2 at P0 to 1:3 at P3 to 3:2 at P7 to 1:1 at P16 to 2.5:1 at P19 to 4:1 at P40 (Figure 3.7). This change is not surprising given the ultimate restriction of tSCs at the NMJ to contact the surface of the axon terminals in the adult (Love and Thompson, 1998). In individual EMs, this is seen in tSC contacts with the surface of the muscle at P16 and P40 that, although diminished from those present at P3, still extend into areas beside axon contacts and in between the developing synaptic gutters (Figure 3.8). Suggestions that at least some of these contacts are with portions of the muscle surface still retaining AChR are obtained from examination of fluorescence micrographs where, at P16, SCs are more extensive at the sides of nerve contacts: these areas have a wider labeling of AChR than the axon terminals themselves. By P40, except those areas where axons and/or SCs run between synaptic gutters without contacting the muscle surface, there is mostly co-extensive labeling of tSCs, axon terminals , and AChR (Figure 3.8).

These observations suggest that the relative adhesiveness of tSCs for the muscle surface steadily decreases as that for the axon terminal itself becomes stronger. These observations also suggest that this restriction is not complete by the conclusion of synapse elimination. Whatever the mechanism of this restriction, it does not appear to involve the localization of the SC-repulsive molecule laminin-beta2, as this molecule is present in the

synaptic basal lamina at the time of extensive tSC contact with the synaptic surface (Figure 3.9). Although this laminin isoform is a major component of the synaptic basal lamina and suggests that wholesale remodeling of the basal lamina is not responsible for these tSC contacts, other laminin isoforms and other basal lamina proteins such as agrin cannot be ruled out for a role in this process.

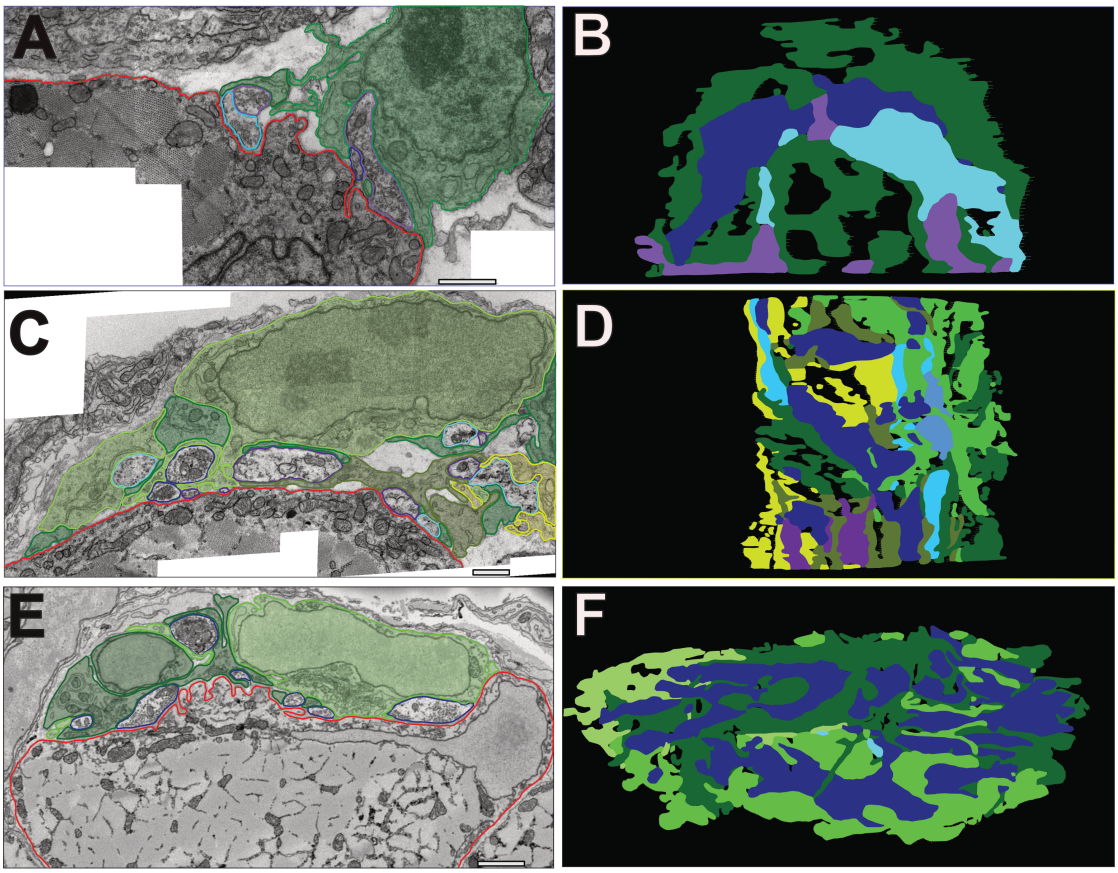

Figure 3.7: Postsynaptic coverage by Schwann cells during synapse elimination. Electron micrographs of NMJs from thin sections in sternomastoid at P0, P3, P7, and P19 (A, C, E, and G) with axon terminals (shades of blue), terminal Schwann cells (green) and muscle fibers (red) outlined on the micrographs. The axon terminals of the NMJs contain synaptic vesicles and come within ~50nm of the muscle fiber surface (red). Terminal Schwann cells (green) extend processes that come as close to the muscle fiber surface as the axon terminals and occupy large portions of the overall contacts with the muscle fiber. Corresponding surface models of contact sites on the postsynaptic muscle fibers made by axon terminals (shades of blue), Schwann cells (shades of green) and vacancies (black) (B, D, F, and H). Terminal Schwann cells proliferate from 1 per NMJ at P0 (A,B) to more than 3 by P3 (C,D). Terminal Schwann cell coverage of the endplate is intermingled early after proliferation (D) and becomes more segregated into maturity (F,H). Postsynaptic contact by terminal Schwann cells peaks during the first postnatal week and remains elevated throughout the period of synapse elimination (I). Scale bars (1µm).

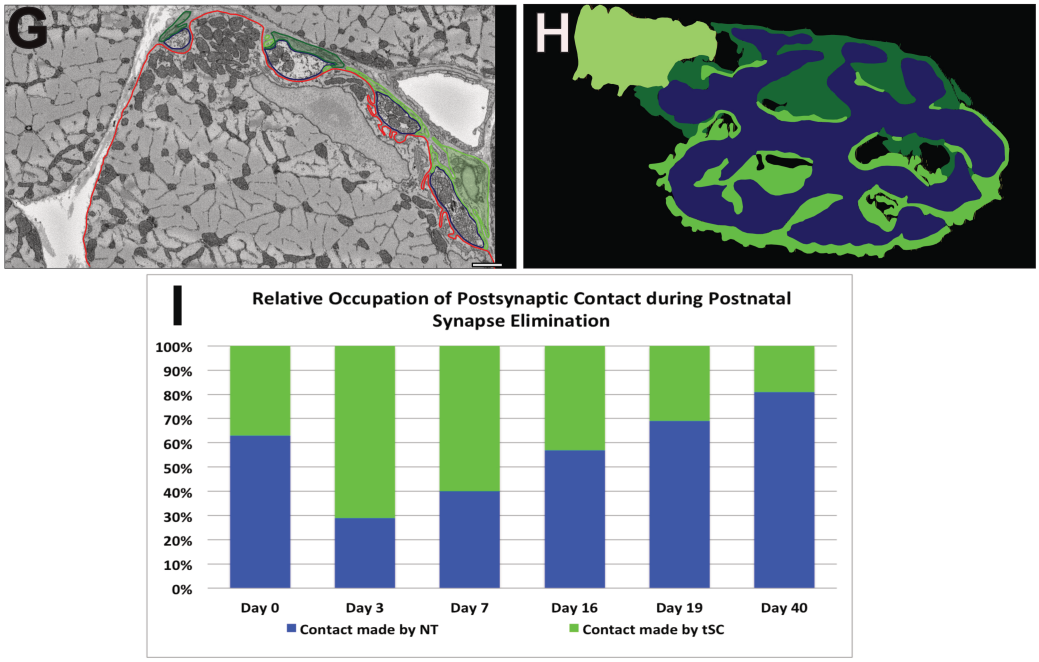

Figure 3.7 Continued

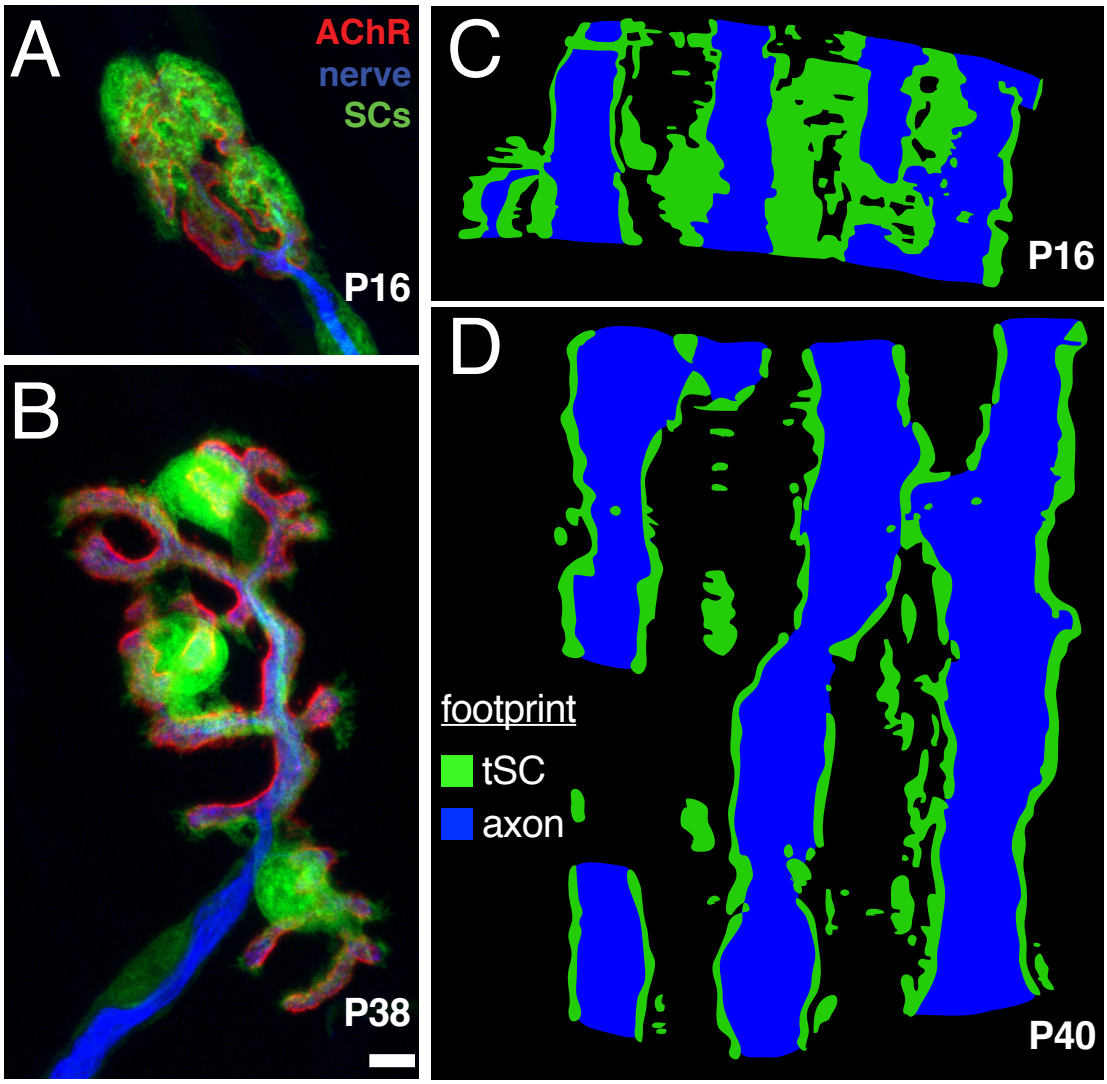

Figure 3.8: tSCs slowly relinquish contact with the muscle and confine their contacts to the nerve terminals. A,B, Fluorescence micrographs of en face views of NMJs labeled with S100-GFP (green) for SCs, antibodies to neurofilament and SV2 (blue) for nerves, and fluorescent BTX (red) for AChRs at P16 and P40, respectively. As the junctions mature, SC processes become largely confined to covering the nerve terminal branches. C, D, Renderings from EMs of the surface of the muscle and the areas contacted by nerve (blue) and SCs (green) (i.e., the nerve and SC footprints) at P16 and P40. The portion of the muscle contacted by the SCs steady diminishes. Coverage of the nerve by SC is not shown here. E, Scale bar, 5μm.

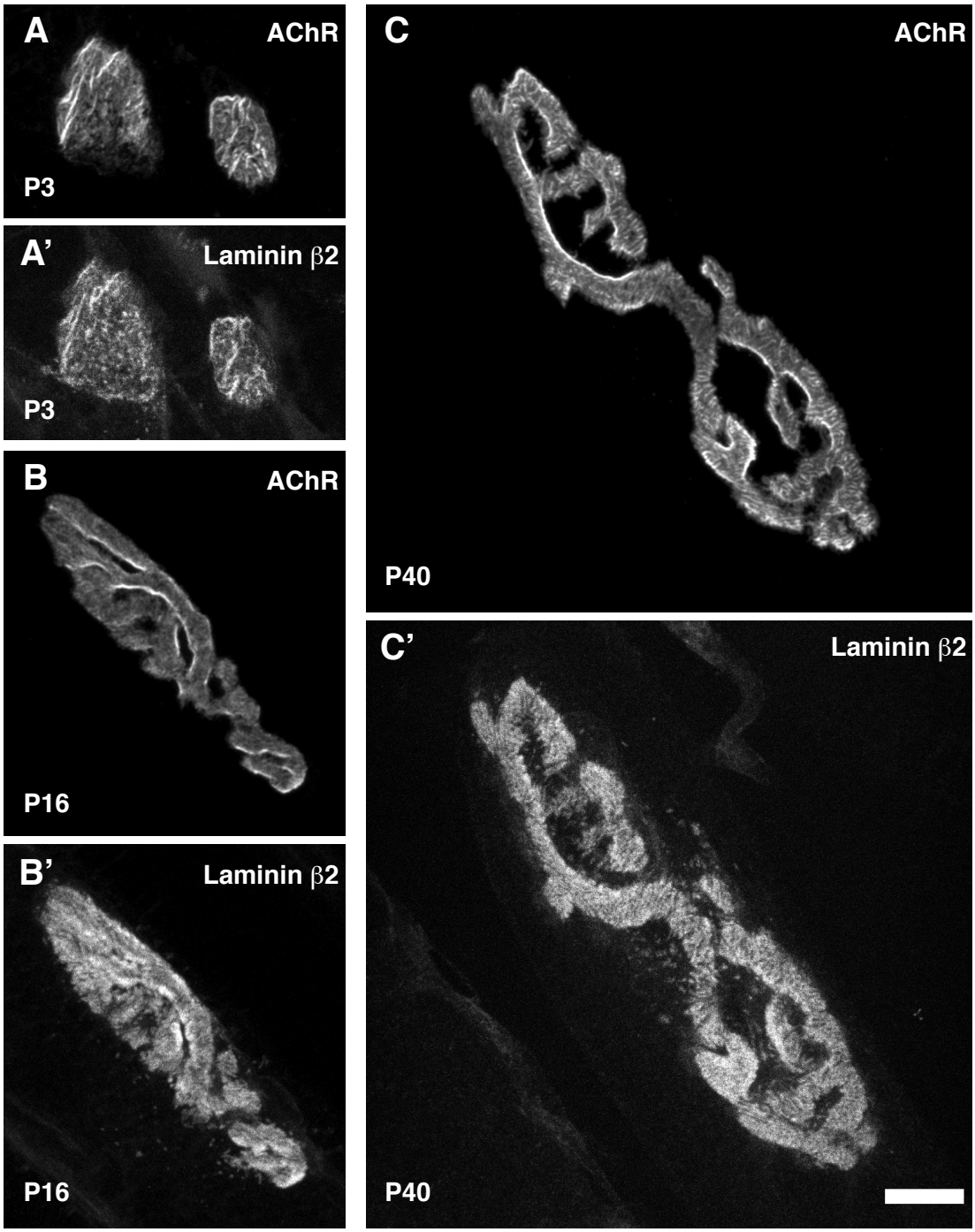

Figure 3.9: Laminin-β2 chain is concentrated at the NMJ during synapse elimination. AChR labeling at P3 (A), P16 (B), P40 (C). Laminin staining at P3 (A'), P16 (B'), and P40 (C'). Scale bar 10μm.

3.9 Discussion

Our experiments document novel behaviors of tSCs at NMJs that have major implications for the roles these cells play in sculpting synapses during development. These roles are illustrated in summary form in Figure 3.10.

Our experiments show that SCs compete with nerve terminals for contact with the AChR-rich area on the surface of the muscle fiber (Fig. 3.10 A-G). This competition is demonstrated by several observations. The SCs contact receptor rich membrane because their occupancy of the endplate site far exceeds that of any discontinuities in the receptors, and in the Ems they appose the muscle surface as close as do the nerve terminals. Although there have been few incidental reports of this relationship at developing junctions studied by EM (Matthews-Bellinger and Salpeter, 1983, Tapia et al., 2012), our study constitutes the first thorough analysis of this tSC apposition at the synaptic site. We show that such apposition is quite substantial, even outstripping that of the nerve terminals themselves by P3. This observation was unexpected, as the contacts of the SCs at the adult NMJ are confined to the nonsynaptic surface of the nerve terminals and at the edges of the nerve terminals (Sanes and Lichtman, 2001). Indeed, these contacts in neonates (separated from the muscle surface by ~50nm) would be impossible to demonstrate with even confocal microscopy given resolution limits. In the act of making contact with the muscle surface, the SCs appear to be displacing the nerve terminals. This is clearly shown by comparing the apposition of the nerves and SCs in the developing endplate: the apposition of the SCs increases from P0 to P3, whereas that of the nerve decreases. This change fits previous EM descriptions of early NMJs that have shown that SC processes penetrate to separate a set of nerve terminals that initially abut each other on the muscle surface (Korneliussen and

Jansen, 1976). Last we observe many instances of SC fingers intruding between the nerve terminals and the muscle fiber, reminiscent of the reports of so-called “synaptic stripping” by glial cells, particularly in cases of axotomy-induced chromatolysis of neurons (Ronnevi, 1978). By preventing postsynaptic action of transmitter at these sites, SCs could be ultimately driving the AChR turnover here. Furthermore, our experiments suggest that the behavior of the SCs at the synapse resemble those of SCs known to occur during peripheral nerve development. Here axons extend into the periphery as naked bundles; the SCs migrate along these nerves, proliferate, and extend processes into the nerve bundles to separate and wrap the individual axons (Peters and Muir, 1959).

The results here strongly suggest the apposition to the muscle fiber membrane by tSCs is at sites of AChR, the level of resolution at the light microscopy level cannot say this for certain. Obvious next steps would be to determine whether tSCs are in fact in direct apposition to AChRs in the postsynaptic membrane using electron microscopy. It is also understood that the AChR staining of the endplate changes drastically during this period (discussed in chapter 1). Labeling AChR for examination under the electron microscope would also allow assessment of any potential differences in AChR staining based on the synaptic footprint of axon terminals, tSCs, and vacancies as we have hypothesized in Figure 3.10.

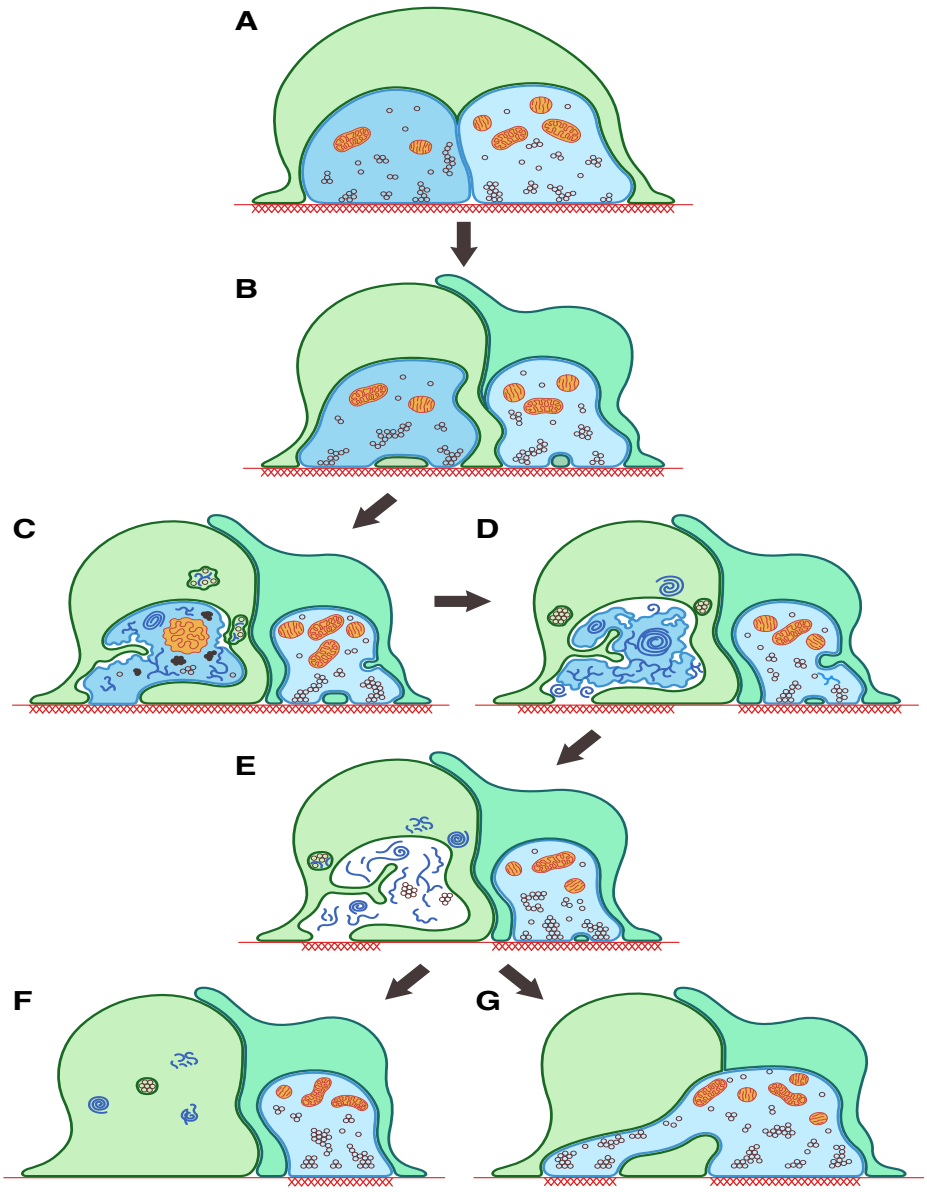

Figure 3.10: tSCs drive postnatal synapse elimination. Summary of findings and their relevance to postnatal synapse elimination at the NMJ. Two different axons (shades of blue) and SCs (shades of green) are depicted at sites where the muscle membrane has a high density of AChRs (red thatching). At the earliest stage shown (A), near the time of birth, several axons (in this case, 2 for simplicity) contact each site in the muscle. The SC(s) arrive after the nerves and initially just cover the nerve terminals. As development proceeds, the tSCs engage in two activities that result in the loss of polyneuronal innervation: (1) They compete with the axons for contact with AChRs, sending processes between and separating the nerve terminals and between the nerve terminals and the muscle fiber (B–E). This eventually results in remodeling (loss) of AChRs at those sites in contact with SCs and that receive no neurotransmitter. (2) They phagocytose and remove axonal boutons in synaptic contact with the muscle; the debris is consumed by SCs as well as left behind in vacancies on the muscle membrane (B–E). This phagocytic attack is directed at all terminals and stochastically results in the destruction of some terminal contacts and creation of vacancies above regions with AChR. At least in some cases, these vacancies are filled on a stochastic basis by terminals of nearby neurons (G). In other cases, these vacancies remain nonsynaptic (F). Artwork courtesy of B. Colyear after a drawing by I.W.S

3.10 Methods

Wild-type C57B/6 mice of either sex, obtained from The Jackson Laboratory and bred in a colony at the University of Texas and Texas A&M University, were killed on postnatal day 0 (P0), P3, P5, P6, P7, P10, P16, P19, P21, or P38-P40 by intraperitoneal injection of Euthasol (Virbac Animal Health). Experimental procedures were approved by the University of Texas and Texas A&M University Institutional Animal Care and Use Committee.

Animals were perfused transcardially with 0.1 M sodium cacodylate buffer, pH 7.4, followed by the same buffer containing 2% PFA and 3% glutaraldehyde. Sternomastoid muscles were removed and fixed overnight at room temperature in the same fixative. Muscles were washed with cacodylate buffer and stained en bloc in 1% osmium tetroxide, 1% ferrocyanide in cacodylate buffer for 5 h, washed with water, and then stained in 1% aqueous uranyl acetate for 2 h. Muscles were dehydrated in graded alcohols and acetone, then embedded in Epon 812. Regions containing neuromuscular junctions were located by thick (0.5–1 μm) sections made on a Leica Ultracut UTC Ultramicrotome with glass knives, stained with 1% toluidine blue, and examined under a light microscope. Blocks were further trimmed using a 45 degree cryotrim tool (Diatome) and serial 65 nm (silver) sections cut with a 35 degree diamond knife (Diatome). Sections were mounted on formvarcoated Synaptek slot grids (Electron Microscopy Sciences) and observed under a FEI Technai Spirit electron microscope with an AMT Advantage HR digital camera. NMJs were identified by the apposition of nerve terminals to within ~50 nm of the muscle fiber surface in the presence of SCs. Digital images of individual NMJs and the immediately surrounding area were captured from each section at a magnification of 16,500. At this

magnification, ~6–12 overlapping images were acquired to include the entire extent of the NMJ. These individual images were then montaged by manual manipulation in Adobe Photoshop to create a single image. Such montaged images over 70–150 serial sections were then imported into the software program Reconstruct (Fiala, 2005), calibrating the pixel dimensions in the images to known distances in the specimen. In software, the montage in each section was aligned linearly to each adjacent montage using 6–8 objects common in both and starting with the central montage in the stack and working toward each the first and last montage. Once aligned, structures of interest in each section were segmented(traced) using the tools provided in the software. Measurements and 3D renderings of these structures were thengenerated in software.

Tissues of the mice at the seventh postnatal day (P7) and P19 were prepared differently and imaged using serial-block-face scanning electron microscopy (SBSEM). Tissue preparation and staining was done with compliance to Renovo Neural Inc. (Cleveland, OH). Briefly, P7 C57/Bl6 mice were transcardially perfused with 2.5% glutaraldehyde and 4% paraformaldehyde in a 0.1M sodium cacodylate buffer. Sternomastoid muscles were then removed and stored in perfusion solution for 1 day prior to staining. Tissue was then stained with uranyl acetate and osmium-ferrocyanide, followed by graded-dehydration and embedded in Epon resin. SBSEM image data sets of postnatal day 7 NMJs were acquired at Renovo Neural Inc. (Cleveland, OH). A sample image is shown in figure 1e. The tissue blocks were mounted, examined, and sectioned in a Zeiss Sigma VP scanning electron micro-scope equipped with a Gatan 3View in-chamber ultra-microtome stage with low-kV backscattered electron detectors optimized for 3View systems. NMJs were initially identified within cross-sections of muscle tissue by axon

terminals in direct apposition to junctional folds on the muscle fiber membrane and capped by terminal Schwann cells. Regions of interest were chosen to include the NMJs in whole cross-section. The first sample block was sectioned cross-sectionally along the long axis of the muscle fibers. A series of 465 EM images in a field size of 130 μm × 50 μm were acquired at 2.2 kV with a resolution of 8.1 nm per pixel and 90 nm per slice. Eight NMJs were captured at P7 with 5 of those NMJs fully reconstructed for synaptic contact areas as described previously for data sets acquired with traditional serial TEM 2 NMJs at P19 were processed similaraly.

In total, we made extensive serial sections from a total of 10 NMJs at P0, 8 at P3, 6 at P7, 2 at P16, and 4 at P40. One P3 muscle provided all 8 NMJs, although two other animals were used to provide 40 semiserial or nonserial sections to confirm the observations made in the serial sections. Of the 8 serially sectioned P3 junctions, 1 (NMJ1) has been completely reconstructed for all parameters reported here, 5 (NMJs 2, 3, 4, 7, and 8) have been completely reconstructed, except that their SCs were not individually identified, and 2 have been partially reconstructed (NMJs 5 and 6). Two animals were used for the serially sectioned P16 muscles; an additional 2 short serials and 10 nonserial sections were made. At P40, 3 animals were used and the four NMJs had between 54 and 231 sections, and approximately a dozen individual sections were made.

Fluorescent labeling of NMJs was performed as described previously (Hayworth et al., 2006, Kang et al., 2007, Lee et al., 2011). Briefly, C57B/6 mice carrying an S100-GFP transgene (to fluorescently label SCs) were anesthetized as described above and transcardially perfused with PBS, pH 7.4. Sternomastoid muscles were dissected and fixed with 4% PFA, pH 7.4, then blocked and permeabilized with a blocking solution (0.2%

BSA-fraction 5, 0.3% Triton X-100, 0.1% NaN3). Presynaptic nerve terminals were labeled with a mouse antineurofilament antibody (2H3; Developmental Studies Hybridoma Bank) and an antibody against a vesicular protein: SV2 (Developmental Studies Hybridoma Bank) or synaptophysin (Invitrogen). AChR-rich plaques were identified using a fluorochrome-conjugated alpha-BTX (Invitrogen). The acquisition of confocal fluorescence images of neuromuscular junctions was performed on a Leica TCS SP5 upright microscope using Leica LAS AF image acquisition software with a 63x oil-immersion objective with a NA of 1.4. Maximum intensity projections and orthogonal slices of image stacks were generated using ImageJ. The presence of tSC somata not in contact with the postsynaptic surface and the curvature of the postsynaptic muscle fiber prevented an accurate measurement of tSC apposition to the AChR-rich portion of muscle membrane through en face views. In attempt to improve our ability to resolve this apposition, we made orthogonal, virtual sections in both the XZ and YZ planes through confocal z stacks near the center of the synapse. Portions of AChR-rich membrane apposed by tSCs and their processes and the lengths of tSC

process that overshoot the postsynaptic surface were measured using iVision software (BioVision Technologies) and computed as a percentage of length of the AChR-positive membrane and found to be 98.1 +/- 0.4% and 4.5 +/- 0.5%, respectively. A total of 46 NMJs from 5 pups were examined in this fashion.

Numerical data are reported as mean +/- SE.

CHAPTER IV

SYNAPTIC FOOTPRINT CONTACTS OF AXON TERMINALS, TERMINAL SCHWANN CELLS, AND VACANCIES SHOW DIFFERENTIAL ACHR STAINING INTENSITY IN THE POSTSYNAPTIC MEMBRANE OF DEVELOPING ENDPLATES

4.1 Introduction

It is well established that each neuromuscular junction (NMJ) of neonatal rodents and other mammals undergoes tremendous remodeling during early postnatal development. Remodeling occurs through the process of synapse elimination, where many of the motor axon inputs to the muscle fibers that are initially established during early development are eliminated (Redfern, 1970; Brown et al., 1976; Balice-Gordon and Thompson, 1988; Tapia et al., 2012). Despite this, the mechanisms that contribute to synapse elimination remain incompletely understood. Recent studies reveal an important role for glial cells, both in muscle and the central nervous system, where elimination is critical for establishing functional neural connectivity in the adult (Awasaki et al., 2004; Song et al., 2008; Fuentes-Medel et al., 2009; Paolicelli et al., 2011; Schafer et al., 2012; Smith et al., 2013). Indeed, the studies from the previous two chapters explain two novel behaviors of terminal Schwann cells (tSCs) that contribute to the process of synapse elimination. First, tSCs prune presynaptic axons and their terminals, contributing to the progressive elimination of inputs in order to achieve singly-innervated NMJs (Smith et al., 2013). Second, tSCs proliferate and extend processes to cover considerable portions of the

postsynaptic membrane, appearing to compete with axon terminals for occupation of the AChR-rich postsynaptic membrane during the period of synapse elimination (Smith et al., 2013).

Although the transition from poly- to single-innervation is a major aspect of the process of synapse elimination, the remodeling is not limited to the presynaptic motor axons. During this period there is also considerable change in the morphology of the AChR patterning in the postsynaptic membrane (Marques et al., 2000) (see figure 4.1).

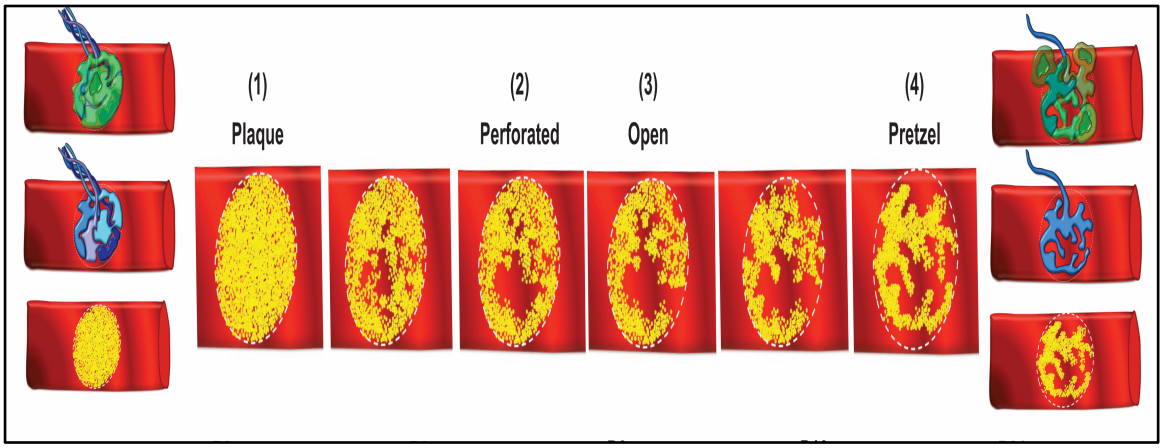

Figure 4.1: Schematic summary of morphological changes at NMJs during synapse elimination. Motor axons shown in shades of blue, muscle fiber in red, terminal Schwann cells green, AChR yellow. All NMJs begin with a plaque-like aggregation of AChR (bottom left) contacted by multiple motor axons (middle left) and a single terminal Schwann cell (top left). Throughout the period of synapse elimination redundant motor axons are eliminated to yield a single motor axon (middle right), terminal Schwann cells proliferate having multiple at adult NMJs (top right) and the AChR morphology is remodeled from plaque to pretzel (bottom right). The initial AChR plaque is remodeled to resemble an intricate pretzel-like configuration during this period as receptors are lost from the postsynaptic membrane in a series of perforations that typically begin at the center of the plaque and accumulate outward (middle series).

It is possible that the behavior of tSCs during the period of synapse elimination, as they proliferate and extend processes covering the postsynaptic membrane, may contribute to the remodeling of the postsynaptic receptor expression (see Figure 3.10). At adult NMJs, Schwann cells occupy the space above the nerve terminal branches, covering the sides not apposed to the muscle fiber surface with their processes (reviewed in Sanes and

Lichtman, 1999). Experimental manipulations suggest that adult tSCs can be induced to intrude between the postsynaptic muscle fiber and the nerve terminal, apparently leading to the abandonment of these portions of the NMJ (Lee et al., 2016). In chapters 2 and 3, I described similar behaviors by tSCs during the period of synapse elimination. The phagocytic removal of axon terminals by tSCs certainly can account for portions of the synapse to be abandoned. Moreover, the extensive contact of tSCs with the postsynaptic membrane, especially at sites where they intrude between axon terminals and the muscle fiber, could contribute to synaptic abandonment through loss of AChR expression (Smith et al., 2013). One drawback of these studies was the lack of knowledge regarding where the AChR were precisely located. Presence of receptors beneath Schwann cell contacts would suggest the possibility that the contacts observed were present at functionally capable sites on the muscle fiber surface. Thus, tSC occupation of these sites, rather than axon terminals, could account for their loss, rather than being silenced by other means.

In this study, I used the electron dense label of horseradish peroxidase (HRP) to mark the location of AChR and combined this with serial electron microscopy of neonatal mouse NMJs. In doing so we have made 3 principle findings: (1) Terminal Schwann cells make extensive close-contacts with the muscle fiber endplate almost exclusively at sites where there is a high density of AChR. (2) AChR remain, at least transiently, at sites that have no axon terminal but are occupied by tSCs. (3) Regions unoccupied by either tSCs or axon terminals, “vacancies”, also possess AChR. These observations suggest, at the very least, interactions between tSCs and AChR (or some component associated with the AChR). Finally, these observations also show that loss of AChR from portions of the

muscle fiber membrane is not a necessary requirement for loss of axon terminals of motor inputs during the period of synapse elimination.

4.2 **Terminal Schwann cell proliferation and extension of postsynaptic coverage occurs simultaneously with postsynaptic remodeling of AChR**

In chapter 3, I show that there is proliferation and expansion of postsynaptic contact made by terminal Schwann cells during the period of synapse elimination. This expansive behavior by tSCs occurs simultaneously during the period of postsynaptic AChR remodeling described in previous reports (Marques et al., 2000). Changes in AChR patterning are described to follow a typical progression, transitioning from the intial plaque of receptors observed at birth, to a fine pretzel pattern in the adult (Marques et al., 2000) (Schematic shown in Figure 4.1; 1. Plaque, 2. Perforated Plaque, 3. Open, 4. Pretzel). The transition from plaque to pretzel occurs through a series of perforations in the initial AChR plaque. While loss of AChR have been correlated with axon terminal loss during synapse elimination (Balice-Gordon and Lichtman, 1994), the role of tSCs have not been examined.

tSC proliferation and coverage of AChR were examined with light microscopy during the period of synapse elimination. Using transgenic mice that express green fluorescent protein in Schwann cells (S-100 eGFP), we labeled the postsynaptic AChR with fluorescently-conjugated α-btx. NMJs were measured for AChR area (μm^2), terminal Schwann cell coverage area (μm^2), and analyzed for degree of overlap between the two (Table 4.1).

Age (Days Postnatal)	Avg. AChR Area (μm²)	Avg. tSC Area (μm²)	% Area Overlap
0 (n=13)	88.84 +/- 32.77	103.03 +/- 29.94	84.54%
3 (n=6)	86.74 +/- 18.16	111.11 +/- 26.42	78.78%
5 (n=10)	192.09 +/- 47.90	210.95 +/- 56.39	91.67%
6 (n=4)	283.07 +/- 90.30	299.71 +/- 80.57	93.41%
9 (n=4)	269.16 +/- 81.01	346.77 +/- 140.77	80.36%
10 (n=11)	271.42 +/- 82.40	324.15 +/- 109.30	86.92%
21 (n=5)	331.83 +/- 43.42	374.59 +/- 40.12	88.58%

Table 4.1: Comparison of coverage area of AChR and tSC from fluorescence microscopy. Average surface area of AChR and tSC coverage at developing NMJs throughout the period of synapse elimination and degree of overlap between labels (shown as percentage). Error shown as standard deviation.

Additionally, we characterized the number of Schwann cells per NMJ and the stage of AChR morphology at 140 NMJs throughout the period of synapse elimination. NMJs were imaged from the day of birth (P0) to roughly 4 months (P120) (P0 n=20, P3 n=27, P5 n=8, P6 n=23, P9 n=14, P10 n= 9, P21 n= 20, P120 n=19). This analysis shows that NMJs undergo proliferation of terminal Schwann cells while simultaneously transforming from plaque to pretzel during the period of synapse elimination (Figure 4.2).

During the transition of AChR morphology and tSC proliferation, the coverage areas of tSC and AChR labeling maintained close association, overlapping by more than 86% on average throughout the period of synapse elimination (P0-P21). This is in agreement with previous observations of greater than 96% co-extensive coverage at postnatal day 3 from confocal analysis (see Figure 3.2 E). Virtual slices through NMJs at P3 imaged with confocal microscopy suggested that the tSC contact with the muscle fiber observed in electron micrographs were indeed in direct contact with AChR-rich regions of the muscle fiber membrane labeled with fluorescently-conjugated α-btx (See Figure 3.2 E).

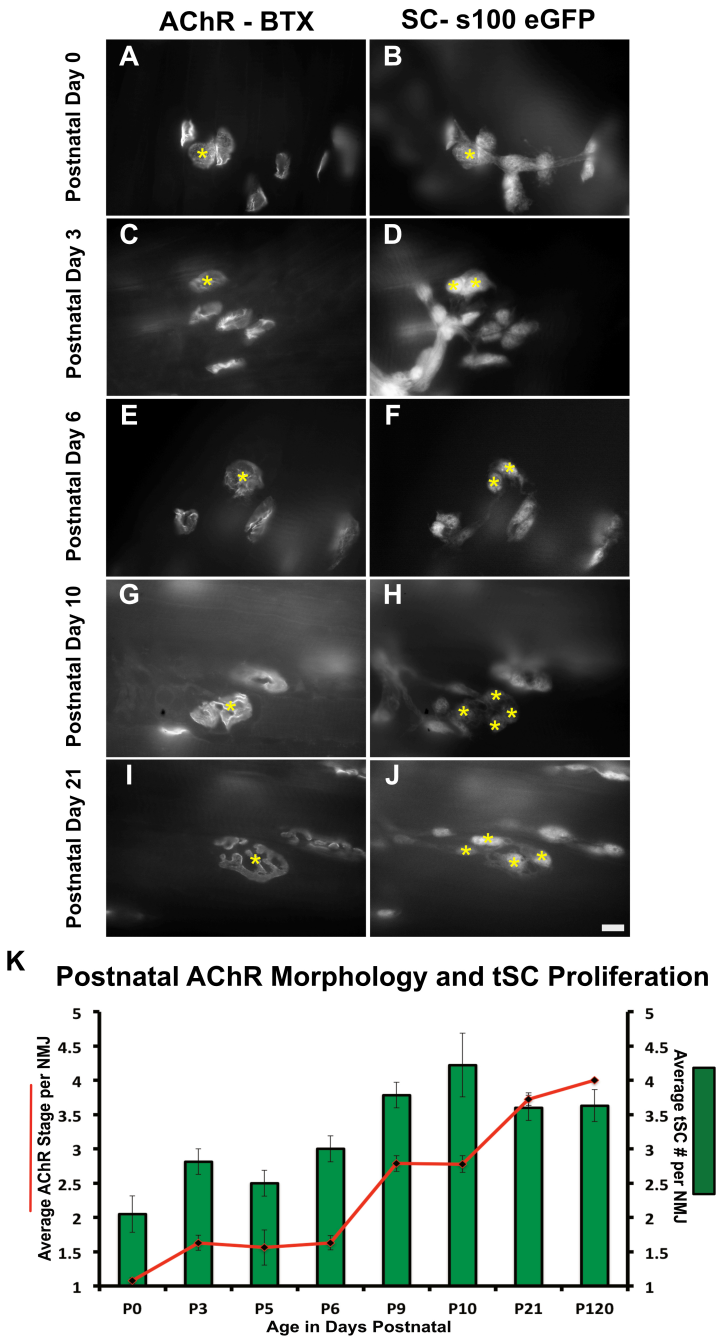

Figure 4.2: Light microscopy observations of AChR morphology and terminal Schwann cell proliferation during synapse elimination. NMJs were labeled with both fluorescently-conjugated btx (A,C,E,G, I) and terminal Schwann cells (B,D,F,H, J) and imaged at P0, P3, P5, P6, P9, P10, P21, and P120. Each NMJ was scored for AChR morphology stage (1= plaque, 2= perforated, 3= open, 4= pretzel) and number of terminal Schwann cells per NMJ at each time-point. Light microscopy observations indicate NMJs begin with a single terminal Schwann cell at birth (B) and proliferate by P3 (D). Most NMJs show perforated AChR by the end of the second postnatal week as shown at P10 (G). Pretzel-like morphology of AChR becomes more prominent by the 3rd week when synapse elimination is largely finished (I). (K) Plot of AChR morphology progression (red line indicates average stage at each time-point, left vertical axis) positively correlates with proliferation of terminal Schwann cells (average number of tSC per timepoint shown by green bars, right vertical axis) during this period. Images aken at 63x magnification, scale 10μm.

4.3 Terminal Schwann cells contact the muscle fiber surface almost exclusively at sites of high-density AChR expression during synapse elimination

In order to determine if tSCs were in direct contact with AChR, electron microscopy imaging was required. AChR were labeled at sternomastoid NMJs in neonates (P4) and adults using biotinylated-btx conjugated to neuravidin-horseradish peroxidase (HRP) and applied DAB-peroxidase solution (Schematic of labeling method in Figure 4.3 A). The resulting electron-dense reaction product strongly demarcated AChR in the muscle fiber membrane. NMJs were located by dark staining of AChR following peroxidase reaction under the light microscope (Figure 4.3 B) and then imaged with electron microscopy showing precise location of AChR in the muscle fiber membrane such as at the adult sternomastoid NMJ shown in Figure 4.3 C.

In addition to imaging adult NMJs, several P4 (n=6) NMJs were imaged with semi-serial or serial electron microscopy (Figure 4.4), with 2 different P4 NMJs serially sectioned, imaged, and reconstructed manually in software (Fiala et al., 2005). Analysis of P4 NMJs showed a plaque-like AChR morphology with even, dense staining along the length of the postsynaptic membrane opposite tSCs and axon terminals of the NMJ (Figure 4.4 and 4.5). Indeed, regions of tSC contacts with the muscle fiber surface were almost exclusively at sites of AChR labeling at all P4 NMJs (Figure 4.5). Analysis of staining in EMs indicates consistent correlation with tSC coverage of the postsynaptic membrane and expression of the AChR on the muscle fiber surface (~96% on average). Furthermore, regions contacted by tSCs were significantly elevated in AChR staining intensity than non-synaptic regions of the muscle fiber membrane (Figure 4.6 and 4.7). Thus, tSCs occupy a considerable portion of the available AChR-rich membrane during synapse elimination.

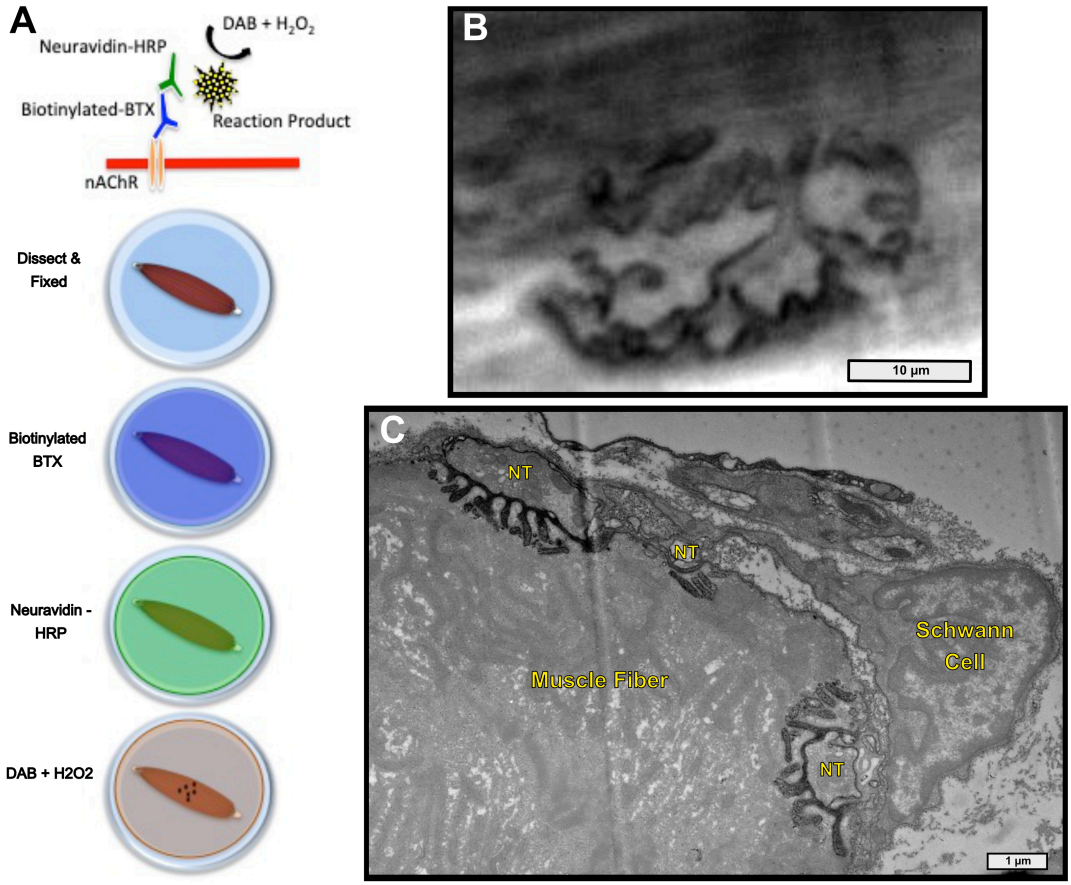

Figure 4.3: Labeling AChR at neonatal and adult NMJs for immuno-electron microscopy. (A) Schematic representation of AChR labeling protocol for imaging with electron microscopy. Muscles were dissected and fixed in a dish, labeled with biotinylated-btx conjugated to neutravidin-HRP and finally reacted with DAB-peroxidase solution to generate electron dense labeling of AChR visible in under the electron microscope. (B) Light micrograph of adult NMJ after HRP-DAB reaction, AChR staining was confirmed by dark reaction product at the endplate and location of NMJs noted prior to processing for electron microscopy. (C) Electron micrograph from thin section of adult sternomastoid NMJ showing AChR labeling at synaptic sites (dark label) occupied by nerve terminals (NT). B, light micrograph taken at 20x scale bar 10µm. C, electron micrograph taken at 7.5kx, scale bar 1µm.

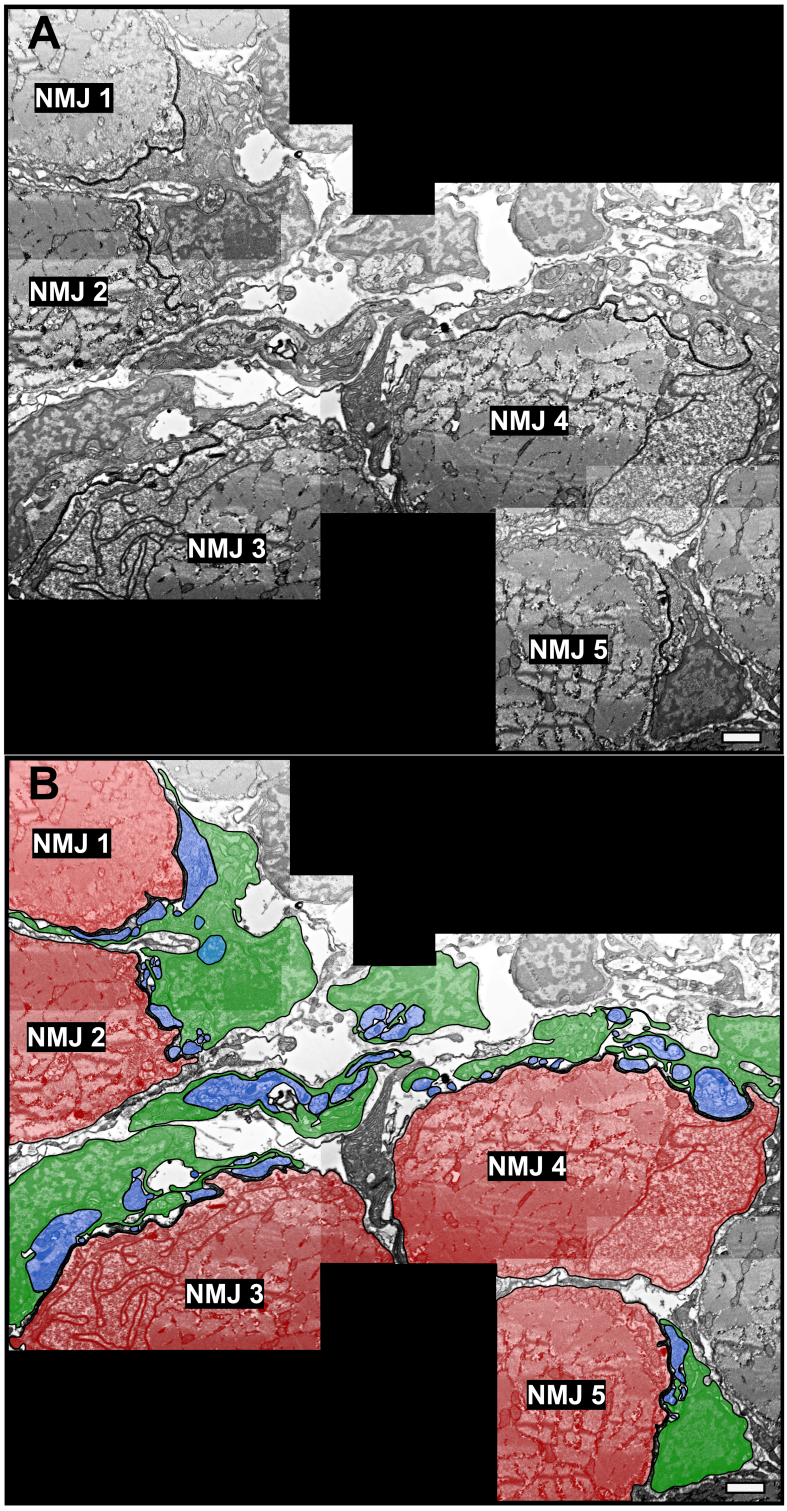

Figure 4.4: AChR staining is plaque-like and coextensive with Schwann cell coverage at postnatal day 4 sternomastoid NMJs. (A) Montage of electron micrographs at P4 showing uniform staining of AChR in postsynaptic membrane at 5 different NMJs (dark label in synaptic cleft). (B) Same montage of electron micrographs with axons and terminal arborizations (blue), terminal Schwann cells (green) and muscle fibers (red) outlined to show co-extensive coverage of AChR. Images taken at 7.5kx, scale bar 1µm.

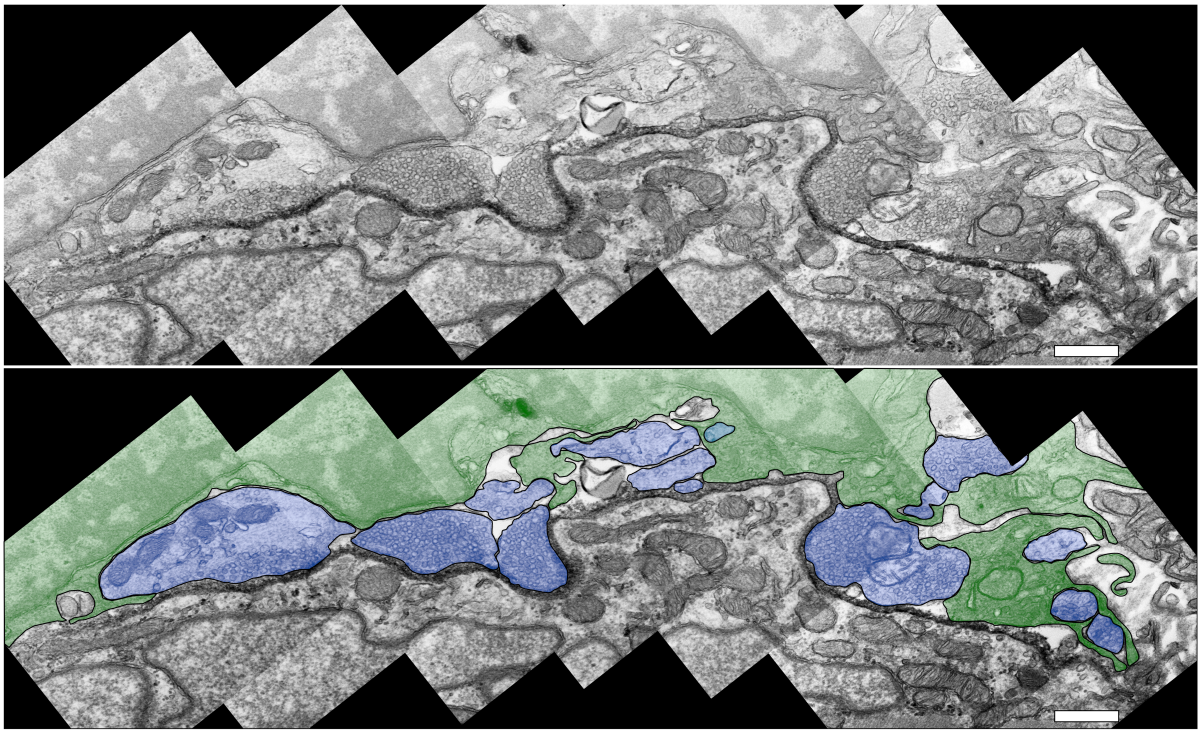

Figure 4.5: High magnification example of AChR labeling at an NMJ from P4 sternomastoid. Terminal Schwann cells shaded green and axon terminals shaded blue. AChR labeling is intense throughout contacts of both axon terminals and terminal Schwann cells. Images taken with TEM at 30kX. Scale bar 500nm.

4.4 Terminal Schwann cell coverage of AChR is transient to the period of synapse elimination

Imaging and analysis of the AChR labeling at P4 NMJs indicates that more than 50% of the AChR-rich membrane is occupied by tSC contacts at this time. My previous serial EM data sets indicate that the extensive postsynaptic contact by tSCs is transient to the period of synapse elimination. However, in adults, axon terminals occupy more than 80% of the postsynaptic coverage (see Figure 3.7). Given this change, I wondered if the AChRs were lost from sites previously occupied by tSCs by examining their labeling profile at adult NMJs. At adult NMJs, I observed much less uniform staining density of

receptors than at P4 NMJs and the degree of contact made by tSCs was greatly reduced, consistent with previous data series (Figure 4.7).

In the electron micrographs of adult NMJs labeled for AChR, staining was confined primarily to the regions contacted by the axon terminals (Figure 4.7 and 4.8). Although the sites of contact by tSCs showed some elevated staining intensities, these contact sites extended minutely into the regions just adjacent to the axon terminals where the tSC processes capped them at the muscle fiber surface (Figure 4.7 and 4.8). This would indicate that the previous postsynaptic membrane occupied by tSCs had lost AChR expression in the muscle fiber membrane. Despite staining being present at these sites, the intensity of AChR label was significantly decreased in comparison to the staining beneath axon terminals (>2-fold) and not significantly elevated over non-synaptic regions of the muscle fiber membrane (Figure 4.8). Interestingly, the relative differences in staining beneath axon terminals versus extrasynaptic membrane increased from P4 to the adult (~1.5 to ~4-fold, respectively) (Compare relative intensities in Figure 4.8 and 4.9). This increase in AChR density agrees with previous reports, indicating the increase in AChR density at NMJs during postnatal development, increasing nearly 100-fold from 10 to 1,000/ μm^2 of muscle fiber membrane (Salpeter et al.,1985).

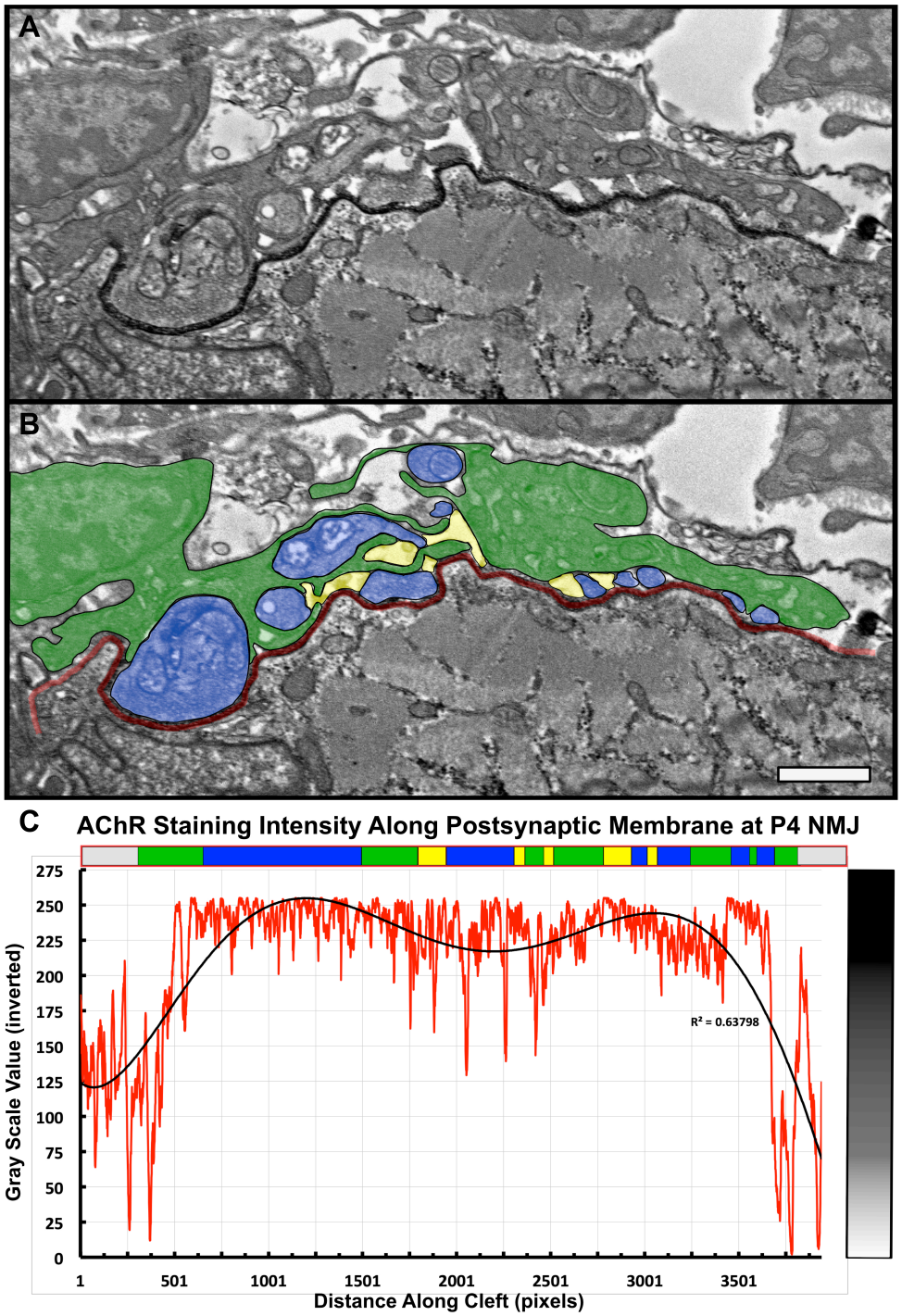

Figure 4.6: AChR labeling at P4 NMJs is demarcated by dense staining throughout the synaptic cleft. (A,B) Electron micrograph of P4 sternomastoid where nerve terminals (blue), Schwann cells (green) and vacancies (yellow) are shown in direct apposition to the postsynaptic muscle fiber membrane. AChR label intensity was measured (red line in B) from extrasynaptic region, through cleft, and opposite extrasynaptic region. Staining beaneath all three components is markedly more dense than extrasynaptic regions. (C) Red line in (B) segmented in Fiji to quantify the average AChR labeling density throughout the length of the postsynaptic membrane at the NMJ. Plot graph corresponds to intensity of AChR (measured in grayscale value averages –Y-axis) labeling along segmented line from left to right (length in pixels-X-axis). Horizontal bar above graph shows corresponding regions contacted by extrasynaptic (gray), axon terminals (blue), terminal Schwann cells (green) and vacancies (yellow).. Gray Scale shown as inverted (0=white, 255=black). Electron micrographs imaged at 12.5kx, scale bar 1µm.

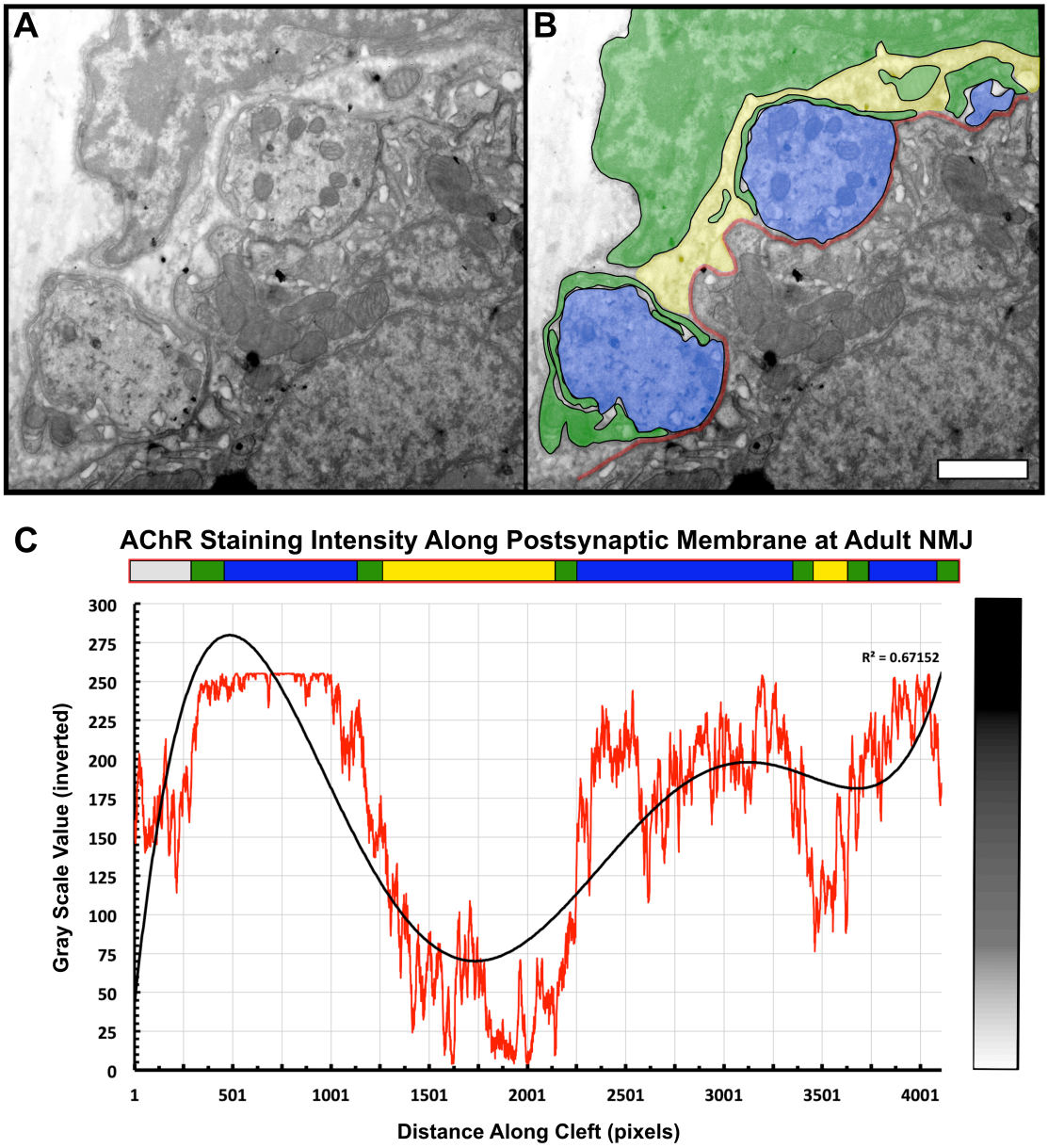

Figure 4.7: Electron microscopy of AChR labeling at adult NMJs. (A) Electron micrograph of adult sternomastoid where axon terminals (NT), Schwann cells and vacancies (Vac) are shown in direct apposition to the postsynaptic muscle fiber where AChR labeling is variable, as opposed to observations of P4 NMJs where a more even distrubution is observed. Here AChR labeling is most intense beneath sites of axon terminal contact. (B) Same micrograph shown in (A) outlined for axon terminals (blue), terminal Schwann cells (green) and vacancies (yellow). (C) Red line in (B) segmented in Fiji to quantify the average AChR labeling density throughout the length of the postsynaptic membrane at the NMJ. Plot graph corresponds to intensity of AChR (measured in grayscale value averages) labeling along segmented line from left to right with bars above graph corresponding to regions contacted by extrasynaptic (gray), axon terminals (blue), terminal Schwann cells (green) and vacancies (yellow). Plot indicates AChR labeling is most intense at sites of axon terminal contact with the muscle fiber as opposed to terminal Schwann cell contacted regions and vacant sites. Electron micrographs imaged at 12.5kx, scale bar 1µm.

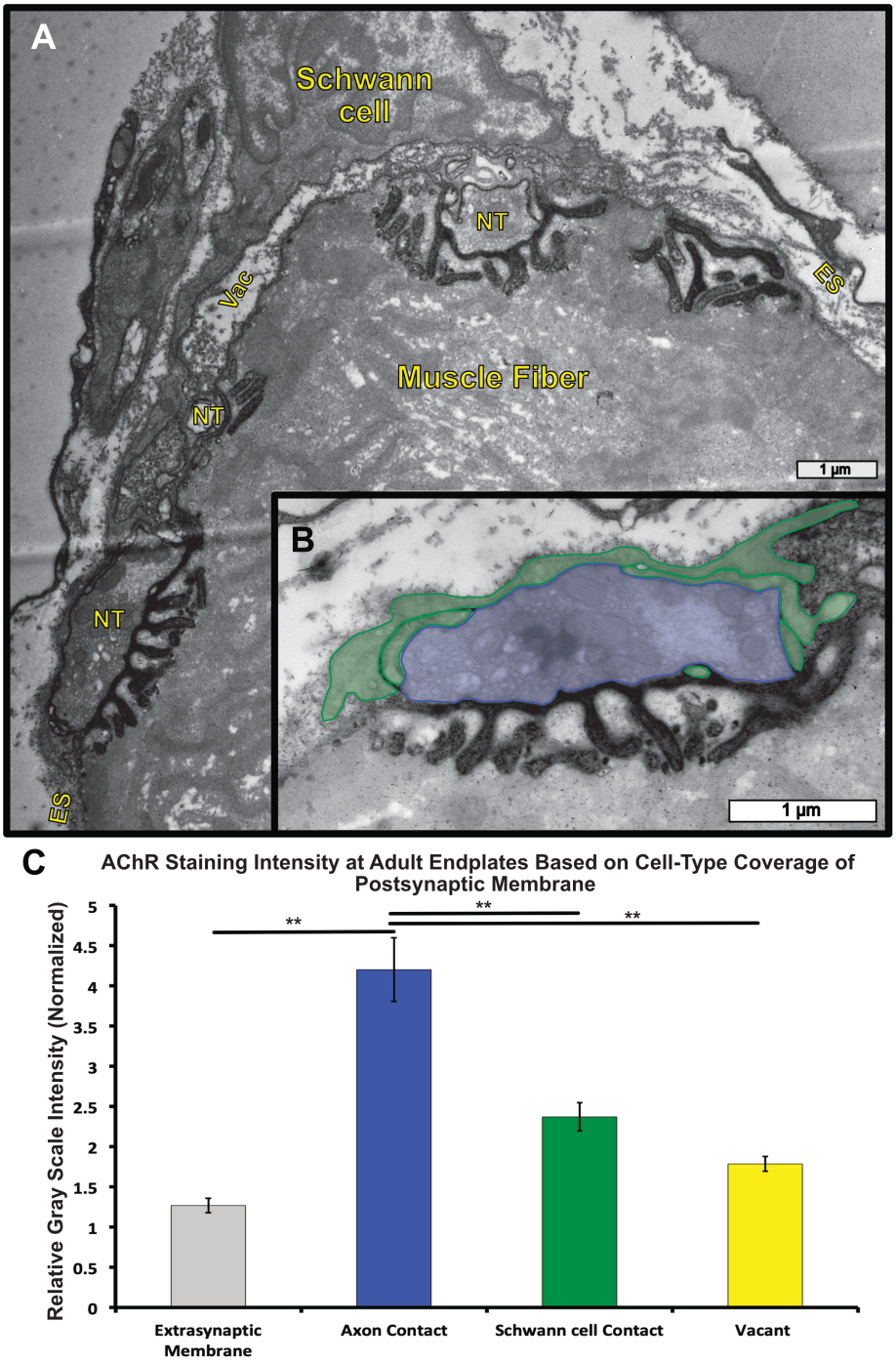

Figure 4.8: Adult micrographs show significantly more intense AChR labeling at sites of axon terminal coverage. (A) Electron micrograph of adult sternomastoid NMJ shows labeling of AChR is predominantly at sites of axon terminal contact with the postsynaptic membrane. These sites are easily noticed by the presence of secondary junctional folds opposite the axon terminals that are laden with synaptic vesicles and mitochondria. (B) Inset of axon terminal on left side of full micrograph in (A) showing axon terminal (blue) and terminal Schwann cell (green) relative to the presence of dense staining of AChR in the postsynaptic membrane. (C) Quantification of average AChR staining density of muscle fiber membrane in extrasynaptic regions (gray), axon terminal apposition sites (blue), terminal Schwann cell apposition sites (green), vacancies (yellow). Staining is significantly elevated at sites of axon terminal apposition to the muscle fiber membrane compared to all other regions. (A) imaged at 7.5kx, scale bar 1µm. B, imaged at 12.5kx, scale bar 1µm. Statistical significance at p value <.05 with ANOVA post-hoc.

4.5 Endplate regions unoccupied by either terminal Schwann cells or axon terminals, "vacancies", possess AChR at postnatal day 4

Analysis of receptor density at P4 NMJs shows 3 distinct tiers of staining intensity. These three tiers correspond to regions contacted by: (1) axon terminals, (2) tSCs, and (3) vacancies (described in ch. 3). Muscle fiber membrane contacted by all three components show elevated intensity of AChR labeling compared to extrasynaptic regions of the muscle fiber membrane (Figure 4.9). Moreover, staining at these three sites were statistically different from one another. Sites contacted by axon terminals show the most intense labeling of AChR, significantly elevated compared to those occupied by tSCs and vacancies. While sites contacted by tSCs were significantly less intense in AChR labeling than axon terminal sites, they remain significantly elevated compared to vacancies within the endplate. Lastly, the label intensity of AChRs at vacancies was significantly reduced compared to sites occupied by axon terminals or tSCs (Figure 4.9). AChR labeling at vacancies was significantly elevated compared to extrasynaptic regions. The presence of AChR at vacancies in early synaptic competition is interesting as these are the contact sites of recently eliminated axon terminals. Vacancies show evidence of axonal cellular debris and were closely associated with tSC processes that also contained similar debris profiles from the axons (see Figures 2.6, 2.7). These images strengthen the argument that tSCs participate in the elimination of losing axon terminals during synaptic competition. It also provides direct evidence that axon terminals can lose synaptic contact sites prior to the loss of the AChR expression in the muscle fiber membrane beneath them as proposed by Balice-Gordon and colleagues (Balice-Gordon and Lichtman, 1994).

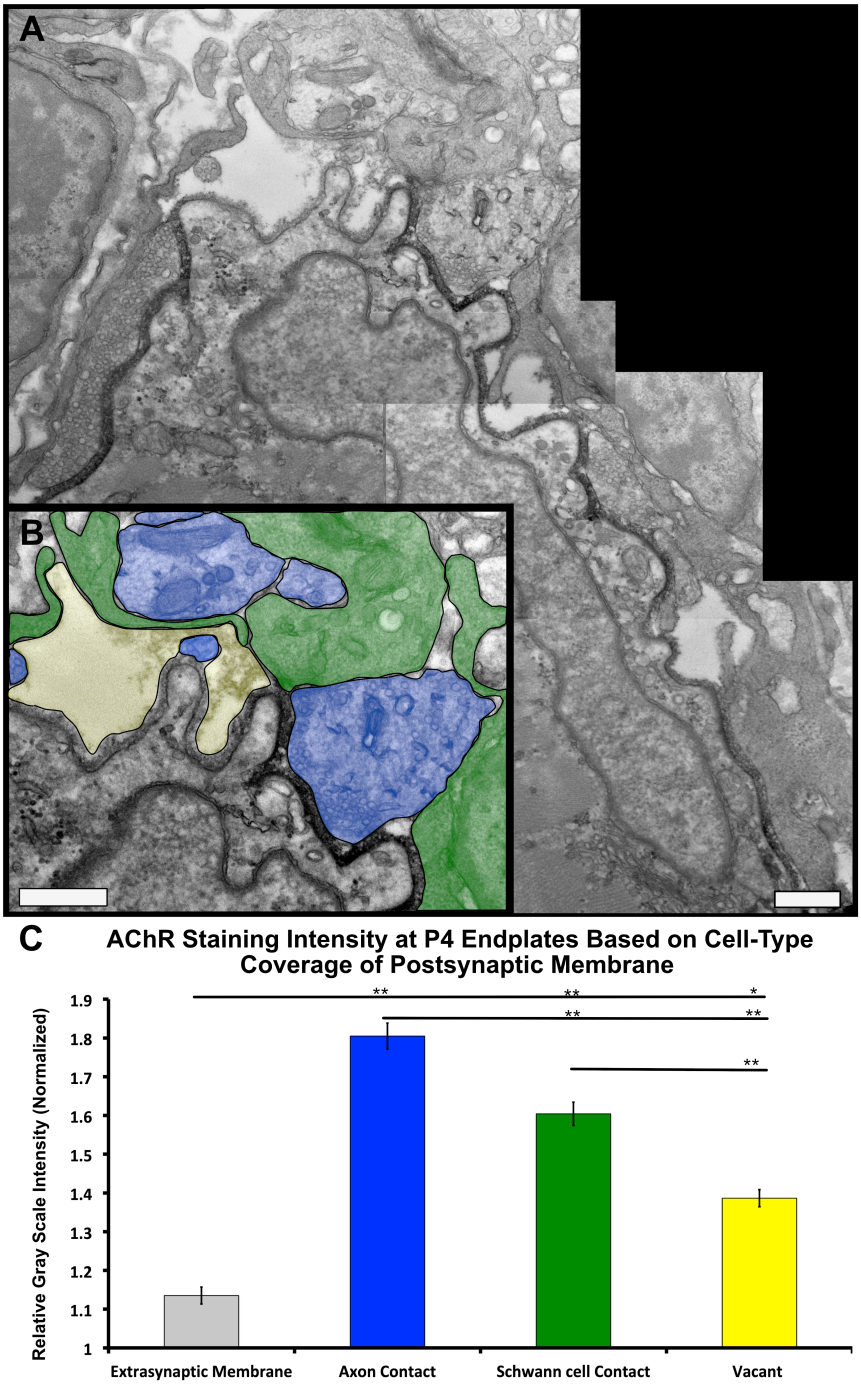

Figure 4.9: P4 micrographs show labeling of AChR is not completely uniform. A, electron micrograph of P4 sternomastoid shows labeling of AChR is dense throughout the synaptic cleft, above that of extrasynaptic regions. B, Inset of axon terminal on left side of full micrograph in (A) showing axon terminal (blue) and terminal Schwann cell (green) relative to the presence of dense staining of AChR in the postsynaptic membrane. C, quantification of average AChR staining density of muscle fiber membrane in extrasynaptic regions (gray), axon terminal apposition sites (blue), terminal Schwann cell apposition sites (green), vacancies (red). Staining at contact sites for axon terminals (blue), terminal Schwann cells (green) and vacancies (red) are all significantly elevated in comparison to extrasynaptic membrane (gray). ANOVA indicates that staining beneath axon terminals is most intense, followed by regions contacted by terminal Schwann cells, followed by vacant regions. A, imaged at 7.5kx, scale bar 1µm. B, imaged at 20kx, scale bar 1µm. Statistical significance at p value <.05 with ANOVA.

4.6 Discussion

Serial electron microscopy of labeled AChR at neonatal and adult NMJs shows that: (1) tSCs make extensive physical contacts with the AChR-rich membrane of the muscle fiber endplate during the period of synapse elimination. (2) tSC occupation of the receptors is transient and confined to the early stages of postnatal development during the period of synapse elimination. (3) The synaptic footprint of axon contacts, tSC contacts, and vacancies at the postsynaptic membrane correspond with distinct differences in postsynaptic intensity of AChR expression. (4) Complete loss of postsynaptic receptor expression is not required for loss of axon terminals during synapse elimination, indicating that the muscle fiber may be leading a part of synapse elimination behaviors, playing an active role, rather than merely inserting AChRs where there is an axon terminal directing the insertion of AChR.

It is well established that the overall morphology of AChR labeling at the endplate undergoes considerable transformation during synapse elimination as the initial plaque of receptors is sculpted into the intricately branched, pretzel-like morphology of singly innervated adult NMJs (Steinbach, 1981; Balice-Gordon and Lichtman, 1993; Marques et al., 2000). It is possible that both the formation of vacancies resulting from axon terminal degradation and postsynaptic occupation by tSCs contribute to the receptor turnover that drives this transformation. The extensive coverage of postsynaptic membrane may influence the activity-driven remodeling of AChR accumulation during postnatal development. Balice-Gordon and colleagues have shown that differences in relative synaptic activity within the endplate can drive changes in receptor expression in the muscle fiber membrane in the adult (Balice-Gordon and Lichtman, 1994). That study showed that

blocking the synaptic activity beneath isolated regions of the endplate using acute application of btx, lead to loss of receptors at those sites while adjacent, active regions showed increasing density of receptors. If differential activity levels within the developing endplate can change receptor distribution patterns, it seems possible that the large contact regions made by tSCs and vacancies could contribute to changes in receptor expression through a similar mechanism during synapse elimination. In theory, regions occupied by tSCs and vacancies would act in a similar fashion to the btx-blockade. In this case, Schwann cells create a physical barrier to synaptic transmission, even at sites where tSC processes intercalate between nerve terminals and the muscle fiber surface. Interestingly, synaptic footprint models reconstructed from P0, P3, and P4 EM series show a considerable amount of contact made by both tSCs and vacancies near the center of the footprint. Notably, AChR density is reduced at the center of reconstructed NMJs in serial TEM analysis as well (See Figure 4.5). The sites of these contacts correspond to the regions of receptor staining that are often lost first from the neonatal plaque of AChRs as they become increasingly perforated in early development (Prozynski et al., 2009). Given the grayscale analysis showing that regions contacted by vacancies and tSCs show reduced expression of receptors when compared to nerve terminals, it seems possible that these contacts may play a role in the differential activity that drives the transformation of the AChR morphology during synapse elimination. However, it must be noted that HRP is a diffusible staining method. This is evident when examining the labeling of adult NMJs where HRP labeling is observed in the depth of junctional folds, where AChRs are not present. Thus, it could also be interpreted that the staining differences observed between sites of axon contact, tSC contact and vacancy contacts are partially a result of the stain

diffusing from the sites of high AChR concentration beneath the axon terminals laterally to sites occupied by tSCs and vacancies.

During denervation studies, tSCs show an affinity for the postsynaptic membrane, remaining in prolonged contact with the post-synaptic AChR while the axons grow back to re-innervate the endplate (Birks et al., 1960; Hesselmans et al., 1993; Culican, 1998). It has also been noted that in the absence of the nerve at NMJs, tSCs are capable of quantal release of acetylcholine, potentially acting as a short-term proxy to stimulate the muscle fiber in the absence of axon terminals being present (Birks et al., 1960). The behavior of tSCs after injury and during reinnervation have long been compared to those observed during postnatal development and synapse elimination. It is possible that tSCs at developing endplates are using their expansive coverage of the AChR to preserve receptors for the eventual expansion of axon terminal coverage as the entire NMJ grows along with the muscle fiber during postnatal development. There may be real differences in transcription and expression between early neonatal and uninjured adult tSCs that may help explain this stark contrast in behavior. Investigating the transcription profiles of neonatal terminal Schwann cells versus those in the adult would offer insight on this discussion.

The evidence of reduced AChR aggregation from acute regions of the endplate at sites of tSC and vacancy-contacted muscle fiber membrane may indicate a more active role for muscle-led synaptic changes. Balice-Gordon and colleagues suggested this after examining relative activity levels at adult endplates and the resulting remodeling of AChR (Balice-Gordon and Lichtman, 1994). The ability of the muscle fiber to choose the winning axon of synapse elimination has also been discussed in terms of the concept of reward and

punishment administered by the muscle fiber through the secretion of "synapto-medin" molecules. Lichtman and colleagues have discussed the possibility of "synaptogenic" and "synaptotoxic" factors secreted by the muscle fiber that feedback to the overlying axon terminals competing during synapse elimination (Reviewed by Sanes and Lichtman, 1999). One such factor has been suggested to act in this fashion, brain derived neurotrophic factor (BDNF). In these studies BDNF is proposed to have two isoforms (mature BDNF and pro BDNF) that exact punishment and reward, respectively, on axon terminals based on their activity (McGurk et al., 2011; Garcia et al., 2011). If this were the case, the coverage of the endplate by tSCs during synapse elimination may provide sufficient spatial separation between competing axon terminals and in theory, allow the muscle fiber better "resolution" to discern between competing inputs and their relative synaptic activity.

While the coverage and contact areas of tSCs at developing endplates may aid in spatial resolution for the muscle fiber's allocation of AChR to more active regions, it may also play a role in propelling the process of elimination by limiting the regions of axon terminal expansion. Considering the confined plaque of AChR expression at developing endplates, the considerable coverage of the AChR-rich membrane by tSCs may drive the competition for synaptic membrane by different axon terminals. The boundaries of AChR expression in the muscle fiber membrane are highly co-extensive with Schwann cell coverage, which may be a means of confining the available space for competition between axonal inputs. As tSCs increase their contacts within the endplate during early postnatal days the available regions for axons to grow and compete for may be even more restricted by the physical presence of tSC occupation of otherwise AChR-rich postsynaptic

landscape. Thus, increased occupation of the AChR-rich endplate membrane may serve to accelerate the progression of synapse elimination.

Evidence from studies examining a line of transgenic mice over-expressing Neuregulin-1-III (NRG), suggests this may be possible. NRG mice show accelerated rates of synapse elimination, primarily attributed to heightened phagocytic activity by tSCs on axon terminals at the NMJ. However, in this study we also performed serial TEM examination of neonatal NMJs and noted that the degree of postsynaptic coverage by tSCs was also increased compared to their wildtype counterparts at postnatal day 3 (Lee et al., 2016). This suggests that the physical contacts made by tSCs in addition to their phagocytic behavior may influence the rate of synapse elimination.

These observations indicate that the proliferation and expansion of tSC contacts show an affinity for regions of AChR-rich membrane at the developing endplate during the period of synapse elimination. The reduction in AChR expression at sites of their contact with the muscle fiber membrane and even more so at the vacant regions brought about by their phagocytic activity on axon terminals suggest they may play a role in the progression of synapse elimination and the remodeling of the AChR aggregation in the postsynaptic membrane.

4.7 Materials

For fluorescence microscopy C57B/6 mice carrying an S100-GFP transgene were used in order to examine SC presence at neonatal NMJs. For electron microscopy, wild-type C57B/6 mice of either sex, obtained from Jackson Laboratory and bred in colonies at the University of Texas at Austin and Texas A&M University. Mice were euthanized on P0, P3, P4, P5, P6, P7,P9, P10, P16, P19, P21 and P40 by intraperitoneal injection of Euthanasol III. P0 indicates the day of birth. Experimental procedures were approved by Texas A&M University Institutional Animal Care and Use Committee.

Animals were perfused transcardially using 0.1M Sodium cacodylate buffer, pH 7.4, followed by the same buffer containing 2% PFA and 3% glutaraldehyde. Sternomastoid and cranial muscles were removed and fixed over-night at room temperature in the same fixative. Muscles were washed with cacodylate buffer and stained en bloc in 1% osmium tetroxide, 1% ferrocyanide in cacodylate buffer for 5 hours, washed with DI water, and then stained in 1% aqueous uranyl acetate for 2 hours. Muscles were then dehydrated in graded ethanols and acetone, then embedded in Epon 812 resin. After embedding, samples were trimmed for thick sectioning (0.5-1μm) where regions of interest, neuromuscular synapses. Using a Leica Ultracut UTC Ultramicrotome with glass knives, thick sections were cut then transferred to glass slides. Dried sections were stained with 1% toluidine blue with borate, and examined under a light microscope. Blocks were further trimmed using a 45 degree cryotrim tool (Diatome), creating secondary block-face. Using a 35 degree diamond knife (Diatome), serial thin sections were cut in continuous ribbons and floated onto water-boats. Sections were mounted on formvar or PEI-coated Synaptek slot grids (Electron Microscopy Sciences) and observed under an FEI Technai Spirit electron microscope with an AMT Advantage HR digital camera or a JOEL – 1200 EX transmission electron microscope with a bottom mounted 3k x 3k slowscan, lens-coupled CCD camera (SIA 15C). Using electron

microscopy, NMJs were identified by the apposition of the nerve terminals to within ~50nm of the muscle-fiber surface in the presence of Schwann cells.

Digital images of individual NMJs and the immediately surrounding area were captured from each section at a magnification of 16,500 for use in assembling series images. (Images were taken at both lower and higher magnification during aspects of observation.) At this magnification, ~6-12 overlapping images were required to include the entire extent of the NMJ. These individual images were then montaged by manual manipulation in Adobe Photoshop to create a single image. Such montaged image series typically consisted of 70-200 sections per series-set. Each series was then imported into the software program Reconstruct (Fiala, 2005), calibrating the pixel dimensions in the micrograph-montages to known distances in the specimen using scale bars and adjusting for the thickness of the individual sections (65nm). Following calibration, each section image was aligned linearly to each adjacent section using 8-10 objects common in both images. To account for drift in the data set alignment, all series were aligned by beginning with a section near the middle of the stack and aligning in a "middle-out" fashion. Once calibrated and aligned, structures of interest in each section were segmented using the tools provided in the software. Measurements and 3D renderings of these structures were then generated in this software.

In total we made extensive serial sections from a total of 10 NMJs at postnatal day 0, 8 at P3, 3 at P4, 5 At P7 (Renovo), 2 at P16, 2 at P19 (Renovo) and 4 at P40. One P3 muscle provided all 8 NMJs, although two other animals were used to provide 40 semiserial or nonserial sections to confirm the observations made in serial sections. Of the 8 serially sectioned P3 NMJs, 2 NMJs (NMJ1 & 4) have been completely reconstructed for all parameters reported here, 4 (NMJs 2, 3,7 and 8) have been completely reconstructed, except that their SCs were not identified individually, and 2 have been partially reconstructed (NMJs 5&6). One animal was used at P4 for serial sectioning where 1 NMJ is completely reconstructed while 2 others have been serially sectioned but are not fully reconstructed. Several other NMJs in the same muscle and/or cranial muscles were

referenced through semi-serial sectioning to confirm ultrastructure observations made in reconstructed series. One animal was used at P7, where 1 NMJ has been completely reconstructed and several more (6) have been partially reconstructed for the muscle fiber, axons, SCs and footprint. Two animals were used for the serial sectioning of P16 muscles; an additional 2 short serials and 10 nonserial sections were made for reference. One animal was used at P19 with one NMJ being fully reconstructed and a second partially reconstructed. At P40, 3 animals were used and the four NMJs had between 54 and 231 sections, and approximately a dozen individual sections were made.

Fluorescent labeling of NMJs was performed as described previously (Hayworth et al., 2006, Kang et al., 2007, Lee et al, 2011). Briefly, C57B/6 mice carrying an S100-GFP transgene (illuminating Schwann cells) were anesthetized as described above and transcardially perfused wityh PBS, pH 7.4. Sternomastoid muscles were dissected and fixed with 4% PFA, pH 7.4, then blocked and permeabilized with a blocking solution (0.2% BSA-fraction 5, 0.3% Triton X-100, 0.1% $NaN_{3)}$. Presynaptic nerve terminals were labeled with a mouse anti-neurofilament antibody (2H3; Developmental Studies Hybridoma Bank) and an antibody against an axonal vesicular protein: SV2 (Develeopmental Studies Hybridoma Bank) or synaptophysin (Invtrogen). AChR-rich plaques were identified using fluorochrome-conjugated alpha BTX (Invtrogen). A total of 140 NMJs from mice during the postnatal period of synapse elimination were examined for AChR morphology and terminal Schwann cell number simultaneously by imaging muscles in whole-mount using 63x oil immersion objective on Leica upright microscope. Image capture and analysis was performed in ilab and ImageJ software.

Muscles were dissected and pinned down in sylgard dishes in oxygenated mammalian Ringer's solution, pH 7.4, 318 mOsm. Ringer's solution was then replaced with the same solution containing biotinylated-BTX [1:250] for 2 hours. While muscles were submerged in BTX-solution, a glass pipette was used periodically to pulse solution over muscles in order to assist infiltration of

BTX into fibers that weren't superficial. Following BTX, muscles were washed thoroughly (5, 5minute washes) in oxygenated Ringer's. Remaining pinned in sylgard dishes, muscles were then submerged in Ringer's with Neutravidin-HRP [1:200] (Thermofisher) for 2 hours at room temperature. Muscles were then washed thoroughly (10washes x 3 minutes each) with ringers in order to insure clearance of any residual HRP not bound to BTX.

After AChR have been labeled with biotinylated-BTX conjugated to Neutravidin-HRP, we proceeded with the Diaminobenzidine (DAB) – Peroxidase reaction. For each set of experiments, DAB-Peroxidase solution (10ml 0.1M phosphate buffer solution, 500µl, 0.3% H_2O_2, 500µl, 0.5% DAB) was freshly prepared and kept on ice, covered from light until ready to use.

Once solutions were prepped and muscle is washed, reactions were performed by submerging muscles in DAB solution in sylgard dishes and using glass pipettes to pulse as mentioned previously. When reacting with the horseradish-peroxidase conjugated to the BTX bound to receptors, the DAB solution generates a reaction product in the form of a dark precipitate at the site. This precipitate is distinct and easily identified, thus the reactions were performed beneath a dissecting microscope and monitored for the appearance of precipitate formations on the muscle fibers, with most reactions becoming visible between 20-30 minutes following the start of the reaction. After reactions were complete, DAB solution was disposed of in the fume hood and muscles were again washed (6 x 5min) prior to secondary fixation and heavy-metal staining for TEM.

Once a-BTX-HRP-DAB treated tissues were sectioned imaged in the electron microscope, labeling of AChRs at NMJs was easily recognized by-eye, showing much more-densely stained synaptic clefts than control tissue. However in order to show this quantitatively and in order to compare AChR-labeling throughout the postsynaptic endplate, individual electron micrographs were analyzed for gray-scale values of the postsynaptic membrane. For gray-scale analysis, images obtained for comparison of synaptic cleft gray-scale values were all imaged using the same

magnification and exposure in the electron microscope. Images were then opened in FIJI and auto-thresholded for brightness/contrast to normalize levels. In addition, each micrograph was quantified for the gray-scale intensity of receptor staining in the synaptic cleft. Measurements were all made using "oval-brush-selection" tool in FIJI, making sure the width of the selection remained constant, encompassing the width of the synaptic cleft. Measurements were constant in width, keeping the area of postsynaptic membrane being analyzed consistent but these measurements varied in length as each measurement was made corresponding to the length of presynaptic coverage by tSCs, NTs and/or vacancies. Segmenting the selections with respect to overlying contacts with the muscle was used in order to discern any differences in staining intensity at areas of the endplate contacted by nerve terminals, Schwann cells, vacancies and/or extra-synaptic regions. Once measurements were made of all segments of synaptic cleft staining on an individual micrograph, all measurements were normalized to the gray-scale value of the muscle-fiber interior. Normalizing in this way helps account for any differences in grayscale value that may be due to slight variations in section thickness and/or beam exposure during acquisition and allows reliable comparison of gray-values between images and sections of serial data sets as well as those between data sets.

Analysis performed on AChR Stage through days postnatal and terminal Schwann cell counts were tested for significance using one-way ANOVA followed by post-hoc analyses (Tukey HSD, Bonferonni Holms, and Scheffe Multicomparison) with alpha = 0.05. Analysis of receptor staining intensity in electron micrographs was evaluated using one-way ANOVA as well, evaluating individual differences between receptor staining intensity at regions extrasynaptic, contacting terminal Schwann cells, contacting axon terminals, and vancancies with post-hoc analysis (Tukey HSD, Bonferonni Holms, and Scheffe Multicomparison) with alpha = 0.05.

CHAPTER V

TERMINAL SCHWANN CELL AND VACANT SITE MEDIATED SYNAPSE ELIMINATION AT DEVELOPING NEUROMUSCULAR JUNCTIONS

5.1 Introduction

The vertebrate neuromuscular junction (NMJ), a synapse between a motor neuron and a muscle fiber, has been intensely studied to understand general synaptic function due to its accessibility and relatively large size compared to other synapses found in the nervous system (Sanes and Lichtman, 1999). Decades of study have expanded our understanding of this synapse and how its components work together: the presynaptic motor axon and its nerve terminal, the postsynaptic muscle fiber and its specialized synaptic region, the endplate, and the non-myelinating terminal Schwann cell (tSC), the glia of the peripheral motor synapse. In a mature NMJ, a single presynaptic nerve terminal releases the neurotransmitter acetylcholine to the endplate where they bind acetylcholine receptors and depolarize the muscle fiber resulting in contraction. However, at birth each endplate is contacted by an excess of nerve terminals and those extra nerve terminals must be removed to ensure proper synaptic function. Thus, the removal of these superfluous nerve inputs, or synapse elimination, is a critical step in the maturation not just of the synapses themselves but also the overall development of the nervous system during the first few weeks of life (Redfern, 1970; Brown et al., 1976; Purves and Lichtman, 1980; Van Essen et al., 1990; Van Ooyen and Willshaw, 1999; Walsh and Lichtman, 2003; Turney and Lichtman, 2012; Smith et al., 2013; Darabid et al., 2014).

Synapse elimination is well characterized as a competitive process of different axons by both experimental and modeling studies (Brown et al., 1976; Betz et al., 1979; Jansen and Fladby, 1990; Walsh and Lichtman, 2003; Darabid et al., 2014). At dually innervated mouse NMJs, one axon was observed to expand its territory as the other retracted (Walsh and Lichtman, 2003). A previous study showed that synapse elimination can be successfully modeled through random competition amongst the different inputs to simulate removal of extra axonal connections in an endplate, achieving single innervation (Turney and Lichtman, 2012). Several other models largely based on interaxonal competition were constructed to match behaviors of synapse elimination (Willshaw, 1981; Gouze et al., 1983; Smalheiser and Crain, 1984; Bennett and Robinson, 1989; Van Essen et al., 1990; Rasmussen and Willshaw, 1993; Stollberg, 1995; Jeanpretre et al., 1996; Elliot and Shadbolt,1996; 1998; Van Ooyen and Willshaw, 1999; Barber and Lichtman, 1999). Though interaxonal competition undoubtedly plays a significant role in the progression of each developing synapse to a mature, singly-innervated form, there is growing evidence that Schwann cells are also important in synapse elimination (Bishop et al., 2004; Song et al., 2008; Lee et al., 2011; Smith et al., 2013; Lee et al., 2016). Schwann cells, tightly associated with motor neurons and their functions, have been observed removing retracting motor axons (Bishop et al., 2004; Song et al., 2008). Moreover, the studies in previous chapters indicate that tSCs are directly involved in the pruning and competing with motor axons for postsynaptic contact during the period of synapse elimination. Specifically, developing mouse NMJs showed that endplates are covered with multiple axons, tSCs, and vacant sites (or vacancies) that have no such contact from either axons or tSCs; the study suggested that tSCs promote postnatal synapse elimination not only by phagocytosis of

axon terminals but also by direct competition with motor axons for occupation of the maturing endplate (Smith et al., 2013). A subsequent study showed that overexpression of neuregulin1 type 3 (NRG1-III), a potent activator of tSCs, led to expedited synapse elimination and that by reducing the activity of endogenous NRG1-III, single-innervation is achieved more slowly than control littermates (Lee et al., 2016). The findings support a direct role of tSCs in synapse elimination and provided a qualitative model of tSC-mediated synapse elimination. However, there is no quantitative model of synapse elimination that incorporates this role despite several models considering dynamic competition of different axons (Willshaw, 1981; Gouze et al., 1983; Smalheiser and Crain, 1984; Bennett and Robinson, 1989; Van Essen et al., 1990; Rasmussen and Willshaw, 1993; Stollberg, 1995; Jeanpretre et al., 1996; Elliot and Shadbolt, 1998; Barber and Lichtman, 1999; Van Ooyen and Willshaw, 1999; Turney et al., 2012), and the possible contribution of the observed vacancies to synapse elimination is little understood.

With this in mind, we developed a quantitative model of synapse elimination that, for the first time, employs the contact areas of tSCs and vacancies in endplates to further understand the roles of tSCs and vacancies in synapse elimination. Based on data from our previous studies (Smith et al., 2013; Lee et al., 2016), the transition probabilities and interactions among tSCs, vacancies, and axons were quantified as the key parameters of the model using Markov chain methods (Jung and Doniach, 2017). Our model simulated synapse elimination reliably, and the simulation results showed the co-existence of tSCs, vacancies, and axons in endplates throughout the entire process of synapse elimination consistent with experimental observations of developing mouse NMJs (Smith et al., 2013). In contrast, when tSCs, vacancies, and axons were assumed to compete with random or

equal transition probabilities, synapse elimination proceeded unreliably in contrast to other models that only consider the competition among different axons (Van Ooyen, 2001). Furthermore, our results exhibited acceleration and delay of synapse elimination depending on degrees of synaptic activity of axons, which are also consistent with other studies and recent observations (Lee et al., 2011; 2016). Our findings suggest that by incorporating active roles for tSCs, axons, and vacancies, our new model provides a broader framework for understanding synapse development and will be useful in further investigation of synapse elimination.

5.2 Synaptic footprint composition changes during postnatal development

Serial electron micrographs of multiple NMJs in sternomastoid muscles at P0, P3, P7, and P16 (Figure 5.1) were examined as in a previous study (Smith et al., 2013). The images in Fig. 1a, c, e, and g show that each endplate is occupied by multiple axons, tSCs, and vacancies. Axon nerve terminals (purple, cyan and blue in Figure 5.1) are outlined in purple, and tSCs surrounding the axons are present at all endplates (color-coded in green in Figure 5.1 b, d, f, and h). Vacant sites (vacancies) devoid of contacts of either tSCs or axons are marked by black lines (Figure 5.1 a) The postsynaptic membranes of the muscle fibers are outlined in red and exhibit junctional folds (JFs) by P7, a feature of normal development and mature NMJs. The three-dimensional (3D) surface models of the tSCs (green), vacancies (black), and axons (other colors) were generated after tracing and segmentation (Figure 5.2a-h) as in the studies in chapters 2 and 3 (Smith et al., 2013).

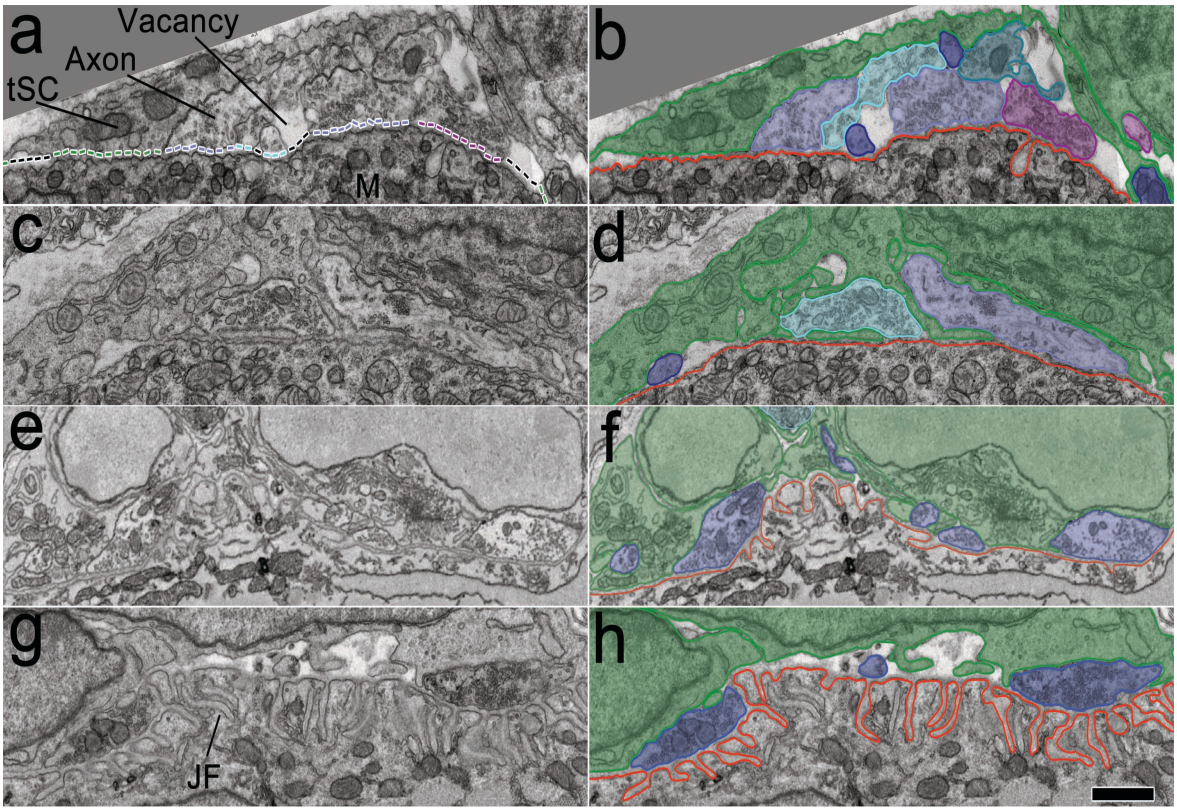

Figure 5.1. Developing sternomastoid NMJs at P0, P3, P7, and P16. (a, c, e, and g) Montaged 2D electron micrographs spanning the entire NMJs in individual thin sections of mouse sternomastoid muscle fibers at P0, P3, P7, and P16, respectively. The nerve terminals of the NMJs contain synaptic vesicles and come within ~50 nm of the surface of a muscle fiber (M). The endplate on the muscle fiber is occupied tSCs (green dotted line), vacancies (black dotted line), and axons (dotted line in color different from green and black). Note that the postsynaptic membranes at P0 and P3 are smooth but show multiple indentations called junctional folds (JFs) at P7 and P16. Multiple axons at the NMJs are also associated with tSCs; vacancies are present, some of which extend to the surfaces of the muscle fibers. (b, d, f, and h) Segmentation of the muscle fiber surfaces (red), terminals (here in shades of blue), axons, tSCs (green), and vacancies at the same NMJs. Red line represents the muscle fiber surface. Scale bar 1μm.

The sites of the tSCs, axons, and vacancies opposed to their endplate were identified (See Figure 5.1a) and their contact areas were measured by computing the entire area of each contact site using their surface models generated after segmentation (See Methods). The measured areas were normalized by dividing the areas by the total areas of tSCs, vacancies, and axons to compare their relative contact areas. From P0 to P3, the relative contact area of tSCs in the endplate increased on average whereas that of axons decreased and the relative area of vacancies changed little (Figure 5.2i) as seen in the previous study (Smith

et al. 2013). We also found that the relative contact area of tSCs changed little between P0 and P3, and then decreased (Figure 5.2i). The dominance of tSC occupation from P3 to P7 is consistent with its active role in synapse elimination by competing against axons to occupy the territory of the endplate proposed in the previous study (Smith et al., 2013). In contrast, the relative contact area of vacancies was found to markedly decrease from P3 to P7 and then change little by P16, whereas the relative contact area of axons significantly increased from P3 to P16 (Figure 5.2i). The increase in the axonal area suggests that axons pursue territory of the endplate more actively than tSCs and vacancies.

Because Schwann cells and axons are both involved in the competition (Smith et al., 2013; Lee et al., 2016), these dynamic changes are expected to be closely related to the process of synapse elimination. However, even with current advanced imaging technologies, direct observation of these dynamic changes is extremely challenging to quantify. Accordingly, we set out to create a modeling approach to investigate the relationship of the dynamic change in the relative areas of tSCs, vacancies, and axons within the endplate during synapse elimination.

5.3 Model of synapse elimination involving direct roles of tSCs and vacancies

Previous modeling studies have shown the transition of a poly-innervated synapse to a single-innervated synapse is a result of competition among different axons in an endplate (Van Ooyen, 2001; Turney and Lichtman, 2012). However, the models did not address the presence of tSCs and vacancies at endplates (Smith et al., 2013). To address their roles, we simplified the contact sites of tSCs, vacancies, and axons in each endplate so that the transition of the endplate is represented as the reorganization of their simplified

contact sites (Figure 5.3a), and based on the previous studies (Smith et al., 2013; Lee et al., 2016), we assumed that tSCs, vacancies, and axons compete against each other (Figure 5.3b). Then a synaptic site formed by an axon has three different transition probabilities: a probability of transitioning into a vacancy (P_{AV}), a probability of transitioning into a tSC (P_{AS}), and a probability of no transition ($P_{AA}=1-P_{AV}-P_{AS}$). Similarly, a synaptic contact site formed by a tSC has three different transition probabilities: a probability of transitioning into a vacancy (P_{SV}), an axon (P_{SA}), and no transition ($P_{SV}=1-P_{VA}-P_{VS}$). A vacant site also has three different transition probabilities: a probability of transitioning into a tSC (P_{VS}), an axon (P_{VA}), and no transition ($P_{VV}=1-P_{VS}-P_{VA}$). Therefore, there are six independent transition probabilities (P_{AV}, P_{AS}, P_{SA}, P_{SV}, P_{VA}, and P_{VS}); however, measuring such transition probabilities experimentally with sufficient observations is presently impossible, so we took a computational modeling approach. We first constructed the initial layout of the endplate composed of multiple contact sites made by tSCs (green), vacancies (black), and axons (other colors) using the empirical data of synaptic footprints gathered from serial images of mouse sternomastoid muscles at P0 (example of individual NMJ Figure 5.4). These initial layouts, as seen in Figure 5.5 a, f, and k, depict the relative contact areas of the sites of tSCS, vacancies, and axons measured in the P0 data sets and the random distribution of those sites. As noted above, it is reasonable to assume that those sites compete to take over other sites in the endplate.

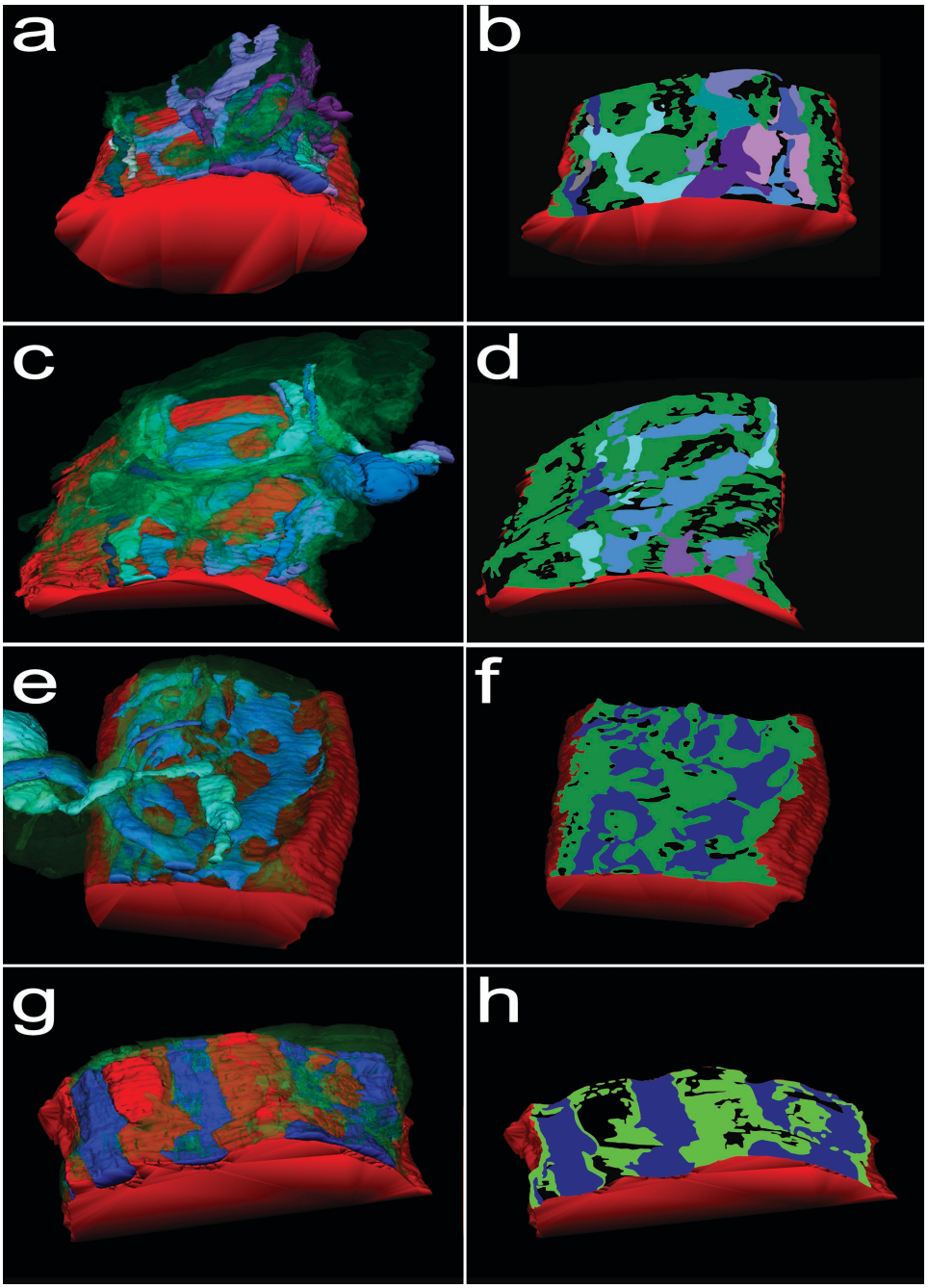

Figure 5.2. Surface models of axons of different neurons, tSCs, and vacancies at the NMJs and their contact areas on their endplate. (a, c, e, and g) Surface rendering of a series of montaged electron micrographs of the sections of the same NMJs at P0, P3, P7, and P16, respectively. Axons, tSCs, and vacancies are color-coded in the same with Figure 1. (b, d, f, and h) The regions of the axons, tSCs, and vacancies in proximity to their muscle fiber or footprints at their endplate were segmented and using the series of their segmented lines the contact regions of the axons, tSCs, and vacancies were marked in color using the same color-code their muscle fiber (red). (i) The average relative areas at P0, P3, P7, and P16. From P0 to P3, the relative contact area of tSCs in the endplate increased from 31.0% to 57.0% on average whereas that of axons decreased from 51.6% to 24.8% on average and also that the relative area of vacancies changed little (17.4% at P0 and 18.3% at P3 on average). The relative contact area of tSCs changed little from 57.0% at P3 to 55.6% at P7 and then decreased to 40.7% at P16. The relative contact area of vacancies markedly decreased from 18.3% at P3 to 4.55% at P7 and then changed little (5.82% at P16) whereas the relative contact area of axons significantly increased from 24.8% at P3 to 39.8% at P7 and then to 53.5% at P16.

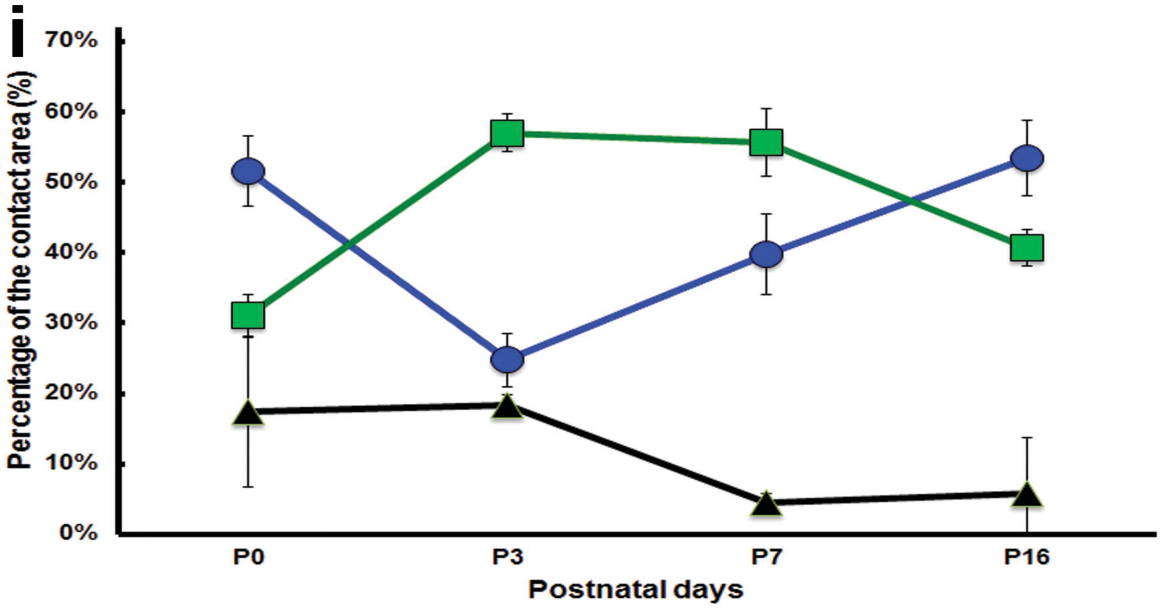

Figure 5.2 Continued

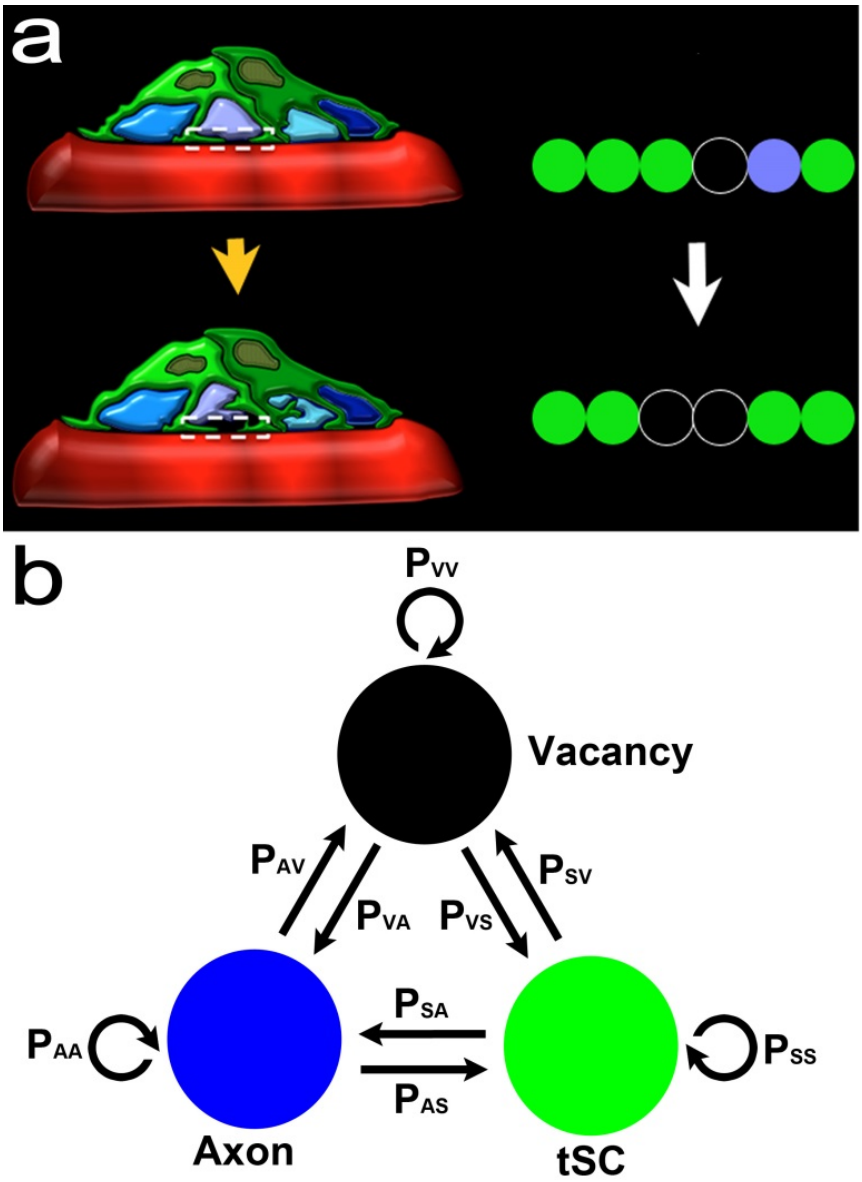

Figure 5.3. Schematic diagram of competing tSCs, vacancies, and axons. (a) An endplate covered with four different types of axon terminals (light blue, purple, cyan, and dark blue) and a tSC (green) transitions into an endplate covered with three of the axon terminals after removal of one axon terminal from the four and a vacancy (black) that takes place of the removed axon. (b) Competition of tSCs, vacancies, and axons. A blue circle represents a synaptic site formed on a muscle fiber by an axon. A green circle represents a synaptic site formed on a muscle fiber by a terminal Schwann cell (tSC). A black circle represents a vacancy having no axon or tSC on a muscle fiber. All the three different synaptic sites can transition from one kind of synaptic sites to another. A contact site formed by an axon has three different transition probabilities: a probability of transitioning into a vacancy (P_{AV}), a probability of transitioning into a tSC (P_{AS}), and a probability of no transition (P_{AA}=1-P_{AV}-P_{AS}). Similarly, a contact site formed by a tSC has three different transition probabilities: a probability of transitioning into a vacancy (P_{SV}), a probability of transitioning into an axon (P_{SA}), and a probability of no transition (P_{SV}=1-P_{VA}-P_{VS}). A vacant site also has three different transition probabilities: a probability of transitioning into a tSC (P_{VS}), a probability of transitioning into an axon (P_{VA}), and a probability of no transition (P_{VV}=1-P_{VS}-P_{VA}).

However, unlike axonal competition models of synapse elimination (Turney and Lichtman, 2012), if those individual sites interact with each other with random transition probabilities, synapse elimination would proceed unreliably because it cannot account for the maintained presence of tSCs and vacancies after synapse elimination is complete. To test this possibility, we generated an idealized endplate randomly occupied by multiple contact sites of tSCs, vacancies, and axons. We kept the area ratios nearly those measured at P0 (See Methods) and assumed that the values of P_{AV}, P_{AS}, P_{SA}, P_{SV}, P_{VA}, and P_{VS} are randomly assigned from 0 to 1 so that a randomly chosen site can be turned into a site of a tSC, a vacancy, or an axon adjacent to the chosen site. The competition process was iterated by repeating the random selection of a site until there is no change in the composition of the sites. The simulation beginning with these initial layouts using random transition probabilities showed that the competition can lead to an entire endplate occupied by only one type of axon after losing all other types of sites at the endplate sharply; however, the competition did not show the stable co-presence of tSCs, vacancies, and a single axon after synapse elimination (Figure 5.5). Moreover, other simulations led to an endplate filled only with tSCs or a completely unoccupied endplate (Figure A1). Even with non-random, equal transition probabilities, synapse elimination did not reliably produce an endplate filled with one axon, tSCs, and vacancies where the values of P_{AV}, P_{AS}, P_{SA}, P_{SV}, P_{VA}, and P_{VS} were one-third (Figures A2 and A3). Although some degrees of randomness and/or equal degrees in the interactions might be present during synapse elimination, our simulation results demonstrated that such randomness or equal fitness is insufficient to reliably recapitulate synapse elimination. Accordingly, we assumed that tSCs, vacancies, and axons have different fixed transition probabilities at least during this period of time.

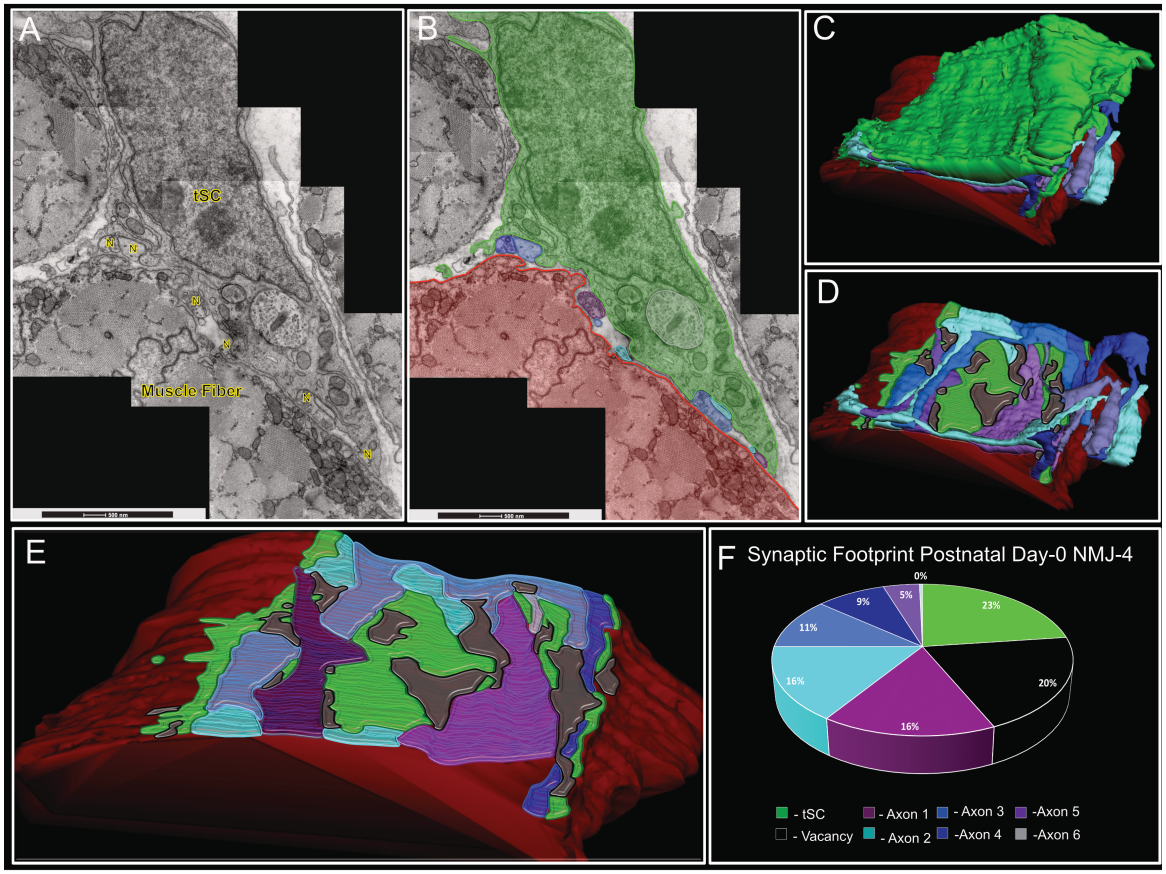

Figure 5.4: Example of P0 NMJ used to generate average starting point for modeling footprints. A, montaged section from P0 sternomastoid NMJ, muscle fiber, nerve terminals (N) and tSCs labeled. B, Same image as in A, segmented for muscle fiber (red), nerve terminals (shades of blue), and tSC (green). C, surface model of NMJ from images in A,B. tSC shown capping axon terminals atop muscle fiber. D, surface model without tSC body. Axons shown (shades of blue), with sites of tSC and vacant contacts with muscle shown (green and black respectively). E, Footprint model of all axons (shades of blue), tSC (green), and vacancies (black). F, Pie chart showing relative surface area contacts made by separate axons, tSC, and vacancies. Scale bar 500nm.

To determine their constant transition probabilities, we developed a stochastic model of synapse elimination that employs the areas of tSCs, vacancies, and axons at different postnatal days and Markov Chain methods that are widely used in biological modeling studies (Allen, 2003; Yakovlev and Yanev, 2006; Wilkinson, 2009; Armond et al., 2014; Soltani et al., 2016; Jung and Doniach, 2017). Our model assumes that tSCs and axons compete against each other as proposed from a previous study (Smith et al., 2013), but here we newly propose that the competition of tSCs and axons is mediated by

vacancies, and different types of axons compete to take over their adjacent vacancy in an endplate (Figure 5.6). Specifically, the model assumes that vacancies mediate the transition between axonal and tSC sites without their direct transition (Figure 5.6), and different axon types compete to occupy nearby sites. These assumptions allow us to describe the stochastic competition process as a Markov process (Wilkinson, 2009; Jung and Doniach, 2017). Accordingly, we have the following equations:

$$\text{Eq. 1: } P_{AA} + P_{AV} = 1 \qquad \text{Eq. 2: } P_{SS} + P_{SV} = 1 \qquad \text{Eq. 3: } P_{VA} + P_{VS} = 1$$

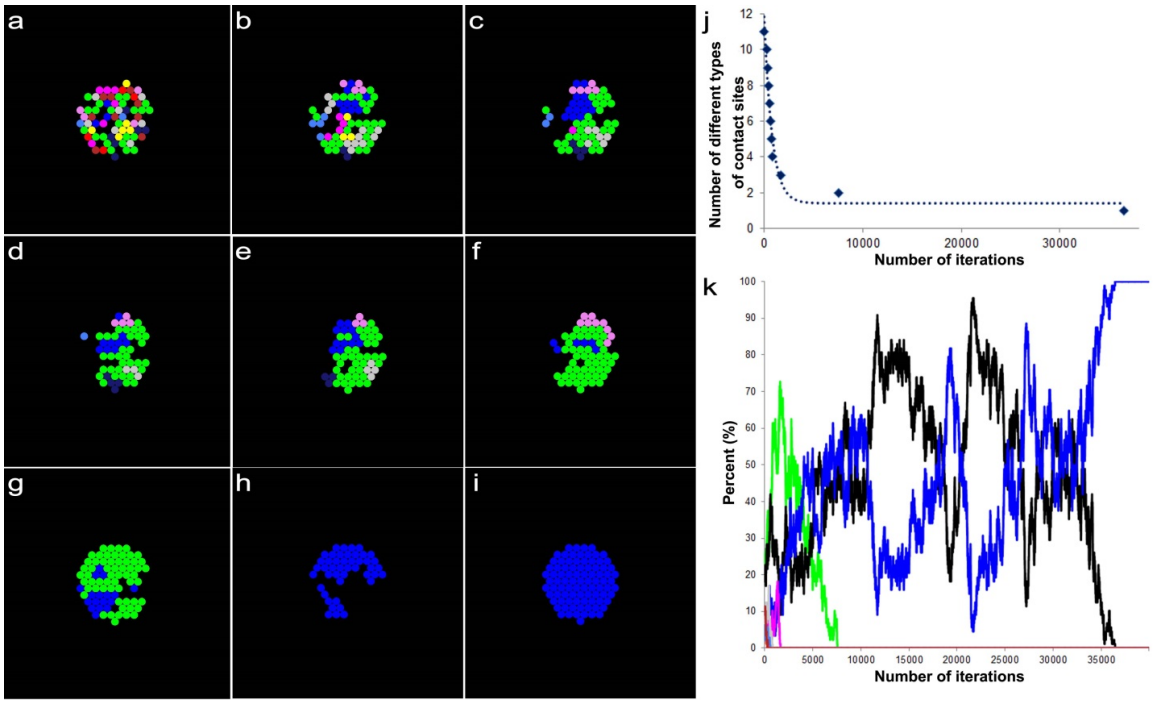

Figure 5.5. An example result based on a model of synaptic competition among axons, tSCs, and vacancies with random transition probabilities. (a) Initially, 9 different axons, tSCs and vacancies form their contact sites randomly in an endplate on a muscle fiber. The initial ratio of their total contact areas (axons:tSCs:vacancies) is about 30:16:54, which was determined from a recent serial electron microscopy study on developing muscle fibers of mouse during synapse elimination (See Methods). (b-h) The competition among axons, tSCs, and vacancies with their random transition probabilities shows elimination of multiple contact sites formed by different axons, tSCs, and vacancies at different iterations of the simulation (400, 500, 600, 700, 800, 1700, and 7600 iterations, respectively). (i) When the simulation reached 36500, synapse elimination is complete. However, only one type of axonal sites remains with no tSC and vacant sites that are present during and after synapse elimination of developing neuromuscular junctions. (j) The number of different types of contact sites in the endplate reduces sharply down to one as the iteration proceeds. (k) Change in the ratio of the contact areas formed by tSCs (green), vacancies (black), and 9 different axons (colors different from green and black) as the simulation based on a stochastic model of tSC and vacancy mediated synapse elimination proceeds.

There are only 3 independent transition probabilities (P_{AV}, P_{SV}, and P_{VS}) because P_{AA}, P_{SS}, and P_{VA} depend on P_{AV}, P_{SV}, and P_{VS} based on the assumed relationship in Eqs. 1-3. In addition, it is assumed that each synaptic site can be occupied by a neighboring axon consistent with other and our studies (Turney and Lichtman, 2012). Thus, when an individual axon occupies multiple neighboring sites near a recently vacated site, that axon has a higher probability of reclaiming that vacancy than axons with fewer sites proximal to the vacated site. As in the previous section, we constructed the initial layout of the endplate composed of multiple contact sites made by tSCs (green), vacancies (black), and axons (other colors) using the empirical data at P0.

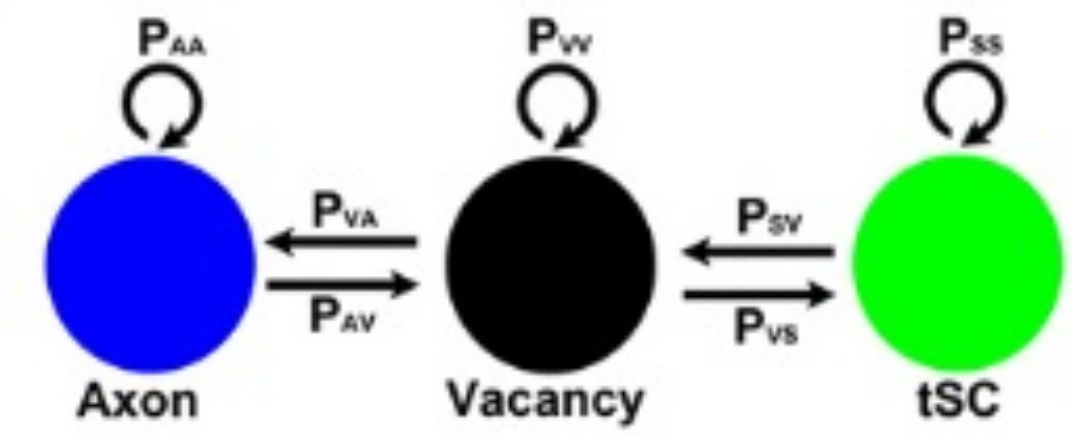

Figure 5.6. Schematic diagram of vacancy mediated competition between tSCs and axons. A model of competition between axonal and tSC sites assumes that tSC-axon competition to occupy the territory of the endplate is mediated by their adjacent vacancies. Accordingly, a synaptic site formed by an axon has two different transition probabilities: the probability of transitioning from an axonal site into a vacancy (P_{AV}) and a probability of no transition (P_{AA}=1-P_{AV}). Similarly, a synaptic contact site formed by a tSC has two different transition probabilities: a probability of transitioning into a vacancy (P_{SV}) and a probability of no transition (P_{SS}=1-P_{SV}); a vacant site that are not an axonal site either a tSC site has two different transition probabilities: a probability of transitioning into an axon (P_{VA}) and a probability of transitioning into a tSC (P_{VS}).

Again these initial layouts (Figure 5.7a, f, and k) depict the relative ratio of the contact sites' areas measured in the P0 data sets and randomly distribute tSC, vacancy, and axon sites in an endplate. Then, the competition process among them was iterated by repeating the random selection of a site in the layout until only one axon (identified by color) remained. As shown in Fig. 5.7, the model with fixed transition probabilities, determined using the measured relative areas of axons, tSCs, and vacancies at P3, reliably reproduced synapse elimination. The results showed that the number of different axons decreases exponentially consistent with other studies (Brown et al., 1976; Barber and Lichtman, 1999; Turney and Lichtman, 2012). The results also showed that the contact sites of tSCs, vacancies, and axons in an endplate interchange dynamically as different axons compete against each other (Fig. 5.7); when synapse elimination is complete, the endplate is occupied by tSCs, vacancies, and only one axon (Fig. 5.7 i-k). The rate of synapse elimination is known to vary between different muscles and even between fibers in the same muscle (Jansen and Fladby, 1990). Consistently, when we repeated the simulation 100 times, the number of iterations varied broadly (the inset of Fig. 5.7k); the average iteration to complete synapse elimination was 10300 ± 6719 (SD). Furthermore, direct measurements of the relative ratios of tSCs, vacancies, and axons at P3 were different from one endplate to another (Fig. 5.8a). Accordingly, it is reasonable to expect that our model using the different ratios may exhibit variable rates of synapse elimination. As expected, simulation results of our model with the different ratios of the 8 measured endplates showed that synapse elimination is complete at very different numbers of iterations, thus variable rates of synapse elimination (Fig. 5.8b). Despite such broad variation, we noted that the number of iterations needed to complete synapse elimination is fewer on average

with large relative areas of tSCs and/or vacancies than those with small relative areas (Fig. 5.8b) suggesting that tSC and vacancy occupation are closely related to the rate of synapse elimination.

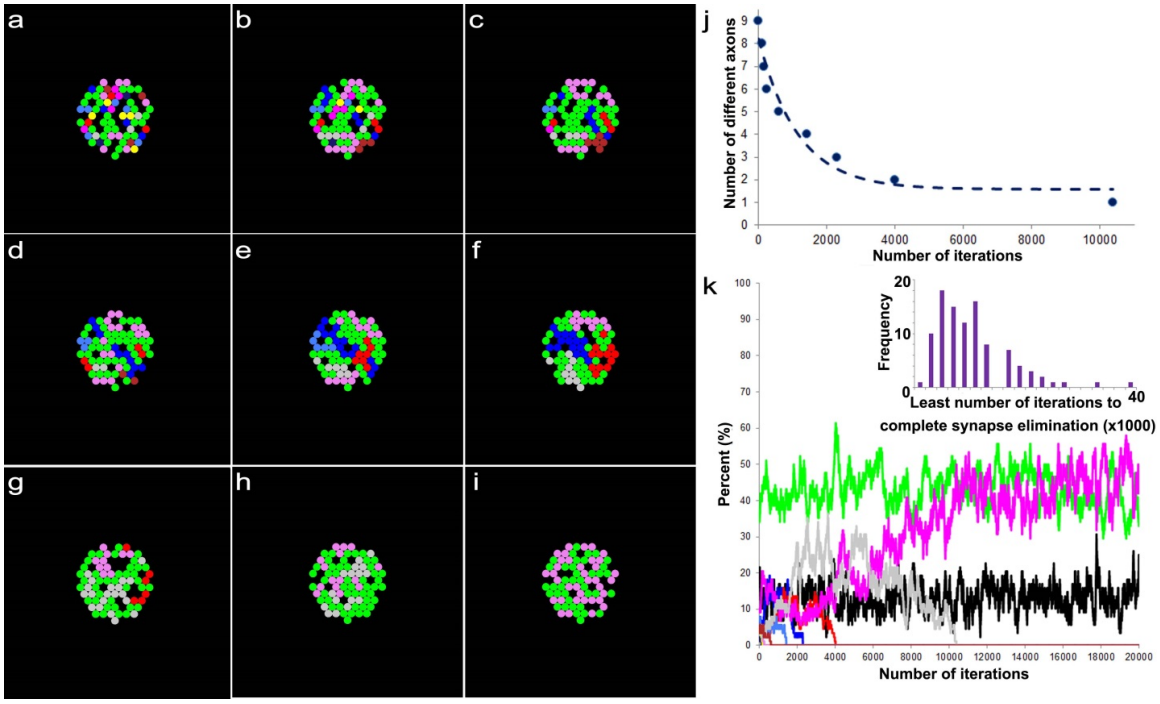

Figure 5.7: An example result based on a model of synaptic competition among axons, tSCs, and vacancies with different constant transition probabilities derived from the area ratios at P3 of the NMJs. Simulations carried out using the same configuration as described in Fig. 3, but the final ratios of tSCs, vacancies and axons are set to be 0.57, 0.18, and 0.25, respectively, which are the ratios at P3 of the NMJs. (a) Initially, 9 different axons, tSCs and vacancies form their contact sites randomly on a muscle fiber with the initial ratio of their total contact areas (axons:tSCs:vacancies), which is about 30:16:54 as Fig. 3. (b-h) The competition among axons, tSCs, and vacancies with their random transition probabilities shows elimination of multiple contact sites formed by different axons, tSCs, and vacancies at different iterations of the simulation (100, 200, 300, 700, 1500, 3400, and 4100 iterations, respectively). (i) When the simulation is at 10,400 iterations, the competition leads to a complete synapse elimination with tSC and vacant sites present demonstrating that optimal transition probabilities reliably simulate synapse elimination. (j) The number of different types of axons in the endplate reduces sharply as the iteration proceeds. (k) Change of ratios of the contact areas formed by tSCs (green), vacancies (black), and 9 different axons (colors different from green and black) as the simulation based on the stochastic model of tSC and vacancy mediated synapse elimination proceeds. Inset: the distribution of the least number of iterations when synapse elimination is complete from 100 repeated simulations.

5.4 Synapse elimination correlated with relative footprint coverage areas of tSCs, vacancies, and axon terminals

To examine the correlation of the rate of synapse elimination with the relative areas of tSCs, vacancies, and axons with regard to their inter-dependence, we combined the relative areas into a composite area by dividing the product of the area of tSCs and that of vacancies by that of axons (Fig. 5.8c). The composite area was found to be negatively correlated with the number of iterations to complete synapse elimination (Spearman Correlation, $p<0.05$) as shown in A4b; the same correlation analysis using manually adjusted relative areas also showed that the composite area is negatively correlated with the number of iterations to complete synapse elimination (Spearman Correlation, $p<0.05$) as shown in A4 indicating that the composite area is positively correlated with the rate of synapse elimination. It is also reasonable to expect that the rate of synapse elimination decreases over time because the synapse elimination is complete in several weeks after birth. As expected, the simulation using the average ratio at P7 showed that synapse elimination is complete after 15700 iterations on average, which is markedly greater than that at P3 (A5). The average iterations needed to complete synapse elimination between P3 and P7 were found to be significantly different ($n=100$, t-test $p<0.05$) indicating that the rate of synapse elimination is slower at P7 than P3. Similarly, simulations using average ratios at P16 showed completed synapse elimination after 15000 iterations on average, also significantly greater than at P3 (A6). The average iterations needed to complete synapse elimination were significantly different between P3 and P16 ($n=100$, t-test $p<0.05$) indicating that the rate is less at P16 than that at P3.

Our results are consistent with our expectation of a decreasing rate of synapse elimination over time. Though the average iterations of the complete synapse elimination between P7 and P16 were not significantly different (t-test, $p = 0.59$), this suggests that the rate has already reached its minimum around P7.

5.5 Synaptic activity-dependent selective and accelerated synapse elimination

It is widely held that synaptic activity is closely related to normal synapse elimination; several experimental studies support that axons having higher synaptic activity tend to remain at their endplate (O'Brien et al., 1978; Thompson, 1983; Magchielse and Meeter, 1986; Nelson et al., 1993). To test whether our model can predict this activity dependent synapse elimination, we assumed that among 9 different axons, one, selected at random, is more active than the others and the active axon sites have 2-fold lower probability of forming a vacancy than other, less active axons (See Methods). We generated the initial layouts using the average relative ratios of tSCs, vacancies, and axons at P0 and determined their transition probabilities using the average relative areas at P3 in the same way with the previous sections. Our simulation results showed that the active axon was the winner with the probability of 97%, consistent with the studies on synapse elimination and synaptic activity. Furthermore, the results showed that synaptic activity accelerates the rate of synapse elimination four-fold compared to that of control NMJs (Fig. 5.8d). When two axons were set to be more active than the others, our simulations predicted that the winning axon came from the active axons with the probability of 98%. Additionally, two active axons further accelerated synapse elimination but only by 10%, indicating that multiple coherently active axons in an endplate weakly promotes competition leading to little or no additional acceleration of synapse elimination (Fig5.8d).

Increasing the number of active axons slowed synapse elimination and the rate became even less than when no axons were assumed to be more active (Fig. 5.8d). This demonstrates that our model can account for activity-dependent axon selection, and the acceleration and delay of synapse elimination it predicts are consistent with other experimental studies (O'Brien et al., 1978; Thompson, 1983; Busetto et al., 2000; Favero et al., 2010; 2012).

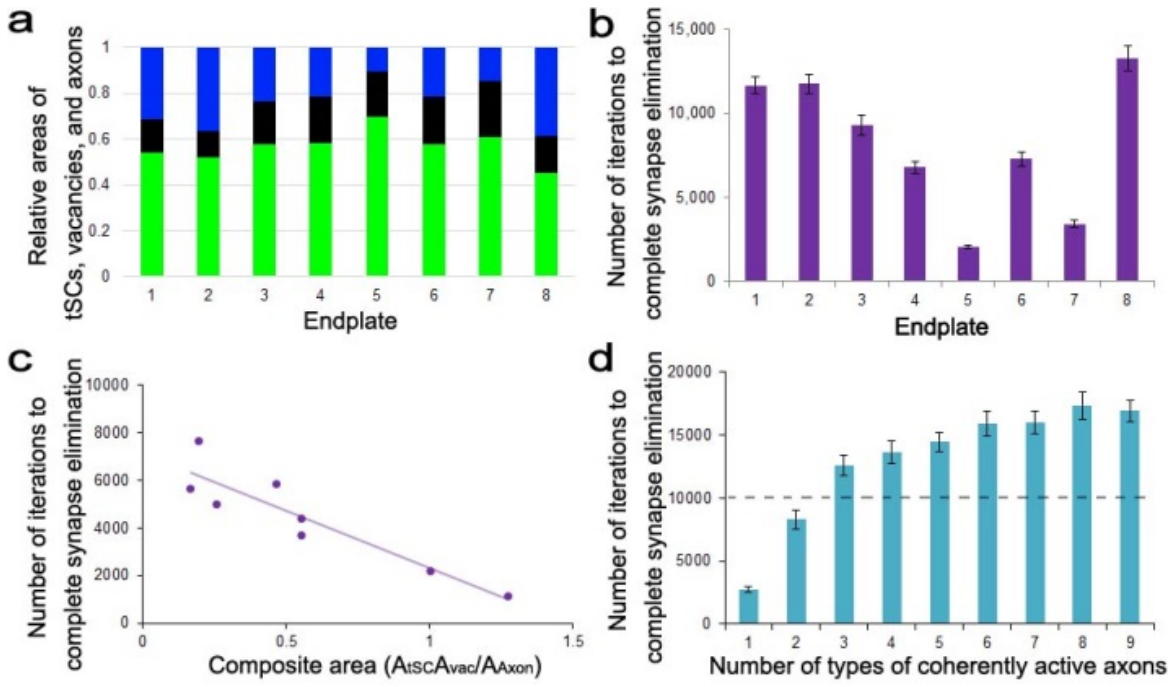

Figure 5.8: Relationships of the simulated average least number of iterations to complete synapse elimination with different ratios of contact areas of tSCs, vacancies, and axons and with synaptic activity. (a) Measured average ratio of contact areas of tSCs (green), vacancies (black), and axons (blue) from each of the 8 different endplates at P3. (b) The average least number of iterations to complete synapse elimination for each of the measured ratios by repeating the simulations 100 times for each. Error bars are standard errors. (c) Negative correlation of the composite area of (a) with the least number of iteration to complete synapse elimination (Spearman correlation, $p<0.05$). (d) Synaptic activity dependent synapse elimination. The simulation repeated 100 times as the number of active axons increased from 1 to 9. The average number of iteration to complete synapse elimination ratio obtained with the average ratio of the areas at P3 (57:18:25) was used as a reference rate of synapse elimination for comparison, and it is represented as a dotted line. When one to three different axons out of nine different axons in the endplate were active, synapse elimination accelerated. In contrast, when more than three different nerves were active, synapse elimination slowed down.

5.6 Discussion

This study developed a stochastic model of synapse elimination that, for the first time, incorporates classical interaxonal competition with the recently proposed competition between tSCs and axons, predicting that the competition is mediated by vacancies, a third endplate occupant. With serial electron micrographs from 25 different developing mouse NMJs, the model employed the relative contact areas of tSCs, vacancies, and axons on muscle fibers as key parameters to determine the degrees of their interaction. Results of the model simulations reliably exhibited co-existence of axons with tSCs and vacancies during synapse elimination and when synapse elimination was complete. Furthermore, our model successfully simulated expedited synapse elimination with synaptic activity, and predicts that the rate of synapse elimination varies during development. By including the relative ratios of the contact areas of these structural components, we can better understand their roles and the mechanisms underlying impaired and enhanced synapse elimination and the development of neural systems.

Interaxonal competition and competition with tSCs for their adjacent vacancies

A competitive process among axons innervating the same muscle fiber is thought to play an important role in synapse elimination. At P0 each axon occupies a similar proportion of the endplate area, so it is impossible to determine which axon will remain after synapse elimination by comparing their areas at this stage. Within days, however, some axon sites are vacated and the vacant sites taken over by different axons leading to the eventual loss of all but one axon. Accordingly, it is reasonable to assume that a vacancy can form randomly by the removal of an axon from the endplate of a muscle fiber.

Any axons in proximity are expected to compete for the newly vacated site. Such competitive processes have been observed in experimental studies and examined theoretically in several modeling studies (Willshaw, 1981; Barber and Lichtman, 1999; Turney and Lichtman, 2012). Specifically, in a model based on evolutionary graph theory, synaptic rearrangement occurs in a neuromuscular junction filled with several different axons; after random removal of sites, neighboring axons with equal fitness compete for the vacated sites, the model successfully simulated the competitive process of synapse elimination (Turney and Lichtman, 2012). However, though they occupy the endplate alongside axons, a role for Schwann cells in synapse elimination (Smith et al., 2013; Lee et al., 2016) is not considered in the model. Since this model is designed to allow only the winning axon to remain after synapse elimination, the coexistence of tSCs and vacancies with it is neither accounted for nor possible (See Fig. 4.5, A1, A2, and A3). While previous studies provided indirect evidence for Schwann cell-axon competition during synapse elimination and propose a qualitative model of Schwann cell mediated synapse elimination (Smith et al., 2013), this and other studies did not provide a quantitative model to characterize such a direct role for Schwann cells.

With respect to vacancies as mediators of competition, we assumed random occurrence of a vacancy in a muscle fiber endplate similar to random competition models of different axons for synapse elimination (Turney and Lichtman, 2012). Furthermore, we extend the random competition to tSCs by assuming that a vacancy can form by removing an axon or a tSC from an endplate. It is reasonable to assume that a vacancy can be formed by removing a tSC from an endplate with the concomitant competition for the

vacated site if a random competitive process occurs between tSCs and axons (Smith et al., 2013; Lee et al., 2016). We assumed that their transition probabilities are closely related to their relative contact areas as determined using their relative areas based on the Markov Chain method, a technique increasingly used to understand the probabilistic behavior of the dynamic stochastic mechanisms associated with biological processes (Wilkinson, 2009). According to our model, axons and Schwann cells do not have equal fitness for taking over vacancies, and assignment of equal or random fitness rendered synapse elimination unreliable (See A1, A2, and A3).

A recent study reported that the relative area occupied by tSCs peaked from P3-P7 compared to the area at P0 and P16, proposing a mechanism of synapse elimination in which tSCs directly compete against axons to take over an endplate. A study by others examining NMJs of soleus muscles of P7-P8 mouse reported that tSCs have different Ca^{2+} responses to weak and strong axons, and proposed another mechanism whereby tSCs differentiate weak axons from strong axons and are involved in selectively removing weak ones, supporting the active role of tSCs in synapse elimination (Darabid et al., 2013). Furthermore, a recent study reported that overexpression of NRG1-III enhanced tSC activity and expedited synapse elimination while reduced NRG1-III slowed synapse elimination (Lee et al. 2016). Those studies raise the possibility that increases in the relative area of tSCs may speed up synapse elimination. When we modified the relative area of tSCs in our models, simulations reflected an enhanced rate of synapse elimination, consistent with the study.

Furthermore, our model predicted that an increase in the relative area of vacancies would enhance synapse elimination more significantly than increasing tSC area alone.

Based on the results, it is expected that relative areas of vacancies are large during the most active phase of synapse elimination. As expected, our measurement of the areas showed that the large relative area of vacancies maintained until P3 whereas the large relative area of tSCs appears between P3 and P7. Such differences may be closely related to the level of tSC activity and tSC-involved mechanisms of regulating the rate of synaptic elimination.

Activity-dependent synapse elimination

Synaptic activity is known to affect the rate of synapse elimination, and a number of studies have concluded that although synaptic activity itself is not a sole decisive factor of synapse elimination (Callaway et al., 1987; Barry and Ribchester, 1995; Costanzo et al., 2000), relatively active axons have competitive advantage (O'Brien et al., 1978; Srihari and Vrobova, 1978; Thompson et al., 1979; Brown et al., 1982; Duxson, 1982; Ding et al., 1983; Ribchester and Taxt, 1983; Ridge and Betz, 1984; Fields and Nelson, 1992; Balice-Gordon and Lichtman, 1994; Personius and Balice-Gordon, 2001; Sanes and Lichtman, 2001; Buffelli et al., 2002; Buffelli et al., 2003; Personius et al., 2007; Favero et al., 2012). Presynaptic block by tetrodotoxin and botulinum toxin and postsynaptic block by α-bungarotoxin and curare led to the prolonging of synapse elimination (Srihari and Vrbova, 1978; Thompson et al., 1979; Brown et al., 1982; Duxson, 1982; Ding et al., 1983).

Electrical stimulation of the nerves of 6-7 day old rat pups at 8 Hz for 4-6 hours per day for 2-4 days was found to decrease the level of polyinnervation from ~85% to ~50% (O'Brien et al., 1978); furthermore, electrical stimulation of muscles also was found to accelerate synapse elimination (Thompson, 1983).

From these studies, it is reasonable to expect that enhancing synaptic activity accelerates synapse elimination and provides the active axon with an advantage. Consistent with prior studies, our simulation results showed that an active axon is more likely to win sole occupancy of the endplate and that such synaptic activity accelerates synapse elimination. Furthermore, our model predicted that when two different axons have the same degree of high synaptic activity compared to other axons, the effect of accelerating synapse elimination is significantly weakened. Our model also predicted that when more than two different axon types have the same degree of high synaptic activity, synapse elimination slows rather than accelerates, suggesting that multiple coherently active axons delay synapse elimination instead of accelerating it. Interestingly, this is consistent with several studies reporting that asynchronous synaptic activity promotes synapse elimination whereas synchronous synaptic activity delays it (Fields and Nelson, 1992; Costanzo et al., 2000; Personius and Balice-Gordon, 2001; Buffelli et al., 2002; Personius et al., 2007; Favero et al., 2012).

As with any model of a biological process, it is impossible to describe all factors in play. For example, intrinsic differences in fitness among multiple axons may be present and the contribution of muscle fibers, such as neurotrophic factor release or removal of acetylcholine receptors (Thompson, 1983; Nelson et al., 1993), may influence the process of synapse elimination.

Such differences are not considered in our model because there are no reliable structural correlates with them yet. Despite these limitations, our stochastic model (see Fig. 5.9) reliably simulates synapse elimination, agrees well with the observed coexistence of Schwann cells, vacancies and axons at endplates at its conclusion, and provides an

explanation of the different dependences of synapse elimination on synchronous and asynchronous synaptic activities. Furthermore, the model reveals a novel role for vacant sites in synapse development closely related to the competition between tSCs and axons. Testing the predictions made by the stochastic model of synapse elimination at single and multiple endplates would contribute to our more complete understanding of synapse elimination and offer insights into the nature of synapse development and network refinement.

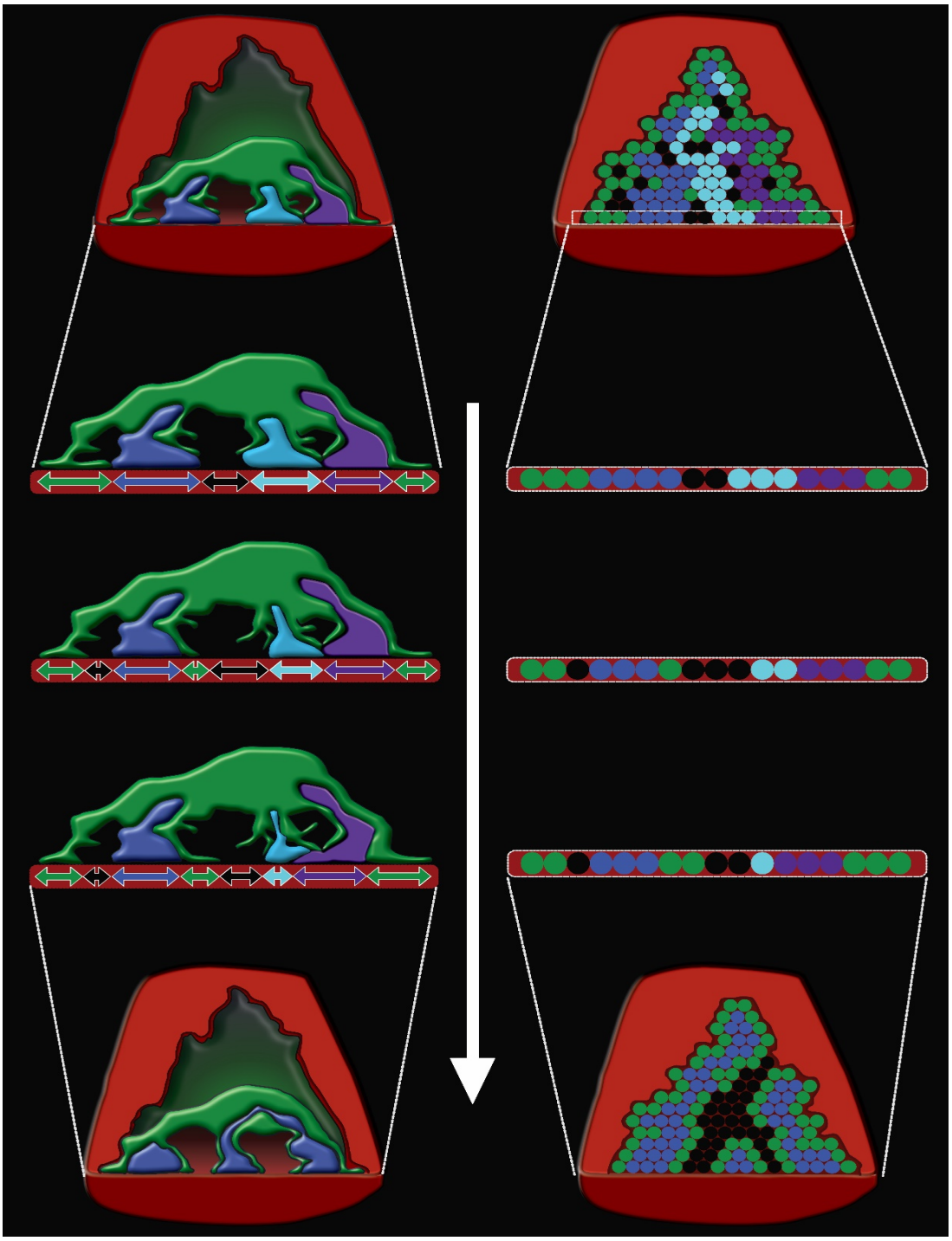

Figure 5.9: A stochastic model of tSC and vacancy mediated synapse elimination. According to the model, a vacant site or vacancy in an endplate of a muscle fiber forms randomly by a removing tSC or nerve terminal of an axon. Subsequently, the vacancy is taken over by adjacent axons or tSCs. The probabilities of their taking over are positively correlated with their relative contact areas. In other words, the greater the contact area of an axon or a tSC surrounding the vacancy is, the greater the probability of its taking over the vacancy is. When the synaptic activity of an axon is greater than other axons in an endplate, the probability of the axon's taking over is greater than other axons consistent with previous and other studies. Furthermore, our model newly predicts that as the relative area of the vacancy in an endplate increases the synapse elimination speeds up raising a testable hypothesis that both the measurable relative areas of vacancies and tSCs are important structural correlates of the rate of synapse elimination.

5.7 Methods

As previously published, 20 different serial electron microscopy data sets from sternomastoid muscles of wild-type C57B/6 mice of either sex were analyzed (Smith et al. 2013, Lee et al. 2016). The mice were obtained from the Jackson Laboratory, bred in a colony at the University of Texas at Austin and Texas A&M at College Station, and killed on the day of birth (P0; n=10), the third postnatal (P3; n=8), and the sixteenth postal natal days (P16; n=2). Experimental procedures were approved by the Institutional Animal Care and Use Committees at the University of Texas and Texas A&M University. The generation of wild-type mice and their sample preparation for electron microscopy for mice of P0, P3, and P16 have been described previously (Smith et al. 2013, Michailov et al. 2004, Li et al. 2011). Simply, animals were perfused transcardially with 0.1M sodium cacodylate buffer, pH 7.4, followed by the same buffer containing 2% paraformaldehyde and 3% glutaraldehyde. Sternomastoid muscles were removed and fixed overnight at room temperature in the same fixative. Muscles were washed with cacodylate buffer and stained en bloc in 1% osmium tetroxide, 1% ferrocyanide in cacodylate buffer for 5 h, washed with water, and then stained in 1% aqueous uranyl acetate for 2 h. Muscles were dehydrated in graded alcohols and acetone, then embedded in Epon 812. Regions containing neuromuscular junctions were located by thick (0.5 – 1 μm) sections made on a Leica Ultracut UTC Ultramicrotome with glass knives, stained with 1% toluidine blue, and examined under a light microscope. Blocks were further trimmed using a 45 degree cryotrim tool (Diatome) and serial 65 nm (silver) sections cut with a 35 degree diamond knife (Diatome). Sections were mounted on formvar-coated Synaptek slot grids (Electron Microscopy Sciences) and observed under a FEI Technai Spirit electron microscope with

an AMT Advantage HR digital camera. NMJs were identified by the apposition of nerve terminals to within ~50 nm of the muscle fiber surface in the presence of SCs. Digital images of individual NMJs and the immediately surrounding area were captured from each section at a magnification of 16,500x. At this magnification, ~6-12 overlapping images were acquired to include the entire extent of the NMJ. These individual images were then montaged by manual manipulation in Adobe Photoshop to create a single image. Such montaged images over 70-150 serial sections were then imported into the software program Reconstruct (Fiala, 2005) and calibrated based on section thickness and known distances in the specimen. In software, the montage in each section was aligned linearly to each adjacent montage using 6-8 objects common in both and starting with the central montage in the stack and working toward each the first and last montage. Once aligned, structures of interest in each section were segmented (traced) using the tools provided in the software. Measurements and 3D renderings of these structures were then generated in software.

Tissues of the mice at the seventh postnatal day (P7) were prepared differently and imaged using serial-block-face scanning electron microscopy (SBSEM). Tissue preparation and staining was done with compliance to Renovo Neural Inc. (Cleveland, OH). Briefly, P7 C57/Bl6 mice were transcardially perfused with 2.5% glutaraldehyde and 4% paraformaldehyde in a 0.1M sodium cacodylate buffer. Sternomastoid muscles were then removed and stored in perfusion solution for 1 day prior to staining. Tissue was then stained with uranyl acetate and osmium-ferrocyanide, followed by graded-dehydration and embedded in Epon resin. SBSEM image data sets of postnatal day 7 NMJs were acquired at Renovo Neural Inc. (Cleveland, OH). A sample image is shown in figure 5.1e. The

tissue blocks were mounted, examined, and sectioned in a Zeiss Sigma VP scanning electron micro-scope equipped with a Gatan 3View in-chamber ultra-microtome stage with low-kV backscattered electron detectors optimized for 3View systems. Neuromuscular junctions were initially identified within cross-sections of muscle tissue by axon terminals in direct apposition to junctional folds on the muscle fiber membrane and capped by terminal Schwann cells. Regions of interest were chosen to include the neuromuscular junctions in whole cross-section. The first sample block was sectioned cross-sectionally along the long axis of the muscle fibers. A series of 465 EM images in a field size of 130 μm × 50 μm were acquired at 2.2 kV with a resolution of 8.1 nm per pixel and 90 nm per slice. Eight NMJs were captured at P7 with 5 of those NMJs fully reconstructed for synaptic contact areas as described previously for data sets acquired with traditional serial TEM.

We used circular contact sites assuming that all of the sites are composed of 9 different axons, tSCs, and vacancies consistent with our observation of them from 2D scanning electron microscope images, and their initial layout is generated based on the recently reported ratios of contact areas of the tSCs, vacancies, and axons at P0.
To simulate the initial layout, it is assumed that tSCs take up about 30% of the total area, which is covered by tSCs, vacant sites about 16%, and axons about 54%, based on their recently measured ratios at P0. All of the sites are randomly formed within a round region of a diameter of 300 pixels, and each site has a diameter of 30 pixels as shown in Figs. 5.5 and 5.7 and all the supplemental figures. Vacant sites are black, tSC sites green, and axonal sites in different colors (blue, red, dark blue, yellow, pink, purple, dark green, gray, and

brown). Thus, each of the 9 different axons takes up about 6% of the total area. Examples of randomly generated initial layouts at P0 are shown in Figs. 5.5a and 5.7a.

We used the optimal probabilities accounting for the synapse elimination and all the ratios of different kinds of synaptic sites using a Markov chain model (Jung and Doniach 2017) assuming that the ratio of their contact areas with a muscle fiber in a neuromuscular junction reflects the efficiency of synapse elimination. We noted that at P3, the ratio of the contact areas of tSC sites greatly increased and gradually decreased later on raising a possibility that the ratio of the areas of tSC sites plays an important role on the process of synapse elimination consistent with the recent study (Smith et al., 2013). Accordingly, the measured ratio of the contact areas of tSC sites, vacancies, and axonal sites at P3 was used here to obtain the optimal transition probabilities by determining the probabilities that can stabilize the ratio using Eq. 4 based on the Markov Chain properties (Jung and Doniach, 2017).

$$\vec{r}_f \begin{bmatrix} P_{SS} & P_{SV} & 0 \\ P_{VS} & 0 & P_{VA} \\ 0 & P_{AV} & P_{AA} \end{bmatrix} = \vec{r}_f \begin{bmatrix} P_{SS} & 1-P_{SS} & 0 \\ P_{VS} & 0 & 1-P_{VS} \\ 0 & P_{AV} & 1-P_{AV} \end{bmatrix} = \vec{r}_f \qquad \text{Eq. 4.}$$

where $\vec{r}_f$, a vector having the final ratios. We have used the average ratios of the developing NMJs at different postnatal days ranging from P0 to P16 as shown in Table 5.1.

Table. 5.1 Average ratios of the contact area of tSCs, mouse NMJs measured at P0, P3, P7, and P16 (n=10, 8, 5, and 2, respectively).

Postnatal days	tSC	Vacancy	Axon
P0	31%	17%	52%
P3	57%	18%	25%
P7	55%	5%	40%
P16	41%	6%	53%

Then, transition probabilities were adjusted to generate the final ratios close to those obtained at P3 from our previous study ($\vec{r}_f$; (Smith et al., 2013)) using multiple neuromuscular junctions of neonatal mice. According to Eq. 4, two independent variables of all the three independent variables can be expressed in terms of the remaining independent variable. Thus, there is only one undetermined transition probability in the matrix. We chose the transition probability from a vacancy to a tSC site (P_{VS}) as the undetermined probability. As P_{VS} is varied, the rest of the transition probabilities are determined using the value of P_{VS} and the ratio at P3. Then, for each specific P_{VS}, the process of the synaptic elimination was iterated until it was complete. But it was noted that for some values of P_{VS} a few other transition probabilities happened to be negative or undetermined. Thus, the value of P_{VS} was set as 0.6, which allowed us to use all of our measured ratios of tSCs, vacancies, and axons such as those of multiple mouse neuromuscular junctions at P3, P7, and P16 and ensured that all the other transition

probabilities were reliably computed from our measured ratios; for the specific P_{VS}, the process of the synaptic elimination was iterated until it was complete or the number of iteration reached a specified maximum number of iteration that was sufficient for completing the synapse elimination (See Figs. 5.7-8, A5, and A6).

To simulate the synaptic activity dependent synapse elimination, the initial layout was constructed in the same way. By assuming that only a type of axons is active in an endplate, all the sites of the active axon among 9 different axons was selected and we set the probability of randomly forming a vacancy for all the sites excluding those of the selected axon to be two times greater than those of the selected axon; then as described above, the process of synapse elimination was iterated until it was complete or the number of iteration reached a specified maximum number of iteration that is sufficient for completing the synapse elimination. We also assumed that more than one type of axons is active in an endplate. In the case, we set the probability of randomly forming a vacancy for all the sites excluding those of the two axons to be two times greater than those of the selected axon (See also Fig. 5.8d).

Because each transition probability might fluctuate randomly, first all of the probabilities are assumed to be random. In each step of the simulation, a contact site from all the sites in an endplate was randomly chosen. Then the site is converted into a different site with randomly assigned transition probabilities. The step was repeated more than 10000 times to ensure that only one type of axonal site survived at most as shown in Fig. 5.5 and A1.

We assumed that all of the probabilities are fixed and the same. Using all the sites randomly assigned in the same way described above, at each step a contact site was randomly chosen from them and transitioned using the transition probabilities of neighboring axons, tSCs or vacancies where all of the probabilities are equal to 0.333. The process was repeated 200000 to make sure that only one type of synaptic site survived at most as shown in A2 and A3.

In order to perform the simulations, a PC computer was used loaded with Windows 7, IDL (Interactive Data Language) and a program written in IDL based on the Markov chain model described previously was employed for the simulations.

CHAPTER VI

SUMMARY

6.1 Introduction

The ability to navigate our environment and perform a vast array of complex mental and physical tasks along with simple yet vital aspects of our lives, such as, eating and breathing are all made possible by the intricate circuitry of our nervous systems. The proper functioning of these neural circuits requires coordination of billions of presynaptic neurons and their postsynaptic target cells that communicate through impulse transmission, where neurotransmitters released from the presynaptic cell act on specific receptor populations on the postsynaptic cell allowing information to pass between the two. Accordingly, the efficacy and specificity between pre and postsynaptic components of these synapses must be highly regulated and carefully constructed to allow such incredible control over the behaviors we perform. Humans and other mammals do not emerge from the womb with this level of precision in neural circuitry; rather it is largely refined over the course of postnatal development. In early life there are abundantly more synapses than are present in the adult due to an over-convergence of presynaptic inputs onto postsynaptic target cells. In a process termed “synapse elimination”, many of these physical synaptic connections are lost, reducing the overall number of synapses present, as less appropriate and/or efficacious synapses are eliminated. Indeed many neurological disorders and diseases are linked to irregularities in the process of refining synapses during development. Thus, identifying the cellular and molecular interactions that influence this process at

individual synapses is integral to gaining a more comprehensive understanding of how nervous systems are formed and refined during development.

Many of the principles of synaptic maturation observed in the central nervous system also apply to synapses in the peripheral nervous system, between presynaptic motor axons and their postsynaptic target muscle fibers at NMJs. In my studies, I utilized these relatively larger and more accessible synapses to examine the process of synapse elimination. Although synapse elimination has been well studied at NMJs, the primary focus has been on the behavior and morphological changes of the motor axons and the postsynaptic muscle fibers. Much less attention has been given to examining the behavior of terminal Schwann cells (tSCs), the glia of NMJs, during the process of synapse elimination at developing neuromuscular junctions. In recent years mounting evidence suggest that glia play an important role in the process of synapse elimination in the central nervous system and provide the basis for my hypothesis that tSCs must be involved in the pruning of motor axons at NMJs as they transition from multi- to singly innervated synapses during the early postnatal process of synapse elimination. Thus, the more specific aim of these experiments was to characterize the behavior of tSCs during the period of synapse elimination and to identify their role in the process.

Although aspects of tSC behavior during the maturation of NMJs have been examined in previous studies, my study stands alone as the most-detailed comprehensive observation of tSCs at developing NMJs. In the course of performing these studies, I have documented novel behaviors of tSCs that indicate they play a role in sculpting aspects of both presynaptic and postsynaptic morphology at NMJs during the period of synapse elimination. In this final chapter, I will summarize the major findings of the experiments

performed in chapters 2 – 5, the relevance of my findings to the literature, and what next steps may be taken to expand our understanding of synapse elimination and the role of tSCs in the process.

6.2 Terminal Schwann cells aid in achieving single innervation of NMJs through phagocytic pruning of presynaptic motor axon terminals

tSCs have been shown to be phagocytic as axons retract and after peripheral nerve injury (Bishop et al., 2004; Song et al., 2008), however this is the first report of this behavior with regard to pruning intact axon terminals at the synaptic interface. Although this is the first documentation of glial mediated elimination of presynaptic axons in the periphery, similar observations have been made from studies examining microglial pruning of presynaptic inputs on hippocampal dendrites and in the binocular zone of the lateral geniculate nucleus (Paolicelli et al., 2011; Schafer et al., 2012). Interestingly, some molecules in this phagocytic activity by glial cells have been identified and suggested to delay the process of synapse elimination if genetically ablated (Song et al., 2008; Schafer et al., 2012; Lee et al., 2016). This delay would indicate that tSC phagocytic activity is an important factor to the progression of synapse elimination and reaching synaptic maturity. Although this has brought a new understanding to tSC roles in synapse elimination, more research is needed to clearly identify how these interactions occur. One interest in the extension of this work is to examine the phagocytic pathways in tSCs and identify candidates for further experiments. For example, in the microglial work discussed above, Schafer and colleagues identified a relationship between immune receptors on the microglia and their ability to perform appropriate synaptic pruning in the developing lateral

geniculate nucleus. It has also been suggested that the complement system may play a role in the process of neuromuscular synapse elimination with regard to neuronal identity (Tetruashvily et al., 2016). An interesting extension of this work would be to investigate the immuno-recognition between tSCs and motor axons at developing neuromuscular junctions. For example, do tSCs also express similar receptors as those shown in microglia and whether genetic manipulation of these receptors could modify the process of synapse elimination? Variations of these experiments could also be designed to assess potential selectivity between individual tSCs and motor axons during the period of synapse elimination.

6.3 Terminal Schwann cells compete with axon terminals for postsynaptic occupation during the process of synapse elimination

Competition is difficult to state definitively, however, several of our observations support this characterization of competition between tSCs and axon terminals. The EMs of neonatal NMJs show tSCs consistently appose the muscle surface just as closely as the axon terminals do, a feature not observed in the adult. Although this is the first study to perform thorough analysis of tSC apposition to the postsynaptic membrane at the endplate, it is supported by incidental reports of this relationship in previous studies (Birks et al., 1960; Matthews-Bellinger and Salpeter, 1983; Hesselmans, 1993; Tapia et al., 2012). Not only are the tSCs in contact with the postsynaptic membrane, the degree of contact is quite substantial, with tSCs occupying more postsynaptic landscape than axon terminals by postnatal day 3 and for most of the period of synapse elimination. The extensive coverage of the postsynaptic membrane at early postnatal time-points was surprising, as the contacts

of the tSCs at the adult NMJ have been consistently observed to be confined to the nonsynaptic surface of the axon terminals and contacting the muscle fiber at the edges of axon terminals (reviewed in Sanes and Lichtman, 2001). Thus, the extensive postsynaptic contact by tSCs appears to be transient to the period of synapse elimination and their processes are retracted upon single innervation in the adult. Another indication that the tSCs are competing with axon terminals for postsynaptic coverage comes from analysis of the their coverage in synaptic footprint models generated from serial EMs at different time-points during early postnatal development. In the act of making contact with the muscle fiber membrane, tSCs appear to be displacing the contacts of axon terminals. Evidence for this displacement in competition comes from serial EM at additional time points in postnatal development in chapter 3 and 5. With this additional imaging, we find that postsynaptic apposition by tSCs is less than that of axon terminals at birth, but increases substantially by postnatal day 3, whereas the axon terminal contact is decreased in that same time. The simultaneous expansion of tSC coverage and reduction in axon coverage indicates that the tSC expansion is not just to regions that are devoid of axon contact, rather, tSCs are displacing axon terminals as they extend their coverage. tSC displacement of axon contacts is easily noted when examining EMs of neonatal NMJs. Here, tSCs are observed intercalated between axon terminals and the muscle fiber surface, rather than just spanning gaps between adjacent axon terminals at the muscle fiber surface. The intercalation of tSCs between axon terminals and the muscle fiber membrane is reminiscent of reports of “synaptic stripping” by glial cells at recently dennervated NMJs (Ronnevi et al., 1978). These observations are also similar to previous EM descriptions of early rodent NMJs that document tSC processes separating sets of axon terminals that

initially abut each other on the surface of the muscle fiber after NMJ formation (Korneliussen and Jansen, 1976). At multi-innervated NMJs it is suggested that the various inputs compete for occupation of the AChR-rich space on the surface of the muscle fiber. In this scenario the surviving axon terminals expand their contact areas to regions vacated by losing terminals (Turney et al., 2012). I have shown that tSCs are responsible for the elimination of these losing terminals and as a result are generating the vacancies that axons are said to compete for. Additionally, I show that tSCs also occupy substantial portions of the available muscle fiber surface at the NMJ, appearing to compete with axon terminals in a similar fashion as proposed by Turney and colleagues (Turney et al., 2012). If this tSC contact was indeed shown to be at sites of AChR expression in the postsynaptic membrane, it would strengthen this argument and provide insight into how the postsynaptic apparatus is changing, regarding AChR patterning. The potential for tSC occupation of the postsynaptic membrane and competing with axon terminals for the AChR-rich membrane of the endplate led to the design of the study in chapter 4 (summarized below).

6.4 Postsynaptic contact by tSCs is primarily at sites of AChR-rich membrane during early stages of synapse elimination

It is conceivable that the intrusion of tSC processes between axon terminals and the postsynaptic membrane could result in blockade/interference of postsynaptic action by acetylcholine and other releasable factors from the axon terminals. Precedent for focal blockade of transmission affecting AChR turnover within the endplate was presented in a study of adult NMJs using acute BTX application (Balice-Gordon and Lichtman, 1994). tSC occupation of AChR-rich portions of the endplate and intercalation between axon

terminals and the muscle fiber may act in a similar fashion. Presuming the substrate for interaxonal competition during synapse elimination is the AChR-rich membrane at the endplate, it is possible that the contacts made by tSCs could help serve to promote competition. The tSCs were first observed to be co-extensive with AChR labeling in the postsynaptic membrane via fluorescence microscopy where their occupancy of the endplate was noted at sites devoid of axon terminal contact and these coverage areas far exceeded any discontinuities in the receptor label (Smith et al., 2013). In serial EM data sets labeled for AChRs, we found that tSC coverage of the endplate is co-extensive with receptor labeling and that tSC contacts with the postsynaptic membrane are primarily at sites of AChR-rich membrane during early stages of synapse elimination. Similar to previous analysis of these contact sites, tSCs occupied the majority of the postsynaptic contacts made when compared to axon terminals. Indeed, tSCs occupy more of the AChR-rich membrane of the endplate during the early stages of synapse elimination. Electron microscopy examination of AChR labeling at adult NMJs showed tSCs occupied very little AChR-rich membrane. The degree of tSC contact to the muscle fiber in these AChR labeled images was similar to unlabeled datasets. As suspected, AChR labeling was significantly elevated at sites of axon terminal contact, while being virtually absent at all other regions of the muscle fiber membrane within the endplate region and extrasynaptic at adult NMJs. These results reinforce the concept that terminal Schwann cells are competing with axon terminals for valuable postsynaptic landscape that could influence the degree of interaxonal competition during synapse elimination.

Further insight into tSC competition with axons and their affect on the rate of synapse elimination could come from ablation studies. If the coverage of tSCs affects the

rate of competition as we propose, ablating individual tSCs during different stages of synapse elimination may test it. Complete ablation of tSCs is known to cause complete degeneration of the synapse (Wolpowitz et al., 2000; Barik et al., 2016), thus it would have to be performed in a way where individual tSCs could be damaged manually through physical disruption or more precisely through laser ablation of individual tSCs. Control NMJs could then be tracked compared to un-damaged NMJs for timing to single innervation, through imaging of separate inputs to the NMJ or electrophysiological recordings. However, the variable timing of synapse elimination per NMJ could complicate these experiments, but with many samples, they could be distinguished statistically.

6.5 Regions of the synaptic footprint occupied by tSCs and vacancies show reduced AChR labeling intensity compared to axon terminals

After establishing that the regions of the synaptic footprint occupied by tSCs at P4 NMJs were indeed at sites labeled for AChRs, I performed further analysis to determine whether the various regions of postsynaptic contact made by axon terminals, tSCs, and vacancies showed any real differences in AChR-label intensity. The results from this analysis suggests that tSCs may contribute to the turnover of AChR accumulated in the muscle fiber membrane during synapse elimination. Similar to previous synaptic footprint models reconstructed from serial EM data sets, the neonatal micrographs labeled for AChR show three types of postsynaptic coverage sites: those contacted by axon terminals, tSCs, and vacancies (previously shown to be sites of eliminated axon terminals via tSC phagocytosis). An obvious pattern emerged when AChR labeling in the EM data was

analyzed for intensity throughout the synaptic footprint. First, all three synaptic footprint regions (axon terminal, tSC, and vacancy) showed significantly more intense labeling than in the muscle fiber membrane outside of the contacts in the extrasynaptic region. Second, there were significant differences in the labeling observed between the regions of postsynaptic membrane occupied by these three components. The most intense labeling was found beneath sites of axon terminals, followed by sites occupied by tSC processes, and the lowest intensity was observed at vacated sites on the postsynaptic membrane. These results agree with previous studies that examined the changes in AChR aggregation and staining as the endplate transitions from the initial plaque of receptors to the intricate pretzel apparatus mirroring sites of axon terminal contact in the adult (Marques et al., 2000; Balice-Gordon and Lichtman, 1994). The location and size of vacancies at these endplates are also reminiscent of the small perforations that are shown to accumulate within the initial plaque. The accumulation of these perforations have been proposed to aid in the sculpting of the plaque to pretzel morphology (Prozynski et al., 2009). Although these findings are slightly different than what I hypothesized at the end of chapter 3 (see figure 3.10), they support the competitive model for tSCs and axon terminals during synapse elimination and may indicate their ability to influence the remodeling of AChR patterning as the initial plaque transitions to the pretzel-like morphology in the adult.

6.6 Synaptic sculpting: modeling tSC mediated synapse elimination at neuromuscular junctions

My data from chapters 2-4 indicate that tSCs participate in eliminating axon terminals and that they cover extensive portions of the valuable postsynaptic membrane at

the endplate. It is possible that the contacts made by tSCs could help serve to promote competition. Previous studies have reported a mechanism of interaxonal competition that results in "synaptic takeover", where the various inputs compete for occupation of the synaptic space on the surface of the muscle fiber, with surviving axon terminals expanding their contact areas to regions vacated by losing terminals (Turney et al., 2012). Turney and colleagues suggest that a mechanism that removes portions of any input results in compensatory growth by other input(s). When modeled using random turnover of inputs, this can result in reliable recapitulation of synapse elimination resulting in singly innervated NMJs. Our results suggest that tSC occupation of the available synaptic space during synapse elimination would aid in driving the process of elimination, increasing the amount of competitive interaction between axon inputs by limiting the available postsynaptic membrane for which they compete. In order to test the possibility of this competitive interaction at the developing endplate, we designed a model of synapse elimination that incorporated the three synaptic footprint characters: axon terminals, tSCs, and vacancies.

We constructed a model where we used the average footprint ratios generated from P0 data sets, but instead of using random and/or equal transition probabilities for site turnover, we used the footprint ratios at later time points (P3 and P7) to develop optimized transition ratios. In doing so, we were able to incorporate the real changes in synaptic footprint coverage we observed in the electron microscopy datasets. Specifically, where tSCs increased their coverage of the postsynaptic membrane relative to the axon terminals during the first week of synapse elimination. Using these optimized transition probabilities, we were able to recapitulate reliable synapse elimination, on every single simulation we

ran. This would suggest that synapse elimination is not entirely random, which is supported by the multitude of studies that indicate there is a competitive advantage to more efficacious inputs often during the process. Moreover, these simulations suggested that tSC occupation and competition for the endplate during the period of synapse elimination is an important aspect of the process, validated by showing tSC coverage of the synaptic footprint was positively correlated with the rate of synapse elimination. For example, when using transition probabilities constructed from the transition from the P0 footprint ratios to those at P3 (where tSC contact is at its peak) and P0 to P7 ratios, we observed that those using the P3 transition ratios completed synapse elimination more quickly. These results are also in agreement with studies we have done examining the rate of synapse elimination in Neuregulin1-III overexpressing mice that experience expedited rates of synapse elimination and where tSC contacts are greater at P3 than in wildtype littermates (Lee et al., 2016). In addition to indicating that tSC contact is positively correlated to the rate of synapse elimination, this model also recapitulated well-understood aspects of synapse morphology and axon activity effects on the rate of synapse elimination. Specifically, simulations reflected segregation of synaptic contact territories by the competing axons as elimination proceeded (Walsh and Lichtman, 2003; Turney et al., 2012) as well as non-linear rates of input elimination (Brown et al., 1976; Bixby and Van Essen, 1979; Balice-Gordon and Thompson, 1988; Balice-Gordon and Lichtman, 1993; Tapia et al., 2012), and an effect of activity dependent competition between the axons (Colman and Lichtman, 1993; Walsh and Lichtman, 2003).

This model supports my hypothesis that terminal Schwann cell expansion and coverage of the developing endplate plays a role in the progression of synapse elimination,

seemingly to expedite the process of interaxonal competition. This is especially interesting when considering certain disease models where synapse elimination is affected, such as, in mouse models of spinal muscular atrophy (Lee et al., 2011) and lysosomal storage disease (Song et al., 2008), where the role of tSCs has been less studied.

6.7 Moving forward

Collectively, the results and observations of my studies have contributed substantially to the comprehensive understanding of the cellular mechanisms and processes involved in the process of neuromuscular synapse elimination. Prior to these studies, tSCs were not known to directly participate in the process of synapse elimination. Moreover, I have described many physical aspects of their morphology during NMJ maturation that were not shown or discussed previously. Despite this advance in appreciating tSCs during NMJ development, there is much more to be learned in order to truly grasp why tSCs behave this way during synapse elimination and how exactly this interaction occurs from a molecular standpoint. An important aspect of these studies is that they do provide the basis for asking these additional questions.

In a broad sense, an important aspect of my work has shown that there are obvious differences in the morphology and behavior of tSCs during early postnatal development versus those in the adult. (1) They show marked differences in their interaction with axons during these two periods. Early on they are highly phagocytic toward axon terminals during the period of elimination, while in the adult they primarily provide trophic support to the motor axon terminals and show very little phagocytic activity. (2) tSCs undergo considerable proliferation at neonatal NMJs, stabilizing their numbers in the adult. What

may trigger this proliferation and what sort of factors may influence this behavior is poorly understood. For that matter, it is still not defined whether these cells locally proliferate through cellular division directly at the NMJ, or whether they are trafficked down the axons themselves. (3) Following proliferation the tSCs show considerable intermingling in their coverage of the NMJ while in the adult they show very segregated coverage of the endplate. (4) They show an incredible affinity for the postsynaptic membrane during early postnatal development and synapse elimination while in the adult they are largely confined to the regions just adjacent to the axon terminals making a fraction of the contact with the postsynaptic surface than what they do during the period of synapse elimination.

The appreciable differences in the behavior and morphology of the tSCs at early postnatal NMJs versus in the adult suggest that they must have very distinct differences in their transcriptional profiles. In the discussion sections of my previous chapters, I have given some thought to the potential molecular pathways that may be involved in the behavior of terminal Schwann cells at NMJs during the period of synapse elimination. For example, changes in immune receptor expression and potentially cell surface adhesion molecules that could explain the stark differences in phagocytic activity and postsynaptic coverage observed in neonates versus adults. I believe these all to be possibilities but, in order to hone in on which molecular candidates may be most useful to pursue, in this line of questioning, whole transcriptome analysis would be integral to success in identifying important factors. Although this is somewhat of a “shotgun” approach, I believe important pathways to focus on would include: complement system componets, cell adhesion molecules, and lysosomal pathways.

Ideally, I would want to isolate tSCs from NMJs at progressive stages of synapse elimination. Given the process is understood to unfold over the first few weeks of postnatal development, it would be important to gather this transcriptome analysis from late stage embryonic NMJs, at birth, several time points in early postnatal development, as well as in the adult. Although conceptually this seems simple, it would require the ability to isolate tSCs from NMJs at every time point, and while not impossible, would be a formidable task. It may not be easy to isolate these cells without also including portions of the axon terminals, which would "muddy" the results. Although the axons could be ablated prior to isolation and removal of the tSCs, this may present complications with transcriptional changes that would occur in the absence of the nerve. Moreover, at early stages of postnatal development it would be difficult to discern between the myelinating Schwann cells that wrap the axons, and the tSCs found at the NMJ. As of now there is not a reliable means of differentiating between the two cell types outside of this myelination, which typically does not occur until the second postnatal week or close to when the NMJs have already completed synapse elimination.

Although these experiments present considerable obstacles to overcome, they represent necessary steps in discerning which molecular pathways and specific proteins are differentially regulated during the period of synapse elimination. Understanding these differences will be critical to making efficient progress in identifying critical pathways for tSC behavior and their involvement in the process of synapse elimination going forward.

REFERENCES

1. Allen, LJS (2003). An introduction to stochastic processes with applications to biology. Upper Saddle River, N.J.: Pearson/Prentice Hall; xiii, 385 p.

2. Anderson, M.J., & Cohen, M.W. (1977). Nerve-induced and spontaneous redistribution of acetylcholine receptors on cultered muscle cells. *J Physiol.,* 268(3): 757-73.

3. Armond, J. W., Saha, K., Rana, A. A., Oates, C. J., Jaenisch, R., Nicodemi, M., & Mukherjee, S. (2015). A stochastic model dissects cell states in biological transition processes. *Sci Rep*, *4*(1), 1-9.

4. Awasaki, T., & Ito, K. (2004). Engulfing Action of Glial Cells Is Required for Programmed Axon Pruning during Drosophila Metamorphosis. *Current Biology*, *14*(8), 668-677.

5. Balice-Gordon, R. J., & Thompson, W. J. (1988). Synaptic rearrangements and alterations in motor unit properties in neonatal rat extensor digitorum longus muscle. *J Physiol., 398*(1), 191-210.

6. Balice-Gordon, R., & Lichtman, J. (1993). In vivo observations of pre- and postsynaptic changes during the transition from multiple to single innervation at developing neuromuscular junctions. *J. Neurosci.*, *13*(2), 834-855.

7. Balice-Gordon, R. J., & Lichtman, J. W. (1994). Long-term synapse loss induced by focal blockade of postsynaptlc receptors. *Nature*, *372*(6506), 519-524.

8. Barber, M. J., & Lichtman, J. W. (1999). Activity-Driven Synapse Elimination Leads Paradoxically to Domination by Inactive Neurons. *J. Neurosci.*, *19*(22), 9975-9985.

9. Barik, A., Li, L., Sathyamurthy, A., Xiong, W.-C., & Mei, L. (2016). Schwann Cells in Neuromuscular Junction Formation and Maintenance. *Journal of Neuroscience*, *36*(38), 9770-9781.

10. Barry, J., & Ribchester, R. (1995). Persistent polyneuronal innervation in partially denervated rat muscle after reinnervation and recovery from prolonged nerve conduction block. *J. Neurosci.*, *15*(10), 6327-6339.

11. Bartol, T., Land, B., Salpeter, E., & Salpeter, M. (1991). Monte Carlo simulation of miniature endplate current generation in the vertebrate neuromuscular junction. *Biophysical Journal*, *59*(6), 1290-1307.

12. Bennett, M.R., & Pettigrew, A.G. (1976). The formation of neuromuscular synapses. *Cold Spring Harb Symp Quant Biol.* 1976;40:409-24.

13. Bennett MR, Robinson J. (1989)Growth and elimination of nerve terminals at synaptic sites during polyneuronal innervation of muscle cells: a trophic hypothesis. *Proc R Soc Lond B Biol Sci*. 1989;235(1281):299-320.

14. Betz, W. J., Caldwell, J. H., & Ribchester, R. R. (1979). The size of motor units during post-natal development of rat lumbrical muscle. *J Physiol., 297*(1), 463-478.

15. Bevan, S., & Steinbach, J.H. (1977). The distribution of alpha-bungarotoxin binding sites of mammalian skeletal muscle developing in vivo. *J. Physiol.* 267(1):195-213.

16. Birks, R., Katz, B., & Miledi, R. (1960). Physiological and structural changes at the amphibian myoneural junction, in the course of nerve degeneration. *J Physiol., 150*(1), 145-168.

17. Bishop, D. L., Misgeld, T., Walsh, M. K., Gan, W.-B., & Lichtman, J. W. (2004). Axon Branch Removal at Developing Synapses by Axosome Shedding. *Neuron*, *44*(4), 651-661.

18. Bixby, J. L., & Van Essen, D. (1979). Regional differences in the timing of synapse elimination in skeletal muscles of the neonatal rabbit. *Brain Research*, *169*(2), 275-286.

19. Bixby, J. L. (1981). Ultrastructural observations on synapse elimination in neonatal rabbit skeletal muscle. *J Neurocytol*, *10*(1), 81-100.

20. Brand-Saberi, B. Wilting, J., Ebensperger, C., & Christ, B. (1996). The formation of somite compartments in the avian embryo. *Int J Dev Biol.* 40(1):411-20. Review.

21. Brill, M. S., Lichtman, J. W., Thompson, W., Zuo, Y., & Misgeld, T. (2011). Spatial constraints dictate glial territories at murine neuromuscular junctions. *J Cell Biol*, *195*(2), 293-305.

22. Brown, M. C., Jansen, J. K., & Van Essen, D. (1976). Polyneuronal innervation of skeletal muscle in new-born rats and its elimination during maturation. *J Physiol., 261*(2), 387-422.

23. Brown, M. C., Hopkins, W. G., & Keynes, R. J. (1982). Short- and long-term effects of paralysis on the motor innervation of two different neonatal mouse muscles. *J Physiol., 329*(1), 439-450.

24. Buffelli, M., Busetto, G., Cangiano, L., & Cangiano, A. (2002). Perinatal switch from synchronous to asynchronous activity of motoneurons: Link with synapse elimination. *Proceedings of the National Academy of Sciences*, *99*(20), 13200-13205.

25. Buffelli, M., Burgess, R. W., Feng, G., Lobe, C. G., Lichtman, J. W., & Sanes, J. R. (2003). Genetic evidence that relative synaptic efficacy biases the outcome of synaptic competition. *Nature*, *424*(6947), 430-434.

26. Burden, S.J., Huijbers, M.G., Remedio, L. (2018). Fundamental molecules and mechanisms for forming and maintaining neuromuscular synapses. *Int J Mol Sci.* 19(2). Pii:E490. Review.

27. Busetto, G., Buffelli, M., Tognana, E., Bellico, F., & Cangiano, A. (2000). Hebbian Mechanisms Revealed by Electrical Stimulation at Developing Rat Neuromuscular Junctions. *J. Neurosci.*, *20*(2), 685-695.

28. Callaway, E. M., Soha, J. M., & Essen, D. C. V. (1987). Competition favouring inactive over active motor neurons during synapse elimination. *Nature*, *328*(6129), 422-426.

29. Cho, S. I., Ko, J., Patton, B. L., Sanes, J. R., & Chiu, A. Y. (1998). Motor neurons and Schwann cells distinguish between synaptic and extrasynaptic isoforms of laminin. *J. Neurobiol.*, 37(3), 339-358.

30. Colman, H., & Lichtman, J. W. (1993). Interactions between Nerve and Muscle: Synapse Elimination at the Developing Neuromuscular Junction. *Developmental Biology*, *156*(1), 1-10.

31. Colman, H., Nabekura, J., Lichtman, J.W. (1997). Alterations in synaptic strength preceding axon withdrawal. *Science.* 275(5298): 356-61.

32. Costanzo, E. M., Barry, J. A., & Ribchester, R. R. (2000). Competition at silent synapses in reinnervated skeletal muscle. *Nat Neurosci*, *3*(7), 694-700.

33. Culican, S. M., Nelson, C. C., & Lichtman, J. W. (1998). Axon Withdrawal during Synapse Elimination at the Neuromuscular Junction Is Accompanied by Disassembly of the Postsynaptic Specialization and Withdrawal of Schwann Cell Processes. *J. Neurosci.*, *18*(13), 4953-4965.

34. Darabid, H., Arbour, D., & Robitaille, R. (2013). Glial Cells Decipher Synaptic Competition at the Mammalian Neuromuscular Junction. *Journal of Neuroscience*, *33*(4), 1297-1313.

35. Darabid, H., Perez-Gonzalez, A. P., & Robitaille, R. (2014). Neuromuscular synaptogenesis: coordinating partners with multiple functions. *Nat Rev Neurosci*, *15*(11), 703-718.

36. Desaki, J., & Uehara, Y. (1981). The overall morphology of neuromuscular junctions as revealed by scanning electron microscopy. *J Neurocytol*, *10*(1), 101-110.

37. Ding, R., Jansen, J. K. S., Laing, N. G., & TannesenH. (1983). The innervation of skeletal muscles in chickens curarized during early development. *J Neurocytol*, *12*(6), 887-919.

38. Duxson, M. J. (1982). The effect of postsynaptic block on development of the neuromuscular junction in postnatal rats. *J Neurocytol*, *11*(3), 395-408.

39. Elliott, T., & Shadbolt, N. (1996). A mathematical model of activity-dependent, anatomical segregation induced by competition for neurotrophic support. *Biological Cybernetics*, *75*(6), 463-470.

40. Elliott, T., & Shadbolt, N. R. (1998). Competition for Neurotrophic Factors: Mathematical Analysis. *Neural Computation*, *10*(8), 1939-1981.

41. Favero, M., Buffelli, M., Cangiano, A., & Busetto, G. (2010). The timing of impulse activity shapes the process of synaptic competition at the neuromuscular junction. *Neuroscience*, *167*(2), 343-353.

42. Favero, M., Busetto, G., & Cangiano, A. (2012). Spike timing plays a key role in synapse elimination at the neuromuscular junction. *Proceedings of the National Academy of Sciences*, *109*(25), E1667-E1675.

43. Fiala, J. C. (2005). Reconstruct: a free editor for serial section microscopy. *J Microsc*, *218*(1), 52-61.

44. Fields, R., & Nelson, P. G. (1992). A Role for Glial Cells in Activity-Dependent Development of the Vertebrate Nervous System. *International review of Neurobiology* 133-214.

45. Fuentes-Medel, Y., Logan, M. A., Ashley, J., Ataman, B., Budnik, V., & Freeman, M. R. (n.d.). Glia and Muscle Sculpt Neuromuscular Arbors by Engulfing Destabilized Synaptic Boutons and Shed Presynaptic Debris. *PLoS Biol*, *7*(8), e1000184.

46. Garcia, N., Tomàs, M., Santafe, M. M., Lanuza, M. A., Besalduch, N., & Tomàs, J. (2011). Blocking p75NTR receptors alters polyinnervationz of neuromuscular synapses during development. *J. Neurosci*. Res., 89(9), 1331-1341.

47. Gautam, M., Noakes, P.G., Moscoso, L., Rupp, F., Scheller, R.H., Merlie, J.P., Sanes, J.R. (1996). Defective neuromuscular synaptogenesis in agrin-deficient mutant mice. *Cell.* 85(4): 525-35.

48. Gouze, J.L., Lasry, J.M., & Changeux, J.P. (1983). Selective stabilization of muscle innervation during development: A mathematical model. *Biol. Cybern.*, *46*(3), 207-215.

49. Harlow, M., Ress, D., Koster, A., Marshall, R. M., Schwarz, M., & McMahan, U. J. (1998). Dissection of active zones at the neuromuscular junction by EM tomography. *Journal of Physiology-Paris*, *92*(2), 75-78.

50. Hayworth, C. R., Moody, S. E., Chodosh, L. A., Krieg, P., Rimer, M., & Thompson, W. J. (2006). Induction of Neuregulin Signaling in Mouse Schwann Cells In Vivo Mimics Responses to Denervation. *Journal of Neuroscience*, *26*(25), 6873-6884.

51. Hesselmans, L. F. G. M., Jennekens, F. G. I., Van Den Oord, C. J. M., Veldman, H., & Vincent, A. (1993). Development of innervation of skeletal muscle fibers in man: Relation to acetylcholine receptors. *Anat. Rec.*, *236*(3), 553-562.

52. Jansen, J., & Fladby, T. (1990). The perinatal reorganization of the innervation of skeletal muscle in mammals. *Progress in Neurobiology*, *34*(1), 39-90.

53. Jeanprêtre, N., Clarke, P., & Gabriel, J.-P. (1996). Competitive exclusion between axons dependent on a single trophic substance: A mathematical analysis. *Mathematical Biosciences*, *135*(1), 23-54.

54. Jirmanov, I., & Thesleff, S. (1972). Ultrastructural study of experimental muscle degeneration and regeneration in the adult rat. *Z.Zellforsch*, *131*(1), 77-97.

55. Jung, J. H., & Doniach, S. (2017). A stochastic model of active zone material mediated synaptic vesicle docking and priming at resting active zones. *Sci Rep*, *7*(1).

56. Kang, H., Tian, L., Son, Y.-J., Zuo, Y., Procaccino, D., Love, F., Hayworth, C., Trachtenberg, J., Mikesh, M., & Sutton, L. (2007). Regulation of the Intermediate Filament Protein Nestin at Rodent Neuromuscular Junctions by Innervation and Activity. *Journal of Neuroscience*, *27*(22), 5948-5957.

57. Kasthuri, N., & Lichtman, J. W. (2003). The role of neuronal identity in synaptic competition. *Nature*, *424*(6947), 426-430.

58. Kastriti, M.E., &Adameyko, I. (2017). Specification, plasticity, and evolutionary origin of peripheral glial cells. *Curr Opin Neurobiol.* 47:196-202. Review.

59. Keller-Peck, C. R., Walsh, M. K., Gan, W.-B., Feng, G., Sanes, J. R., & Lichtman, J. W. (2001). Asynchronous Synapse Elimination in Neonatal Motor Units. *Neuron*, *31*(3), 381-394.

60. Kelly, A. M. (1969). The fine structure of motor endplate morphogenesis. *The Journal of Cell Biology*, *42*(1), 154-169.

61. Ko, C.-P., & Robitaille, R. (2015). Perisynaptic Schwann Cells at the Neuromuscular Synapse: Adaptable, Multitasking Glial Cells. *Cold Spring Harb Perspect Biol*, *7*(10), a020503.

62. Korneliussen, H., & Jansen, J. K. S. (1976). Morphological aspects of the elimination of polyneuronal innervation of skeletal muscle fibres in newborn rats. *J Neurocytol*, *5*(5), 591-604.

63. Kummer, T. T., Misgeld, T., Lichtman, J. W., & Sanes, J. R. (2004). Nerve-independent formation of a topologically complex postsynaptic apparatus. *J Cell Biol*, *164*(7), 1077-1087.

64. Kummer, T.T., Misgeld, T., & Sanes, J.R. (2006). Assembly of the postsynaptic membrane at the neuromuscular junction: paradigm lost. *Curr Opin Neurobiol.* 16(1): 74-82.

65. Li, L., Xiong, W.C., & Mei, L. (2017). Neuomuscular junction formation, aging, and disorders. *Annu. Rev. Physiol.* 80: 159-88. Review.

66. Leber, S.M., Breedlove, S.M., & Sanes, J.R. (1990). Lineage, arrangement, and death of clonally related motoneurons in chick spinal cord. *J Neurosci.* 10(7): 2451-62. Review.

67. Lee, Y. il, Mikesh, M., Smith, I., Rimer, M., & Thompson, W. (2011). Muscles in a mouse model of spinal muscular atrophy show profound defects in neuromuscular development even in the absence of failure in neuromuscular transmission or loss of motor neurons. *Developmental Biology*, *356*(2), 432-444.

68. Lee, Y. il, Li, Y., Mikesh, M., Smith, I., Nave, K.-A., Schwab, M. H., & Thompson, W. J. (2016). Neuregulin1 displayed on motor axons regulates terminal Schwann cell-mediated synapse elimination at developing neuromuscular junctions. *Proc Natl Acad Sci USA*, 113(4), E479-E487.

69. Li, Y., Lee, Y. i., & Thompson, W. J. (2011). Changes in Aging Mouse Neuromuscular Junctions Are Explained by Degeneration and Regeneration of Muscle Fiber Segments at the Synapse. *Journal of Neuroscience*, *31*(42), 14910-14919.

70. Lin, S., Landmann, L., Reugg, M.A., & Brenner, H.R. (2008). The role of nerve- versus muscle-derived factors in mammalian neuromuscular junction formation. *J. Neurosci.* 28(13): 3333-3340.

71. Love, F. M., & Thompson, W. J. (1998). Schwann Cells Proliferate at Rat Neuromuscular Junctions during Development and Regeneration. *J. Neurosci.*, *18*(22), 9376-9385.

72. Magchielse, T., & Meeter, E. (1986). The effect of neuronal activity on the competitive elimination of neuromuscular junctions in tissue culture. *Brain Research*, *390*(2), 211-220.

73. Marques, M. J., Conchello, J.-A., & Lichtman, J. W. (2000). From Plaque to Pretzel: Fold Formation and Acetylcholine Receptor Loss at the Developing Neuromuscular Junction. *J. Neurosci.*, *20*(10), 3663-3675.

74. Matthews-Bellinger, J., & Salpeter, M. (1983). Fine structural distribution of acetylcholine receptors at developing mouse neuromuscular junctions. *J. Neurosci.*, *3*(3), 644-657.

75. McGurk, J. S., Shim, S., Kim, J. Y., Wen, Z., Song, H., & Ming, G.- l. (2011). Postsynaptic TRPC1 Function Contributes to BDNF-Induced Synaptic Potentiation at the Developing Neuromuscular Junction. *J. Neurosci*, 31(41), 14754-14762.

76. McMahan, U.J., Sanes, J.R., & Marshall, L.M. (1978). Cholinesterase is associated with the basal lamina at the neuromuscular junction. *Nature.* 271:172-174.

77. McMahan, U.J. (1990). The agrin hypothesis. *Cold Spring Harb Symp Quant Biol.* 55:407-18. Review.

78. Miledi, R., & Slater, C.R. (1968). Electrophysiology and electron-microscopy of rat neuromuscular junctions after nerve degeneration. *Proc. Roy. Soc. B.* 169:289-306.

79. Miledi, R., & Slater, C. R. (1970). On the degeneration of rat neuromuscular junctions after nerve section. *J Physiol., 207*(2), 507-528.

80. Nelson, P. G., Fields, R. D., Yu, C., & Liu, Y. (1993). Synapse elimination from the mouse neuromuscular junctionin vitro: A non-hebbian activity-dependent process. *J. Neurobiol.*, *24*(11), 1517-1530.

81. Nguyen, Q. T., Sanes, J. R., & Lichtman, J. W. (2002). Pre-existing pathways promote precise projection patterns. *Nat Neurosci*, *5*(9), 861-867.

82. Njå, A., & Purves, D. (1978). The effects of nerve growth factor and its antiserum on synapses in the superior cervical ganglion of the guinea-pig. *J Physiol., 277*(1), 55-75.

83. Noakes, P. G., Gautam, M., Mudd, J., Sanes, J. R., & Merlie, J. P. (1995). Aberrant differentiation of neuromuscular junctions in mice lacking s-laminin/laminin β2. *Nature*, 374(6519), 258-262.

84. O'Brien, R. A., Ostberg, A. J., & Vrbová, G. (1978). Observations on the elimination of polyneuronal innervation in developing mammalian skeletal muscle. *J Physiol., 282*(1), 571-582.

85. Ontell, M., Bourke, D., & Hughes, D. (1988). Cytoarchitecture of the fetal murine soleus muscle. *Am. J. Anat.*, *181*(3), 267-278.

86. Ooyen, A. (2001). Competition in the development of nerve connections: a review of models. *Network: Computation in Neural Systems*, *12*(1), 1-47.

87. Paolicelli, R. C., Bolasco, G., Pagani, F., Maggi, L., Scianni, M., Panzanelli, P., Giustetto, M., Ferreira, T. A., Guiducci, E., & Dumas, L. (2011). Synaptic Pruning by Microglia Is Necessary for Normal Brain Development. *Science*, *333*(6048), 1456-1458.

88. Patton, B.L. (2003). Basal lamina and the organization of neuromuscular synapses. *J. Neurocytol.* 32(5-8): 883-903. Review.

89. Personius, K. E., & Balice-Gordon, R. J. (2001). Loss of Correlated Motor Neuron Activity during Synaptic Competition at Developing Neuromuscular Synapses. *Neuron*, *31*(3), 395-408.

90. Personius, K. E., Chang, Q., Mentis, G. Z., O'Donovan, M. J., & Balice-Gordon, R. J. (2007). Reduced gap junctional coupling leads to uncorrelated motor neuron firing and precocious neuromuscular synapse elimination. *Proceedings of the National Academy of Sciences*, *104*(28), 11808-11813.

91. Peters, A., & Muir, A. R. (1959). The relationship between axons and Schwann cells during development of peripheral nerves in the rat. *Exp Physiol*, *44*(1), 117-130.

92. Proszynski, T. J., & Sanes, J. R. (2013). Amotl2 interacts with LL5 , localizes to podosomes and regulates postsynaptic differentiation in muscle. *Journal of Cell Science*, 126(10), 2225-2235.

93. Purves, D., & Lichtman, J. (1980). Elimination of synapses in the developing nervous system. *Science*, *210*(4466), 153-157.

94. Rasmussen, C. E., & Willshaw, D. J. (1993). Presynaptic and postsynaptic competition in models for the development of neuromuscular connections. *Biol. Cybern.*, *68*(5), 409-419.

95. Reddy, L. V., Koirala, S., Sugiura, Y., Herrera, A. A., & Ko, C.-P. (2003). Glial Cells Maintain Synaptic Structure and Function and Promote Development of the Neuromuscular Junction In Vivo. *Neuron*, *40*(3), 563-580.

96. Redfern, P. A. (1970). Neuromuscular transmission in new-born rats. *J Physiol., 209*(3), 701-709.

97. Ribchester, R. R., & Taxt, T. (1983). Motor unit size and synaptic competition in rat lumbrical muscles reinnervated by active and inactive motor axons. *J Physiol., 344*(1), 89-111.

98. Rich, M., & Lichtman, J. (1989). In vivo visualization of pre- and postsynaptic changes during synapse elimination in reinnervated mouse muscle. *J. Neurosci.*, *9*(5), 1781-1805.

99. Ridge, R., & Betz, W. (1984). The effect of selective, chronic stimulation on motor unit size in developing rat muscle. *J. Neurosci.*, *4*(10), 2614-2620.

100. Riethmacher, D., Sonnenberg-Riethmacher, E., Brinkmann, V., Yamaai, T., Lewin, G.R., & Birchmeier, C. (1997). Severe neuropathies in mice with targeted mutations in the ERbB3 receptor. *Nature.* 389(6652): 725-30.

101. Riley, D. A. (1977). Spontaneous elimination of nerve terminals from the endplates of developing skeletal myofibers. *Brain Research*, *134*(2), 279-285.

102. Riley, D. A. (1981). Ultrastructural evidence for axon retraction during the spontaneous elimination of polyneuronal innervation of the rat soleus muscle. *J Neurocytol*, *10*(3), 425-440.

103. Rimer, M., Mathiesen, I., Lomo, T., & McMahan, U.J. (1997). Gamma-AChR/ epsilon-AChR switch at agrin-induced postsynaptic-like apparatus in skeletal muscle. *Mol Cell Neurosci.* 9(4): 254-63.

104. Ronnevi, L.-O. (1978). Origin of the glial processes responsible for the spontaneous postnatal phagocytosis of boutons on cat spinal motoneurons. *Cell Tissue Res.*, *189*(2).

105. Rosenberry, T.L., & Richardson, J.M. (1977). Structure of 18S and 14S acetylcholinesterase. Identification of collagen-like subunits that are linked by di-sulfide bonds to catalytic subunits. *Biochemistry.* 16, 3550-3558.

106. Rosenthal, J. L., & Taraskevich, P. S. (1977). Reduction of multiaxonal innervation at the neuromuscular junction of the rat during development. *J Physiol., 270*(2), 299-310.

107. Salpeter, M.M. (1969). Electron microscope radioautography as a quantitative tool in enzyme cytochemistry II. The distribution of DFP-reactive sites at motor endplates of a vertebrate twitch muscle. *Journal of Cell Biology.* 42, 122-134.

108. Salpeter, M.M., Rogers, A.W., Kasprzak, H., & McHenry, F.A. (1978). Acetylcholinesterase in the fast extraocular muscle of the mouse by light and electron microscope autoradiography. *Journal of Cell Biology.* 78, 274-286.

109. Salpeter, M. (1985). Nicotinic acetylcholine receptors in vertebrate muscle: Properties, distribution and neural control. *Progress in Neurobiology*, *25*(4), 297-325.

110. Salpeter, M. M. (1988). Distribution of extrajunctional acetylcholine receptors on a vertebrate muscle: evaluated by using a scanning electron microscope autoradiographic procedure. *The Journal of Cell Biology*, *106*(6), 2087-2093.

111. Sanes, J.R., Apel, E.D., Burgess, R.W., Emerson, R.B., Feng, G., Guatam, M., Glass, D., Grady, R.M., Krejci, E., Lichtman, J.W., Lu, J.T., Massoulie, J., Miner, J.H., Moscoso, L.M., Ngyuyen, Q., Nichol, M., Noakes, P.G., Patton, B.L., Son, Y.J., Yancopoulos, G.D., Zhou, H. (1998). Development of the neuromuscular junction: genetic analysis in mice. *J Physiol Paris.* 92(3-4): 167-72. Review

112. Sanes, J. R., & Lichtman, J. W. (1999).Development of the vertebrate neuromuscular junction. *Annu. Rev. Neurosci.*, *22*(1), 389-442.

113. Sanes, J. R., & Lichtman, J. W. (2001). Induction, assembly, maturation and maintenance of a postsynaptic apparatus. *Nat Rev Neurosci*, *2*(11), 791-805.

114. Schafer, D., Lehrman, E., Kautzman, A., Koyama, R., Mardinly, A., Yamasaki, R., Ransohoff, R., Greenberg, M., Barres, B., & Stevens, B. (2012). Microglia Sculpt Postnatal Neural Circuits in an Activity and Complement-Dependent Manner. *Neuron*, *74*(4), 691-705.

115. Slater, C. R. (1982). Postnatal maturation of nerve-muscle junctions in hindlimb muscles of the mouse. *Developmental Biology*, *94*(1), 11-22.

116. Smalheiser, N. R., & Crain, S. M. (1984). The possible role of ?sibling neurite bias? in the coordination of neurite extension, branching, and survival. *J. Neurobiol.*, *15*(6), 517-529.

117. Smith, I. W., Mikesh, M., Lee, Y. i., & Thompson, W. J. (2013). Terminal Schwann Cells Participate in the Competition Underlying Neuromuscular Synapse Elimination. *Journal of Neuroscience*, 33(45), 17724-17736.

118. Soltani, M., Vargas-Garcia, C. A., Antunes, D., & Singh, A. (n.d.). Intercellular Variability in Protein Levels from Stochastic Expression and Noisy Cell Cycle Processes. *PLoS Comput Biol*, *12*(8), e1004972.

119. Son, Y.J., & Thompson, W.J. (1995). Nerve sprouting in muscle is induced and guided by processes extended by Schwann cells. *Neuron.* 14(1): 133-41.

120. Son, Y.J., & Thompson, W.J. (1995). Schwann cell processes guide regeneration of peripheral axons. *Neuron.* 14(1): 125-32.

121. Son, Y.J., Trachtenberg, J.T., & Thompson, W.J. (1996). Schwann cells induce and guide sprouting and reinnervation of neuromuscular junctions. *Trends Neurosci.* 19(7): 280-5. Review.

122. Song, J. W., Misgeld, T., Kang, H., Knecht, S., Lu, J., Cao, Y., Cotman, S. L., Bishop, D. L., & Lichtman, J. W. (2008). Lysosomal Activity Associated with Developmental Axon Pruning. *Journal of Neuroscience*, *28*(36), 8993-9001.

123. Srihari, T., & Vrbova G. (1978). The role of muscle activity in the differentiation of neuromuscular junctions in slow and fast chick muscles. *J Neurocytol*, *7*(5), 529-540.

124. Steinbach, J. H. (1981). Developmental changes in acetylcholine receptor aggregates at rat skeletal neuromuscular junctions. *Developmental Biology*, *84*(2), 267-276.

125. Stollberg, J. (1995). Synapse elimination, the size principle, and Hebbian synapses. *J. Neurobiol.*, *26*(2), 273-282.

126. Szule, J. A., Jung, J. H., & McMahan, U. J. (2015). The structure and function of 'active zone material' at synapses. *Phil. Trans. R. Soc. B*, *370*(1672), 20140189.

127. Tapia, J., Wylie, J., Kasthuri, N., Hayworth, K., Schalek, R., Berger, D., Guatimosim, C., Seung, H., & Lichtman, J. (2012). Pervasive Synaptic Branch Removal in the Mammalian Neuromuscular System at Birth. *Neuron*, *74*(5), 816-829.

128. Teravainen, H. (1968). Development of the myoneural junction in the rat. *Z. Zellforsch.*, *87*(2), 249-265.

129. Tetruashvily, M.M., McDonald, M.A., Frietze, K.K., & Boulanger, L.M. (2016). MHCI promotes developmental synapse elimination and aging-related synapse loss at the vertebrate neuromuscular junction. *Brain Behav Immun.* 56:197-208.

130. Thompson, W., Kuffler, D., & Jansen, J. (1979). The effect of prolonged, reversible block of nerve impulses on the elimination of polyneuronal innervation of new-born rat skeletal muscle fibers. *Neuroscience*, *4*(2), 271-281.

131. Thompson, W. (1983). Synapse elimination in neonatal rat muscle is sensitive to pattern of muscle use. *Nature*, *302*(5909), 614-616.

132. Trachtenberg, J.T., & Thompson, W.J. (1996). Schwann cell apoptosis at developing neuromuscular junctions is regulated by glial growth factor. *Nature.* 379(6561):174-7.

133. Trachtenberg, J.T., & Thompson, W.J. (1997). Nerve terminal withdrawal from rat neuromuscular junctions induced by Neuregulin and Schwann cells. *J. Neurosci.* 17(16): 6243-55.

134. Turney, S. G., & Lichtman, J. W. (2012). Reversing the Outcome of Synapse Elimination at Developing Neuromuscular Junctions In Vivo: Evidence for Synaptic Competition and Its Mechanism. *PLoS Biol*, *10*(6), e1001352.

135. Van Essen, D. C., Gordon, H., Soha, J. M., & Fraser, S. E. (1990). Synaptic dynamics at the neuromuscular junction: Mechanisms and models. *J. Neurobiol.*, *21*(1), 223-249.

136. Van Ooyen, A., & Willshaw, D. J. (1999). Poly- and Mononeuronal Innervation in a Model for the Development of Neuromuscular Connections. *Journal of Theoretical Biology*, *196*(4), 495-511.

137. Van Ooyen, A. (2001). Competition in the development of nerve connections: a review of models. *Network.* 12(1):R1-47. Review.

138. Walsh, M. K., & Lichtman, J. W. (2003). In Vivo Time-Lapse Imaging of Synaptic Takeover Associated with Naturally Occurring Synapse Elimination. *Neuron*, *37*(1), 67-73.

139. Watts, R. J., Schuldiner, O., Perrino, J., Larsen, C., & Luo, L. (2004). Glia Engulf Degenerating Axons during Developmental Axon Pruning. *Current Biology*, *14*(8), 678-684.

140. Wilkinson, D. J. (2009). Stochastic modelling for quantitative description of heterogeneous biological systems. *Nat Rev Genet*, *10*(2), 122-133.

141. Willshaw DJ. (1981). The establishment and the subsequent elimination of polyneuronal innervation of developing muscle: theoretical considerations. *Proc R Soc Lond B Biol Sci*. 1981;212(1187):233-52.

142. Wolpowitz, D., Mason, T. B., Dietrich, P., Mendelsohn, M., Talmage, D. A., & Role, L. W. (2000). Cysteine-Rich Domain Isoforms of the Neuregulin-1 Gene Are Required for Maintenance of Peripheral Synapses. *Neuron*, *25*(1), 79-91.

143. Woodhoo, A., & Sommer, L. (2008). Development of the Schwann cell lineage: From the neural crest to the myelinated nerve. *Glia*, *56*(14), 1481-1490.

144. Yakovlev, A., & Yanev, N. (2006). Branching stochastic processes with immigration in analysis of renewing cell populations. *Mathematical Biosciences*, *203*(1), 37-63.

APPENDIX A

SIMULATING SYNAPTIC COMPETITION USING RANDOMLY VARIED TRANSITION PROBABILITIES AMONG AXONS, TERMINAL SCHWANN CELLS, AND VACANCIES

Previous models have shown that by random turnover of synaptic sites, multi-innervated synapses may achieve single innervation. Thus, we began our experiments by utilizing a model, where each synaptic site had a random transition probability with each iteration of the simulation. However, here we have determined the initial layout of the endplate contacts made by tSCs (green), vacancies (black), and axons (shades of blue) using the data of synaptic footprints gathered from TEM series of mouse sternomastoid muscles at P0. These initial layouts as seen in figure A1a, f, and k depict the relative ratio of contacts observed in the P0 data sets. Simulation of these initial layouts using random transition probabilities was often unsuccessful. In some instances, only tSCs remain without an axon (Figure A1 a-e), while in others the opposite is true (Figure A1 f-j). Moreover, some simulations lead to completely unoccupied NMJs (Figure A1 k-o). Although this model was able to produce proper synapse elimination at times, it was not a reliable model for producing proper synapse elimination. Thus, a model based on randomly varying transition probabilities for synaptic sites occupied by tSCs, vacancies, and axons is not sufficient to reliably recapitulate proper synapse elimination.

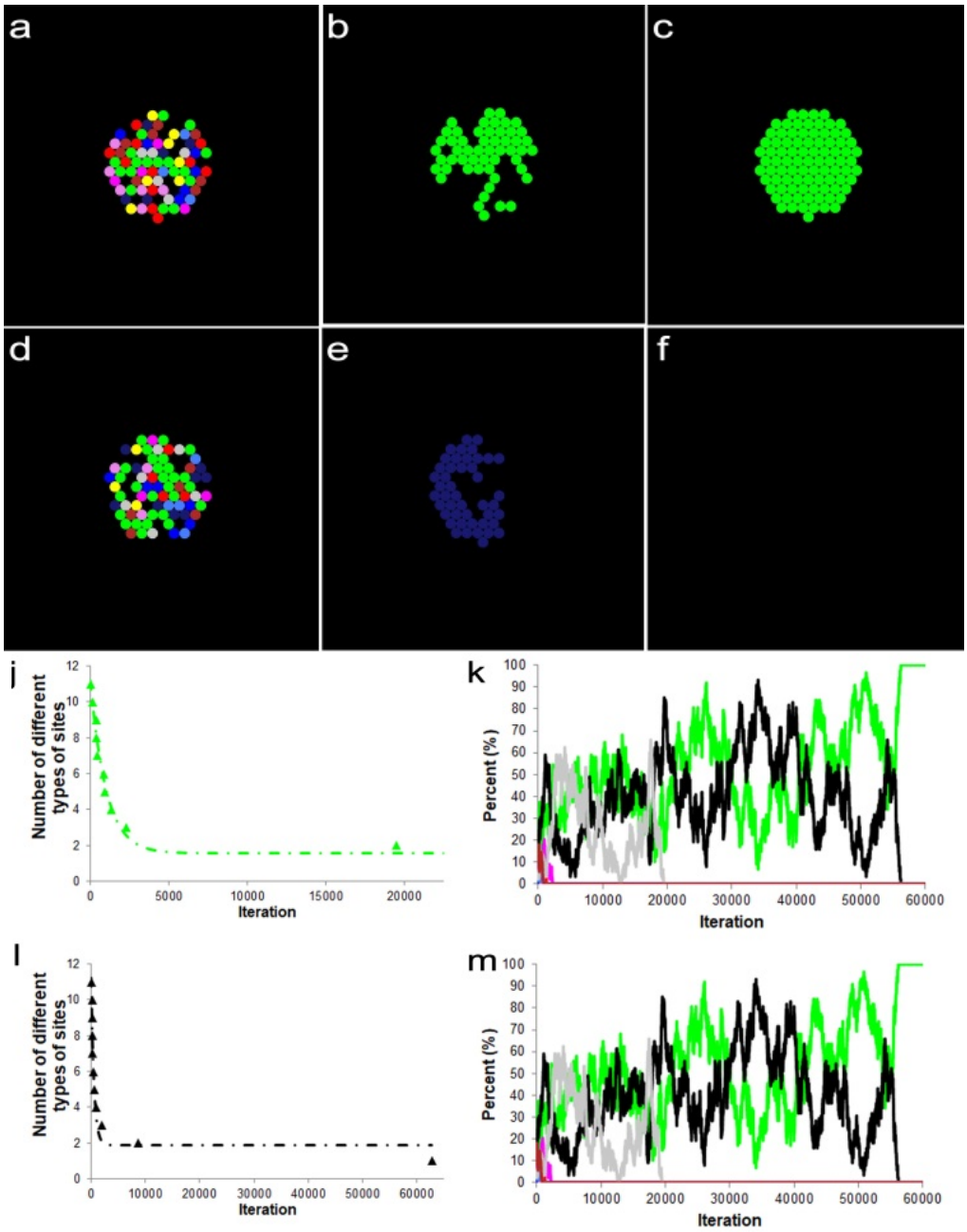

Figure A1: Two different example results based on a model of synaptic competition among axons, tSCs, and vacancies with random transition probabilities. A green circle represents a synaptic site formed on a muscle fiber by a terminal Schwann cell (tSC). A black empty spot represents a vacant site or a vacancy having no axon or tSC on a muscle fiber. Circles having other 9 different colors represent synaptic sites formed on a muscle fiber by 9 different axons. The simulations are repeated for 40000 times. (a, d) Initially, 9 different axons, tSCs and vacancies form their contact sites randomly on a muscle fiber. The initial ratio of their total contact areas (axons:tSCs:vacancies) is about about 30:16:54, which was determined from a recent serial electron microscopy study on developing muscle fibers of mouse during synapse elimination (See Methods). (b, e) The competition among axons, tSCs, and vacancies with their random transition probabilities shows elimination of multiple contact sites formed by different axons, tSCs, and vacancies when the iteration is 40000. (c, f) When the simulation is complete, the competition often leads to a complete synapse elimination. However, it can also generate contact sites formed by only tSCs or vacancies demonstrating that random transition probabilities among them cannot account for synapse elimination. (j, l) The number of remaining types of axons rapidly decreases consistent with other studies. (k, m) The ratios of each type of contact sites formed by 9 different axons, a tSC, and a vacancy varies as the simulation proceeded with 60000 iterations showing that only one type of contact sites remains.

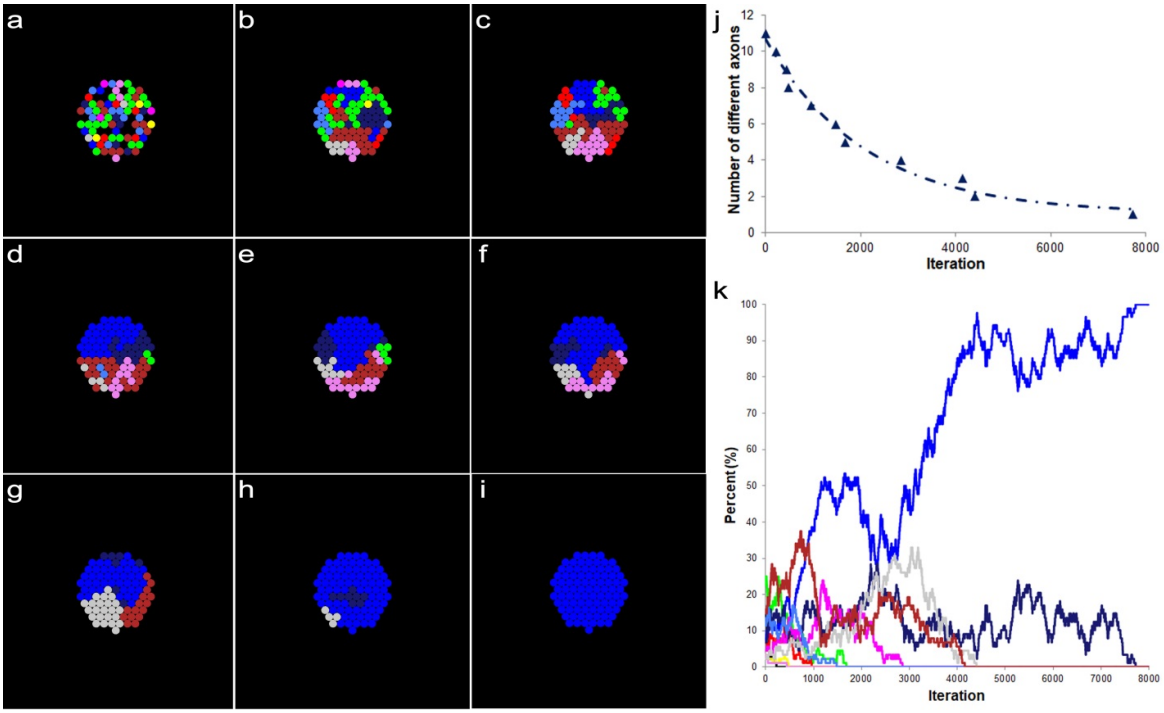

Figure A2: An example result based on a model of synaptic competition among axons, tSCs, and vacancies with equal transition probabilities. (a) Initially, 9 different axons, tSCs and vacancies form their contact sites randomly in an endplate on a muscle fiber. The initial ratio of their total contact areas (axons:tSCs:vacancies) is about 30:16:54, which was determined from a recent serial electron microscopy study on developing muscle fibers of mouse during synapse elimination (See Methods). (b-h) The competition among axons, tSCs, and vacancies with their random transition probabilities shows elimination of multiple contact sites formed by different axons, tSCs, and vacancies at different iterations of the simulation (300, 500, 1000, 1500, 1700, 2900, and 4200 iterations, respectively). (i) When the simulation reached 7800, synapse elimination is complete. However, only one type of axonal sites remains with no tSC and vacant sites that are present during and after synapse elimination of developing neuromuscular junctions. (j) The number of different types of axons in the endplate reduces sharply as the iteration proceeds similar to A1 and Figs. 5.3 and 5.5. (k) Change in the ratio of the contact areas formed by tSCs (green), vacancies (black), and 9 different axons (colors different from green and black) as the simulation based on a stochastic model of tSC and vacancy mediated synapse elimination proceeds.

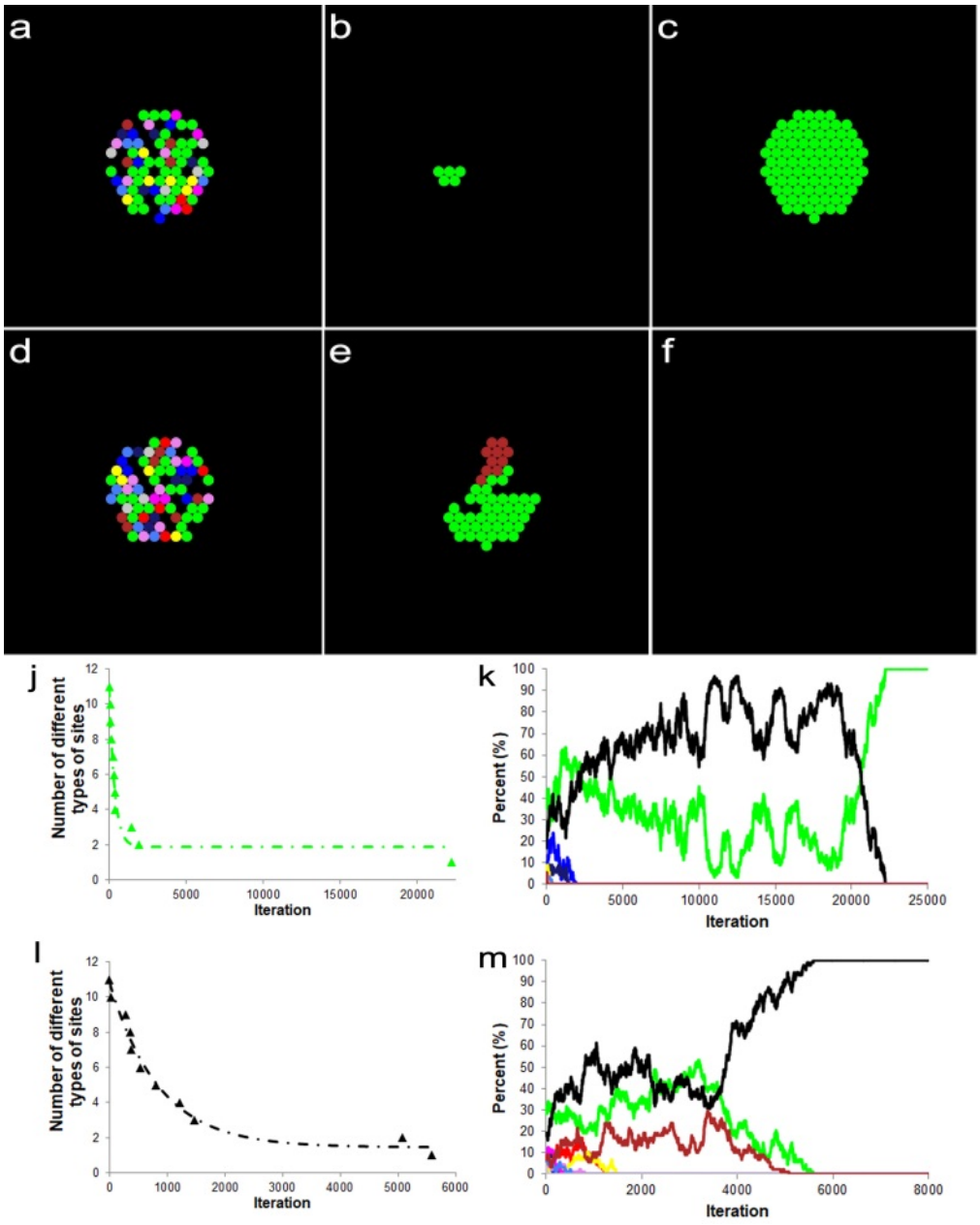

Figure A3: Two different example results based on a model of synaptic competition among axons, tSCs, and vacancies with equal transition probabilities. A green circle represents a synaptic site formed on a muscle fiber by a terminal Schwann cell (tSC). A black empty spot represents a vacant site or a vacancy having no axon or tSC on a muscle fiber. Circles having other 9 different colors represent synaptic sites formed on a muscle fiber by 9 different axons. The simulations proceeded until synapse elimination was complete. (a, d) Initially, 9 different axons, tSCs and vacancies form their contact sites randomly on a muscle fiber. The initial ratio of their total contact areas (axons:tSCs:vacancies) is about about 30:16:54, which was determined from a recent serial electron microscopy study on developing muscle fibers of mouse during synapse elimination (See Methods). (b, e) The competition among axons, tSCs, and vacancies with their random transition probabilities shows elimination of multiple contact sites formed by different axons, tSCs, and vacancies when the iteration is 15000 and 4000, respectively. (c, f) When the simulation is complete, it often generates contact sites formed by only tSCs or vacancies demonstrating that random transition probabilities among them cannot account for synapse elimination. (j, l) The number of remaining types of axons rapidly decreases consistent with other studies. (k, m) The ratios of each type of contact sites formed by 9 different axons, a tSC, and a vacancy varies as the simulation proceeded with 25000 iterations and 8000 iterations, respectively, showing that only one type of contact sites remains.

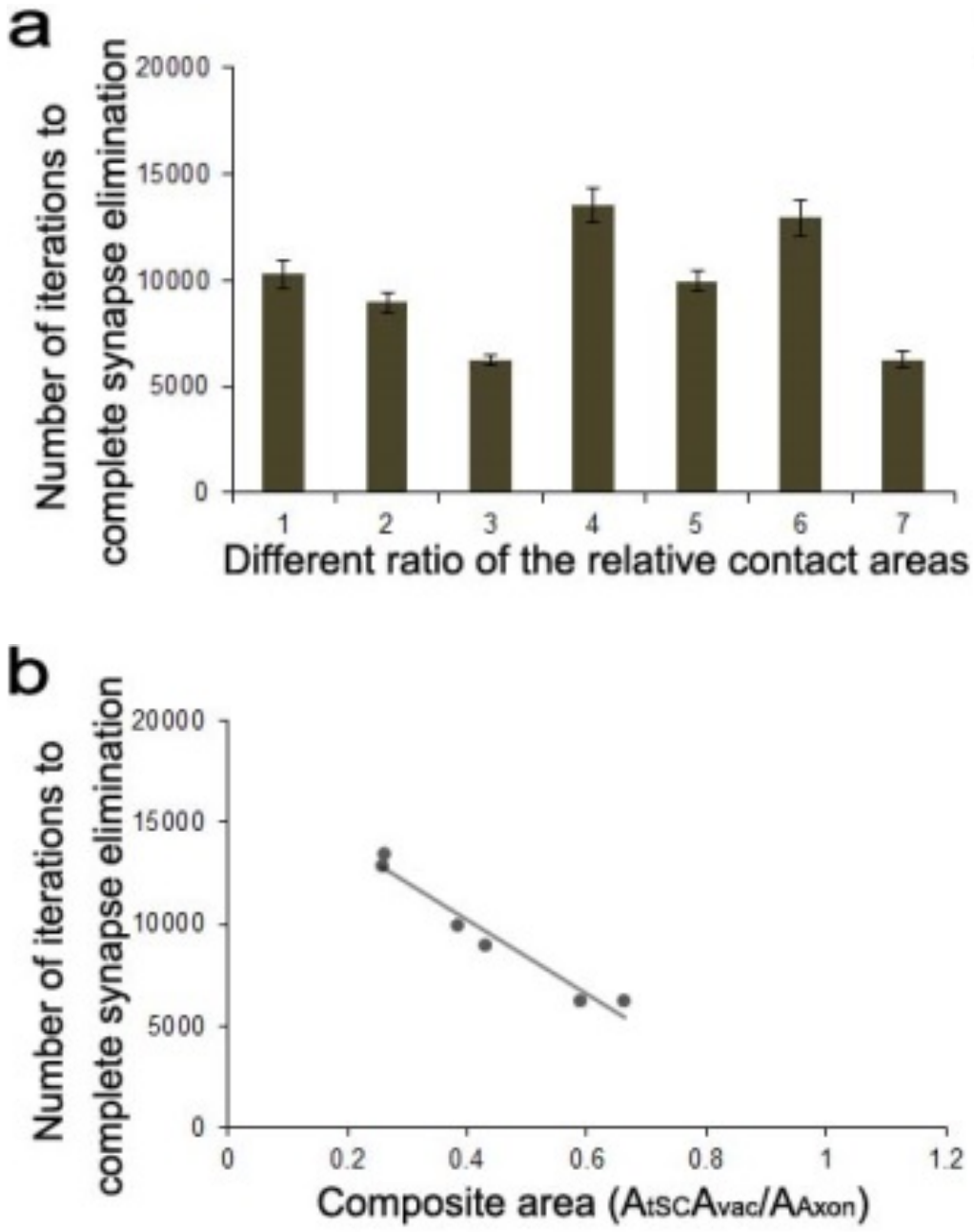

Figure A4:Relationships of the simulated average least number of iterations to complete synapse elimination with arbitrarily adjusted ratios of contact areas of tSCs, vacancies, and axons. (a) The average least number of iterations to complete synapse elimination for each of the six arbitrarily different ratios of postsynaptic contact areas by increasing or decreasing the portion of the area of tSCs, vacancies, and axons, respectively. The ratio at P3 (57:18:25) is used as a reference ratio for comparison (first bar). The changed ratios were 54:24:22 (second bar), 63:15:22 (third bar), 54:15:31 (fourth bar), 60:12:28 (fifth bar), 51:21:28 (sixth bar), and 60:21:19 (seventh bar). (b) Relationship of the composite area with the number of iterations to complete synapse elimination. All of the three fractions of the areas are combined into a variable called a composite area. The composite area is the product of the fraction of the area of tSCs and that of vacancies divided by that of axons. The composite area negatively correlates with the least number of iteration to complete synapse elimination (Spearman correlation, $p<0.05$).

To test whether our model can reliably predict the relationship between the rate of synapse elimination with the relative ratio of tSCs or that of vacancies, we increased the average relative ratios of tSCs or vacancies from their average ratios at P3 and ran the simulation of our model using the changed ratios. First, we increased the relative ratio of the vacancies from 0.18 to 0.24 and decreased each ratio of the tSCs and the axons by 0.03 each to keep the ratio of the relative area of tSCs to axons constant (0.54 for the tSCs and 0.28 for the axons). Simulation results using the adjusted ratios showed that the increased ratio of the vacancies accelerated synapse elimination (S4) by about 80%, indicating that vacancy area has a strong positive correlation with the rate of synapse elimination. Next, we increased the relative ratio of the tSCs from 0.57 to 0.63 and decreased vacancies and axons each by 0.03 (0.15 and 0.22 respectively). Synapse elimination was expedited with the increased ratio of tSCs by about 8%, indicating that the ratio of the tSCs has a positive correlation with the rate of synapse elimination but not as strongly as that of the vacancies. Our results demonstrate that the model can predict the positive correlation between the rate of synapse elimination and the ratio of the relative contact area formed by tSCs consistent with other studies (Smith et al., 2013; Lee et al., 2016) and the relative area formed by vacancies. These results show that an increase in the relative area of tSCs and/or vacancies accelerates synapse elimination in our model (Figure A4). We can then expect that an increase in the relative axon area will slow down synapse elimination. As expected, when we increased the relative ratio of the axons from 0.25 to 0.31 and decreased the ratio of tSCs and vacancies each by 0.03 (0.54 and 0.21 respectively), our simulation showed that the rate of synapse elimination was delayed by about 28%, indicating that the ratio of the axons has a negative correlation with the rate of synapse elimination (Figure A4 A). We

then decreased the relative ratio of the vacancies from 0.18 to 0.12 and increased the ratio of tSCs and axons each by 0.03 to keep their relative ratios constant (0.60 and 0.28 respectively). Our simulation showed that the rate of synapse elimination decreased by about 36% (Figure A4 A), which indicates again that the ratio of the vacancies has a positive correlation with the rate of synapse elimination. As we decreased the relative ratio of the tSCs from 0.57 to 0.51 and increased the ratio of the vacancies and axons each by 0.03 (0.21 and 0.28, respectively), we observed a decrease in the rate of synapse elimination of about 4%. This indicates that tSC ratio has a positive correlation with the rate of synapse elimination, but not as strong as that of vacancies, consistent with previous results (Figure A4 A). Finally, when we decreased the relative ratio of the axons from 0.25 to 0.19 and increased the ratio of tSCs and vacancies each by 0.03 (0.54 and 0.21 respectively), our simulation showed that the rate of synapse elimination increased by about 57%, again indicating that the ratio of the axons is negatively correlated with the rate of synapse elimination (Figure A4 A). These results and those reported above demonstrate that the model reliably predicts a close correlation between the rate of synapse elimination and the ratio of the contact areas formed by axons, tSCs, and vacancies consistent with our previous results and studies (Smith et al., 2013; Lee et al., 2016; Lee et al., 2011) . They also support the direct involvement of vacancies in synapse elimination. However, the seemingly positive correlation of the rate of synapse elimination with the relative area of tSCs and that of vacancies need to be interpreted with caution because the relative areas of tSCs, vacancies, and axons are inter-dependent. By using the composite area defined as the product of the relative area of tSCs (A_{tSC}) and that of vacancies (A_{vac}) divided by the relative area of Axons (A_{Axon}), we found that the composite area is negatively correlated

with the number of iterations to complete synapse elimination (Spearman Correlation, $p<0.05$) as shown in figure A4, B.

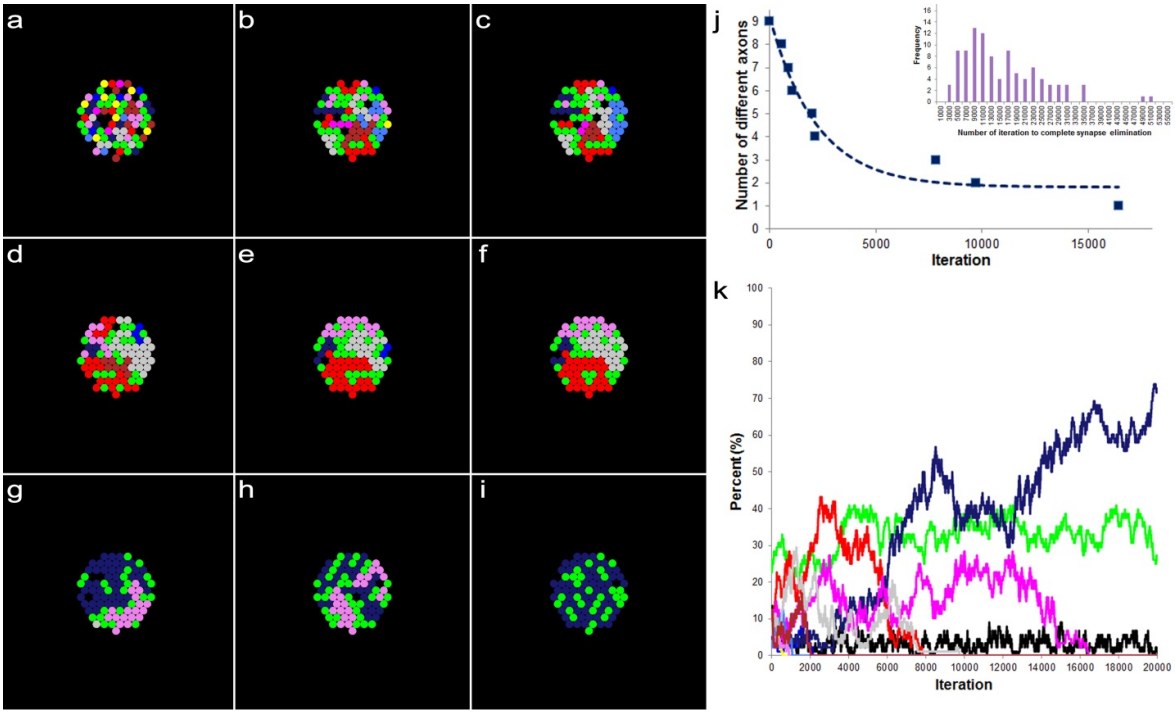

Figure A5: An example result based on a model of synaptic competition among axons, tSCs, and vacancies with different constant transition probabilities derived from the area ratios at P7 of the NMJs. Simulations carried out using the same configuration as described in Fig. 5.5, but the final ratios of tSCs, vacancies and axons are set to be 0.55, 0.05, and 0.40, respectively, which are the ratios at P7 of the NMJs (See Methods). (a) Initially, 9 different axons, tSCs and vacancies form their contact sites randomly on a muscle fiber with the initial ratio of their total contact areas (axons:tSCs:vacancies), which is about 30:16:54 as Fig. 5.5. (b-h) The competition among axons, tSCs, and vacancies with their random transition probabilities shows elimination of multiple contact sites formed by different axons, tSCs, and vacancies at different iterations of the simulation (600, 900, 1100, 2100, 2200, 7900, and 9800 iterations, respectively). (i) When the simulation is at 16,500 iterations, the competition leads to a complete synapse elimination with tSC and vacant sites present demonstrating that optimal transition probabilities reliably simulate synapse elimination. (j) The number of different types of axons in the endplate reduces sharply as the iteration proceeds. Inset: a distribution of the least number of iterations to complete synapse elimination for 100 repeated simulations (15730 ± 943, Mean ± SE). (k) Change of ratios of the contact areas formed by tSCs (green), vacancies (black), and 9 different axons (colors different from green and black) as the simulation based on the stochastic model of tSC and vacancy mediated synapse elimination proceeds. Inset: the distribution of the least number of iterations when synapse elimination is complete from 100 repeated simulations.

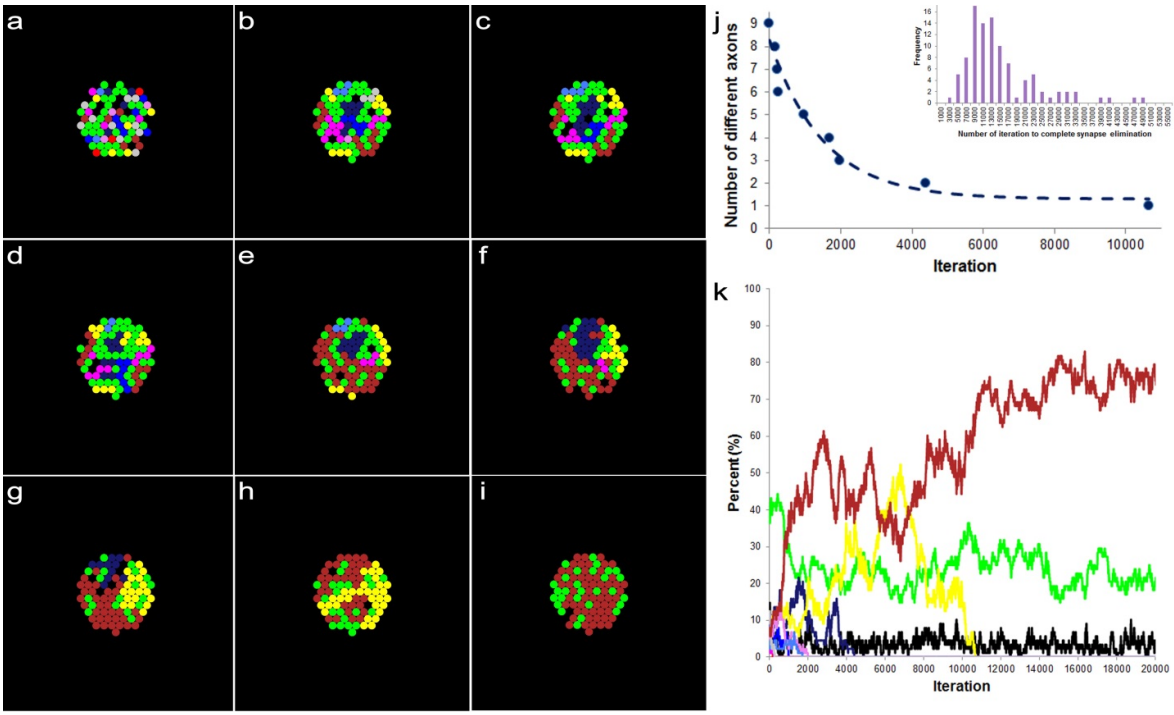

Figure A6: An example result based on a model of synaptic competition among axons, tSCs, and vacancies with different constant transition probabilities derived from the area ratios at P16 of the NMJs. Simulations carried out using the same configuration as described in Fig. 5.5, but the final ratios of tSCs, vacancies and axons are set to be 0.41, 0.06, and 0.53, respectively, which are the ratios at P16 of the NMJs (See Methods). (a) Initially, 9 different axons, tSCs and vacancies form their contact sites randomly on a muscle fiber with the initial ratio of their total contact areas (axons:tSCs:vacancies), which is about 30:16:54 as Fig. 5.5. (b-h) The competition among axons, tSCs, and vacancies with their random transition probabilities shows elimination of multiple contact sites formed by different axons, tSCs, and vacancies at different iterations of the simulation (200, 300, 400, 1000, 1700, 2000, and 4400 iterations, respectively). (i) When the simulation is at 10,600 iterations, the competition leads to a complete synapse elimination with tSC and vacant sites present demonstrating that optimal transition probabilities reliably simulate synapse elimination. (j) The number of different types of axons in the endplate reduces sharply as the iteration proceeds. Inset: a distribution of the least number of iterations to complete synapse elimination for 100 repeated simulations (15016 ± 902, Mean ± SE). (k) Change of ratios of the contact areas formed by tSCs (green), vacancies (black), and 9 different axons (colors different from green and black) as the simulation based on the stochastic model of tSC and vacancy mediated synapse elimination proceeds. Inset: the distribution of the least number of iterations when synapse elimination is complete from 100 repeated simulations.

Methods

Simulations based on Random Transition Probabilities

Because each transition probability might fluctuate randomly, first all of the probabilities are assumed to be random. In each step of the simulation, a contact site from all the sites in an endplate was randomly chosen. Then the site is converted into a different site with randomly assigned transition probabilities. The step was repeated more than 10000 times to ensure that only one type of axonal site survived at most as shown in Fig. 4 and A.1.

Simulations based on Equal Transition Probabilities

We assumed that all of the probabilities are fixed and the same. Using all the sites randomly assigned in the same way described above, at each step a contact site was randomly chosen from them and transitioned using the transition probabilities of neighboring axons, tSCs or vacancies where all of the probabilities are equal to 0.333. The process was repeated 200000 to make sure that only one type of synaptic site survived at most as shown in A.2 and A.3.